THE EFFECTS OF CHEMOTHERAPEUTIC AGENTS ON EPIDERMAL KERATINOCYTES MODIFIED WITH HUMAN PAPILLOMAVIRUS (HPV) GENES

By

LEE MEI WEI

A dissertation submitted to the Department of Pre-Clinical Science,
Faculty of Medicine and Health Sciences,
Universiti Tunku Abdul Rahman,
in partial fulfilment of the requirements for the degree of
Master of Medical Sciences

April 2018

ABSTRACT

THE EFFECTS OF CHEMOTHERAPEUTIC AGENTS ON EPIDERMAL KERATINOCYTES MODIFIED WITH HUMAN PAPILLOMAVIRUS (HPV) GENES

Lee Mei Wei

Human Papillomavirus type 16 (HPV16) is associated with various epithelial malignancies including cervical and head-and-neck cancers. HPV16-positive head-and-neck cancers and cancer cell lines have been reported to be more sensitive to irradiation and chemotherapy than HPV16-negative ones. To study the relationship between HPV16 and chemosensitivity in cancer, *in vitro* study models are needed. Hence, the primary objective of this study is to generate HPV16-associated models by employing epidermal keratinocytes. The second objective is to investigate the susceptibility of these models to two standard chemotherapeutic agents, cisplatin and topotecan as a proof of concept and the third objective is to test the potential cytotoxicity of novel natural flavones, eupatorin and sinensetin, and synthetic compounds tribenzyltin carboxylates 1 & 4 (TC1 & TC4) using the models.

To represent the precancerous stage of HPV16-associated carcinogenesis, a normal immortalised epidermal keratinocytes (NIKS) cell line was modified to harbour episomal HPV16 genome using lipid-based transfection. To represent the cancerous stage, HPV16 E6 and/or E7 were

introduced into NIKS cells by retrovirus transduction. HPV16 episomes were maintained up to passage 21 in the HPV16-precancerous model. RT-PCR and western blot analyses showed stable expression of the E6/E7 mRNA and protein in the models. Both the cancerous and pre-cancerous models demonstrated higher susceptibility to cisplatin and topotecan than the parental immortalised cells. Cells modified to express E6 or E7 alone were more sensitive to eupatorin/sinensetin compared to E6/E7 co-expression. Cells harbouring HPV16 episomes and those carrying the E6 oncogene were more sensitive to TC1 but all the models were insensitive to TC4. In conclusion, HPV16-associated cell models were established and their greater susceptibility to cisplatin and topotecan treatment compared to parental control cells was demonstrated. The increased sensitivity of the experimental cell lines relative to the control was also demonstrated for selective natural and synthetic compounds.

ACKNOWLEDGEMENTS

Foremost, I would like to express my sincere gratitude and appreciation to my supervisors, Prof. Dr. Yap Sook Fan and Assist. Prof. Dr. Leong Pooi Pooi for their continuous support of my master studies and research. I appreciate their patience, guidance and vast knowledge in my research areas, especially their assistance in the thesis writing.

I would like to thank Dr. Ken Raj, our collaborator from Health and Protection Agency, United Kingdom and Prof. Ngeow Yun Fong from UTAR for their supports in providing invaluable research advices and research materials at times of critical need. A special thanks to Dr. Kenny Voon Gah Leong from International Medical University (IMU), Malaysia for his persistence, understanding and kindness in helping out in this research project. I would like to thank to Dr. Kiew Lik Voon for his sharing knowledge in drug testing part of the study. Further, I would like to extend my sincere appreciation to Prof. Choo Kong Bung for his continuous encouragement, motivation, patience and guidance throughout the thesis writing period.

To my lab mates, especially to Ms. Wong Tze Hann and Ms. Nalini Devi Verusingam for all the hard times we were working together throughout this study; their support and constructive discussions helped me a lot in overcoming setbacks and stay focused in my research.

This project would not have been possible without the financial assistance of UTAR Research Fund; account number 6200/Y30, 6200/Y41, and 6200/Y50. Finally, I am immensely grateful to my parents for their understanding and spiritual support over the years in completing this study.

APPROVAL SHEET

This dissertation entitled "**THE EFFECTS OF CHEMOTHERAPEUTIC AGENTS ON EPIDERMAL KERATINOCYTES MODIFIED WITH HUMAN PAPILLOMAVIRUS (HPV) GENES"** was prepared by LEE MEI WEI and submitted as partial fulfilment of the requirements for the degree of Master of Medical Sciences at University Tunku Abdul Rahman.

Approved by:

_____ Date: ……

(Prof. Dr. Yap Sook Fan)
Professor/ Supervisor
Department of Pre-clinical sciences
Faculty of Medicine and Health Sciences
Universiti Tunku Abdul Rahman

_____

(Assistant Professor Dr. Leong Pooi Pooi) Date:……...
Assistant Professor/ Co-supervisor
Department of Pre-clinical sciences
Faculty of Medicine and Health Sciences
Universiti Tunku Abdul Rahman

FACULTY OF MEDICINE AND HEALTH SCIENCES

UNIVERSITI TUNKU ABDUL RAHMAN

Date: 27th April 2018

SUBMISSION OF DISSERTATION

It is hereby certified that **Lee Mei Wei** (ID number: **14UMM06114**) has completed this dissertation entitled "THE EFFECTS OF CHEMOTHERAPEUTIC AGENTS ON EPIDERMAL KERATINOCYTES MODIFIED WITH HUMAN PAPILLOMAVIRUS (HPV) GENES" under the supervision of Prof. Dr. Yap Sook Fan (Supervisor) and Assistant Prof. Dr. Leong Pooi Pooi (Co-supervisor) from the Department of Pre-clinical Sciences, Faculty of Medicine and Health Sciences.

I understand that University will upload a softcopy of my dissertation in pdf format into UTAR Institutional Repository, which may be made accessible to UTAR community and public.

Yours truly,

_____

(Lee Mei Wei)

DECLARATION

I hereby declare that the dissertation is based on my original work except for quotations and citations which have been duly acknowledged. I also declare that is has not been previously or concurrently submitted for any other degree at UTAR or other institutions.

_____

LEE MEI WEI

Date: 27th April 2018

TABLE OF CONTENTS

	PAGE
ABSTRACT	**ii**
ACKNOWLEDGEMENTS	**iv**
APPROVAL SHEET	**vi**
SUBMISSION SHEET	**vii**
DECLARATION	**viii**
LIST OF TABLES	**xv**
LIST OF FIGURES	**xvi**
LIST OF ABBREVIATIONS	**xviii**

CHAPTERS

1.0	**INTRODUCTION**	1
2.0	**LITERATURE REVIEW**	6
2.1	Human Papillomavirus (HPV)	6
2.1.1	Classification and Types of HPV	6
2.1.2	HPV Genome Organisation	9
2.1.3	HPV Viral Life Cycle	9
2.1.3.1	Early Event: Non-Vegetative Genome Amplification	12
2.1.3.2	Late Event: Vegetative Genome Amplification	14
2.1.4	Functions of HPV16 Genes	16
2.1.4.1	The E6 protein: Structure and Functions	19

2.1.4.2 The E7 Protein: Structure and Functions 22
2.2 Human Papillomavirus-associated Cancers 24
2.2.1 Cervical carcinoma (Cx Ca) 24
2.2.2 Head-and-Neck Squamous Cell Carcinoma (HNSCC) 25
2.2.3 Other HPV-related Diseases 28
2.3 Prevention, Current Treatments, and Challenges in HPV16-associated Cancers 29
2.4 *In-vitro* Models for Disease Studies of HPV-associated Cancers 30
2.4.1 The Use of Normal Immortalized Keratinocytes, NIKS 32
2.5 Chemosensitivity of HPV-associated Tumours and Cell Lines 33
2.6 Mechanisms of Cisplatin and Topotecan Action 35
2.6.1 Cisplatin and Mechanism of Action 35
2.6.2 Topotecan and Mechanism of Action 37
2.7 The Use of Natural Flavonoids Compounds in Cancer Treatment 40
2.7.1 Eupatorin and Sinensetin 40
2.8 The Use of Novel Synthetic Compounds in Cancer Treatment 41
2.8.1 Tribenzyltin Carboxylates (TC) 1 and 4 41

3.0 MATERIALS AND METHODS 43

3.1 Cell Lines 43
3.1.1 Normal Immortalised Keratinocytes, NIKS 43
3.1.2 Mouse Embryonic Fibroblast Cell Line, 3T3-J2 47
3.1.2.1 Irradiation of 3T3-J2 Cells to Serve as Feeder Layers 48
3.1.3 HPV16-positive Cell Line, CaSki 48

	3.1.4 Retrovirus Packaging Cell Line, Phoenix	49
3.2	Plasmid Constructs and Primers	50
	3.2.1 Plasmid DNA Constructs	50
	3.2.2 Primers Used in the Study	50
3.3	Preparation of Bacteria Culture Media and Antibiotic	53
	3.3.1 Lysogeny (LB) Agar Plate	53
	3.3.2 Lysogeny (LB) Media	54
	3.3.3 Ampicillin Stock Solution	54
3.4	Preparation of Plasmids DNA	55
	3.4.1 Transformation of *E. coli* with Plasmid DNA	55
	3.4.2 Identification of Positive Clones by Colony PCR	55
	3.4.3 Agarose Gel Electrophoresis	58
	3.4.4 Expansion Culture of Transformed *E. coli* Clones	58
	3.4.5 Plasmid DNA Extraction	59
	3.4.6 Preparation of Re-circularised HPV16 DNA	61
3.5	Establishment of HPV16 Precancerous Models: NIKS-HPV16$_{EPI}$	63
	3.5.1 Co-transfection of Re-Circularised Full HPV16 Genome and pcDNA into NIKS	63
3.6	Establishment of HPV16 Cancerous Models: NIKS-HPV16$_{INT}$	68
	3.6.1 Production of Recombinant Retroviruses	68
	3.6.2 Retroviral Transduction of NIKS cells	70
3.7	Characterisation of the HPV16 Modified Cell Lines	71
	3.7.1 Assessment of Gene Expression	71
	3.7.1.1 Total Ribonucleic Acid (RNA) Extraction	71
	3.7.1.2 Conversion of RNA into cDNA	73
	3.7.1.3 Polymerase Chain Reaction (PCR)	76

3.7.2 Analysis of Protein Expression by Western Blot 78
3.7.2.1 Buffers and Solutions 78
3.7.2.2 Protein Lysate Preparation 78
3.7.2.3 Protein Quantification 81
3.7.2.4 Protein Separation by SDS-polyacrylamide Gel Electrophoresis (SDS-PAGE) 81
3.7.2.5 Wet Transfer of Proteins from Gel to Nitrocellulose Membrane 83
3.7.2.6 Blocking of Nitrocellulose Membrane 84
3.7.2.7 Reaction with Primary and Secondary Antibodies 84
3.7.2.8 Chemiluminescence Detection 85
3.7.2.9 Membrane Stripping and Reprobing 86
3.7.3 Southern Blot Analysis for Assessment of the Integration Status of the HPV16 Genome 86
3.7.3.1 Restriction Enzyme Digestion and Gel Electrophoresis 88
3.7.3.2 Probe Preparation and Labelling 88
3.7.3.3 Southern Blot Transfer 88
3.7.3.4 Hybridisation and Autoradiography 89
3.8 Cell proliferation analysis by MTT assay 89
3.9 Susceptibility of HPV-modified Cell Lines to Standard Chemotherapeutic Agents 90
3.9.1 Assessment of Cytotoxicity 90
3.10 Treatment of Cells with Natural and Synthetic Compounds 92
3.10.1 Determination of Cytotoxic Effects of Natural and Synthetic Compounds by MTT 92

4.0 RESULTS 94

4.1 Study Design 94
Part I: Generation and Characterisation of HPV16-Associated Models 96
Part I(a): HPV16 "Precancerous" Models: NIKS-HPV16$_{EPI}$ 96
4.2 Generation of the "Precancerous" Model 96
4.3 Characteristics of the Transfected Cells 100
4.3.1 HPV16 Genome Integration Status 100
4.3.2 E6 and E7 mRNA Transcription Status 102
4.3.3 E6 and E7 Protein Expression Status 102
Part I(b): HPV16 "Cancerous" Models: NIKS-HPV16$_{INT}$ 104
4.4 Production of E6, E7 or E6E7 Retroviruses 104
4.5 Generation of the "Cancerous" Models 106
4.6 Characteristics of Transduced Cells 109
4.6.1 E6 and E7 mRNA Transcription Status 109
4.6.2 E6 and E7 Protein Expression Status 109
Part II: Verification of the Reported Increased Chemosensitivity of HPV-associated Tumours Compared to Non-HPV associated Tumours using the HPV16- models 111
4.7 Optimal Seeding Densities of the Cell Lines 111
4.8 Cytotoxic Effects of Cisplatin 114
4.9 Cytotoxic Effects of Topotecan 117
Part III: Effects of Selective Natural and Synthetic Compounds on the HPV16-associated Cell Lines 120
4.10 Effects of Eupatorin 120
4.11 Effects of Sinensetin 123
4.12 Effects of Tribenzytin Carboxylates 1 (TC1) 125
4.13 Effects of Tribenzytin Carboxylates 4 (TC4) 128

5.0 DISCUSSION 109

5.1 Characteristics of NIKS Cells modified to Harbour the HPV Genome in Episomal Form or the HPV E6 and/or E7 Oncogenes 131
5.2 Increased Sensitivity of HPV16 Models to Cisplatin 133

Treatment Compared to the Parental NIKS Cells
5.3 Topotecan Induces the Highest Growth Inhibition in NIKS Cells Expressing the E7 Gene Alone 137
5.4 Eupatorin and Sinensetin Exert Higher Growth Inhibition when E6 or E7 was Acting Alone than when E6 and E7 are Co-expressed 140
5.5 TC1 but not TC4 Induces Growth Inhibition in the HPV16 Precancerous Models 143

6.0 CONCLUSIONS 148

6.1 Major Findings of the Present Study 148
6.2 Limitations of the Study 149

REFERENCES 151

APPENDICES 175

LIST OF TABLES

Table		Page
3.1	Cell lines used in the study	44
3.2	Plasmids used to generate experimental models	51
3.3	Primers used in mRNA RT-PCR	52
3.4	PCR components for colony PCR	56
3.5	PCR cycling profile for colony PCR	57
3.6	Ligation reaction mixture set-up for preparation of circular HPV16	62
3.7	Preparation of transfection mixes using Lipofectamine® 3000	66
3.8	Production of recombinant retroviruses preparation of transfection mixture using the calcium phosphate	69
3.9	Reverse-transcription reaction mixture (Step 1)	74
3.10	Reverse-transcription reaction mixture (Step 2)	75
3.11	PCR reaction mixture	77
3.12	Preparation of buffers and solutions	79
4.1	Cytotoxic effects of cisplatin and topotecan on the HPV16 models	116
4.2	Effects of the natural compounds, eupatorin and sinensetin on the HPV16 models	122
4.3	Effects of novel synthetic compounds, tribenzyltin carboxylates 1 (TC1) and 4 (TC4) on HPV16 models	127

LIST OF FIGURES

Figure		Page
2.1	Phylogenetic tree of 170 human papillomavirus types categorised based on the sequence of the L1 open reading frame	7
2.2	Normal and human papillomavirus-infected stratified cervical squamous epithelial cells	11
2.3	Terminology used in classification and grading of cervical cancer	26
2.4	Mitochondrial (intrinsic) and death-receptor (extrinsic) apoptotic pathways activated by cisplatin	36
2.5	Mechanism of action of topotecan	39
3.1	Identification of HPV16-full genome fragment by restriction enzyme digestion	64
4.1	Overview of the study design	95
4.2	Microscopic images of NIKS cells	98
4.3	Morphology of blasticidin-treated HPV16 modified NIKS cells	99
4.4	Southern blot analysis of NIKS cells transfected with HPV16 genome	101
4.5	Expression of E6 and E7 in NIKS cells transfected with the HPV16 genome from passage (P) 5 to 30	103
4.6	Morphology and GFP-staining of transfected Phoenix cells.	105
4.7	Post-transduction of NIKS cells from 24 to 72 h	107
4.8	Geneticin treatment of the HPV16 cancerous model	108
4.9	Expression of E6 and E7 mRNA and protein in NIKS transduced with HPV16 E6, E7 or E6/E7 genes	110
4.10	Cell proliferation of the HPV16 precancerous model	112
4.11	Cell proliferation of the HPV16 cancerous models	113

4.12	Cisplatin-induced inhibition of cell growth on the HPV models	115
4.13	Topotecan-induced inhibition cell growth inhibition on the HPV models	119
4.14	Effects of eupatorin on cell growth of the HPV models	121
4.15	Effects of sinensetin on cell growth of the HPV models	124
4.16	Effects of tribenzyltin carboxylates 1 (TC1) on cell growth of the HPV models	126
4.17	Tribenzyltin carboxylates 4 (TC4) effects on cell growth of the HPV models.	129
5.1	Proposed pathways of the interactions between the HPV16 E6 or E7 oncogenes and cisplatin	136
5.2	Proposed pathways of the interactions between the HPV16 E7 oncogenes and topotecan	139
5.3	Proposed mechanism of action of eupatorin	141
5.4	Proposed mechanism of action of sinensetin	144
5.5	Proposed mechanism of action of tribenzyltin carboxylates 1 (TC1)	146

LIST OF ABBREVIATIONS

µ	Mu
32P-dCTP	Phosphorus-32-deoxycytidine triphosphate
3D	Three-dimensional
3T3-J2	Mouse embryonic fibroblast, J2-clone cell line
4T1	Mammary/breast carcinoma cell line
A_{570}	Absorbance at 570nm wavelength
AGS	Human gastric carcinoma cell line
APAF	Apoptotic protease activating factor
APS	Ammonium persulfate
ASC-US	Atypical squamous cells of undetermined significance
ATM	Ataxia telangiectasia mutated
ATP	Adenosine triphosphate
ATR	Ataxia telangiectasia and rad3-related
BAX / BAK	Bcl (B-cell lymphoma)-2-like protein 4
Bel-7402	Human hepatocellular carcinoma cell line
bp	base pairs
BSA	Bovine serum albumin
CAL27	Oral adenosquamous carcinoma cell line
CasKi	HPV16-positive cervical cancer cell line
CCD	Charge-coupled device
CCL23	Oral adenosquamous carcinoma cell line
CCL23AS	Oral adenosquamous carcinoma cell line
CDC25A	Cell division cycle 25A
CDK	Cyclin dependent kinase
cDNA	Complementary DNA
Chk1	Checkpoint kinase-1
CIN	Intraepithelial neoplasia
CO_2	Carbon dioxide
CR	Conserved region
CXXC	Cysteines (C) separated by amino acid (X)
ddH2O	Double-distilled water

DED	Death effector domain
DEPC	Diethylpyrocarbonate
DISC	Death inducing signalling complex
DMEM	Dulbecco's modified eagle medium
DMSO	Dimethyl sulfoxide
DNA	Deoxyribonucleic acid
dNTP	Deoxynucleoside triphosphate
DSB	Double-tranded breakage
E	Early
E. coli	*Escherichia coli*
E2F	Elongation 2 promoter binding factor
E6AP	E6-associated protein
ECL	Enhanced chemiluminescent
ECM	Extracellular matrix
EDTA	Ethylenediaminetetraacetic acid
EGF	Epidermal growth factor
EGFR	Epidermal growth factor receptor
EV	Epidermodyplasia verruciformis
EV	Empty vector
FADD	Fas-associated death domain
FasL	Fas ligand
FBS	Fetal bovine serum
FLT1	Fms-like tyrosine kinase gene
γ	Gamma
G418	Geneticin
GADD45	Growth arrest and DNA damage-inducible 45
GADPH	Glyceraldehyde 3-phosphate dehydrogenase
GFP	Green fluorescence protein
HCl	Hydrochloride acid
hDIg	Human homologue of the Drosophila discs-large tumor suppressor
HeLa	HPV18-positive cervical cancer cell line
HL-60	Human promyelocytic leukemia cell line

HNSCC	Head-and-neck squamous cell carcinoma
HPV	Human papillomavirus
HRAS	Harvey rat sarcoma viral oncogene homolog
HRP	Horseradish peroxidase
HSIL	High-grade squamous intraepithelial lesion
HSPG	Heparan sulfate proteoglycan
hSrib	Human homologue of the Drosophila scribble protein
hTERT	Human telomerase reverse transcriptase
HUVEC	Human umbilical vascular endothelial cell line
IC_{50}	Half maximal inhibitory concentration
IgG	Immunoglobulin G
IL8	Interleukin-8
JNK/p38	Jun N-terminal kinase/ phosphorylated p38
K562	Human immortalised myelogenous leukemia cell line
kb	kilobase pairs
KB	Epidermoid carcinoma cell line
kDa	Kilo-dalton
KDR1	Kinase insert domain receptor
L	Late
LAST	Lower anogenital squamous terminology standardisation
LB	Lysogeny broth
LCR	Long control region
LSIL	Low-grade squamous intraepithelial lesion
LXXLL	Leucine (L) separated by amino acid (X)
MAGI	Membrane associated guanylate kinase
MCF-7	Human breast adenocarcinoma cell line
MDA-MB231	Human breast adenocarcinoma cell line
MEKK	MAPK/Erk kinases
$MgCl_2$	Magnesium chloride
MHC	Major histocompatibility complex
MMC	Mitomycin-C
MOLT-4	Mixture of established human T-lymphoid cell line
mSin3A/HDAC	mSin3A/histone deacetylase

MTT	3-(4,5-dimethylthiazolyl-2)-2,5-diphenyltetrazolium bromide
NaCl	Sodium chloride
NC	Negative control
NIKS	Normal immortalised keratinocytes
NILM	Negative for intraepithelial lesion
Oligo(dT)$_{18}$	Oligodeoxythymidylic acid
OPSCC	Oropharygeal squamous cell carcinoma
ORF	Open reading frame
P	Passage
p21^{CIP1}/ p21	Cyclin-dependent kinase inhibitor 1A (CDKN1A)
p27^{KIP1} / p27	Cyclin-dependent kinase inhibitor 1B (CDKN1B)
p53	p53 tumor suppresor gene
P640	HPV16 late promoter
P97	HPV16 early promoter
PAGE	Polyacrylamide gel electrophoresis
Pap	Papanicolaou
PBS	Phosphate bufferred saline
PCNA	Proliferating cell nuclear antigen
PCR	Polymerase chain reaction
PDZ-BM	PDZ-binding motif
pH	Potential hydrogen
PIN	Penile intraepithelial neoplasia
pRb	Retinoblastoma tumor suppressor gene
PTPN	Non-receptor tyrosine phosphatase protein
PV	Papillomavirus
RIPA	Radioimmunoprecipitation assay
RNA	Ribonucleic acid
RPA	Replication protein A
rpm	Revolutions per minute
RPMI1640	Roswell Park Memorial Institute 1640
RPMI8226	Human myeloma cell line
RT-PCR	Reverse-transcription polymerase chain reaction
SDS	Sodium dodecyl sulphate

SiHa	HPV18-positive uterus cancer cell line
TAC	Transit amplifying cell
TAE	Tris-acetate-EDTA
TBS	Tris-bufferred saline
TBST	Tris-buffered saline with tween-20
TC1	Tribenzyltin carboxylates 1
TC4	Tribenzyltin carboxylates 4
TE	Tris-EDTA
TEMED	Tetramethylethylenediamine
TNF	Tumour necrosis factor
TNFR-1	Tumour necrosis factor receptor-1
TNF-α	Tumour necrosis factor-α
topo I	Topoisomerase I
TRADD	TNFR-1-associated death domain
TRAIL	TNF-related apoptosis inducing ligand
TRAIL-R1	TNF-related apoptosis inducing ligand receptor-1
TRAIL-R2	TNF-related apoptosis inducing ligand receptor-2
TZ	Transformation zone
URR	Upstream regulatory region
UV	Ultraviolet
V	Volt
VEGF	Vascular endothelial growth factor
VEGFR	Vascular endothelial growth factor receptor
VIN	Vulva intraepithelial neoplasia
W12	HPV16-positive cell line with episomal HPV16 genome
xg	Times gravity
α	Alpha
β	Beta
β-actin	Beta-actin
δ	Delta
ν	Nu

CHAPTER 1

INTRODUCTION

The incidence of cancers is increasing worldwide. It has been estimated that approximately 5 - 15% of human cancers are caused by viral infections (Baseman and Koutsky, 2005; Ault, 2006; Palefsky, 2010; Schiffman et al., 2016). Human papillomavirus (HPV) infection is one of the most common sexually transmitted viral diseases in both men and women. The high-risk HPV types, specifically HPV type-16 (HPV16) and HPV type-18 (HPV18) are the causative agents responsible for various epithelial malignancies in particular cervical and head-and-neck cancers. HPV infections are often transient and in the majority of cases, the immune system of the HPV-infected individuals eliminate the infection within 12 to 24 months (Juckett et al., 2010; Sudenga and Shrestha, 2013). However, HPV16 infection in particular is highly persistent, and remains asymptomatically in the host for 5 to 15 years (Braaten and Laufer, 2008; Sudenga and Shrestha, 2013), frequently leading to aggressive HPV16-related cancers, especially in cervical cancer among infected women.

To date, more than 150 HPV subtypes have been identified. They are grouped based on differences in the viral genomic DNA sequences and clinical manifestations into high-risk and low-risk types. (Doorbar et al., 2015; Kim, 2016).

The low-risk HPV types, typically represented by HPV type-6 and -11, are known to cause benign genital lesions. The high-risk HPV types, commonly HPV type-16 and -18, are found in various epithelial cancers, such as cancers of the cervix, head-and-neck, anus, vulvovagina and penis (Bansal et al., 2016).

HPV infection is acquired through direct skin-to-skin contact at the squamous epithelial tissue and the HPV lifecycle is tightly associated with differentiation of keratinocytes. HPV infection is initiated via micro-abrasions at the proliferative basal keratinocytes, and viral DNA replication is relatively low at the early stage of infection (Kajitani et al., 2012; Pinidis et al., 2016). At the later stage of HPV infection, cells infected by high-risk oncogenic virus express two major oncoproteins, the early genes E6 and E7, which function during productive HPV infection to subvert normal cell growth regulatory pathways to allow viral replication. Both E6 and E7 play important roles in carcinogenesis by inducing cellular transformation through deregulation of fundamental cellular events, including apoptosis, cell cycle and DNA repair (Longworth and Laimins, 2004; Tommasino, 2014). Prolonged infection in susceptible individuals is associated with random integration of the HPV genome into the host genome leading to uncontrolled expression of the E6 and E7 genes, driving the cells to acquire an invasive cancer phenotype (Psyrri and DiMaio, 2008; Pinidis et al., 2016).

Cervical cancer, one of the major causes of cancer death worldwide, is associated with HPV infection in over 99% of cases. Early detection of these

cancers is vital to decrease the morbidity and mortality of the disease. This is promoted by the Papanicolaou (Pap) smear screening. More recently, testing for HPV infection in the susceptible population has also been advocated. HPV testing allows the detection of high-risk HPV types, which can act as a surrogate marker for the risk of cervical cancer development (Burd, 2003; Lorincz et al., 2013). In addition, prevention of HPV-related cancers can be achieved by vaccination of uninfected individuals (Braaten and Laufer, 2008). However, due to inadequate coverage of Pap smear screening, much less HPV testing and vaccination, cervical cancer remains a major cause of cancer death among women. This is particularly relevant in poorer regions where, as a result, cervical cases are often detected at late stage of the disease. Furthermore, although the current standard treatment options for HPV-associated cancers comprising surgery, radiotherapy and chemotherapy (Urban et al., 2014; Vokes et al., 2015) can be effective, these treatments carry many side effects. Therefore, it is necessary for continued research on finding more effective therapeutic options with maximal benefits but minimal detrimental effects.

Interestingly, HPV16-associated head-and-neck cancers were found to be more prone to elimination by radiation and chemotherapy than HPV-negative cancers *in vitro* and *in vivo* (Ang et al., 2010; Ziemann et al., 2015). This observation is contrary to the fact that HPV16 E6 and E7 are known to promote evasion of apoptosis and induction of cellular immortalisation, both of which are features of neoplasia. These findings have been reported in HPV-associated head-and-neck squamous cell carcinoma (HNSCC) as well as in cervical cancer (Sultana

et al., 2003; Fakhry et al., 2008; Ang et al., 2010; Ziemann et al., 2015). This phenomenon of HPV-positive cells being more susceptible to chemotherapeutic agent is intriguing and is the basis of our interest in establishing epidermal keratinocyte-based models harbouring the episomal HPV genome, as well as that carrying the HPV16 E6 and E7 oncogenes to further examine this observation.

The cells that harbour the HPV genome as episomes are used, albeit simplistically, to represent the precancerous stage of cellular transformation in the evolution of the cancer. Cells that carry the E6 or E7 oncogene singly or in combination are taken to emulate the stage of carcinogenesis process where the HPV genome is integrated into the host genome, an important step in the carcinogenesis process. These models will be named for convenience as precancerous and cancerous models respectively in the rest of the thesis. These cell models were used as drug screening platforms in this study, primarily for proof of concept that HPV-associated cancers are more sensitive to chemotherapy. The hypothesis, therefore, is that the epidermal keratinocyte-based HPV16 models established in this study are more susceptible to selective chemotherapeutic drugs. To test this hypothesis, susceptibility of the cell models to standard chemotherapeutic agents compared to control (parental) cells was studied. It is proposed that the established cell models, if verified, could serve as tools for testing synthetic and natural compounds for their potential effects as chemotherapeutic agents.

Hence, the objectives of this study are:

1) To generate epithelial cell-based models to represent the HPV16-associated precancerous and cancerous stages of the carcinogenesis process
2) To evaluate the susceptibility of these models, relative to unmodified parental cells, to two standard chemotherapeutic agents
3) To test the effects of selected natural and synthetic compounds on the HPV16-modified cell lines

CHAPTER 2

LITERATURE REVIEW

2.1 Human Papillomavirus (HPV)

Epithelial malignancy caused by human papillomaviruses, particularly the oncogenic HPV type-16 (HPV16) is a major concern worldwide. Hence, active research on HPV16 and HPV-associated malignancies is on-going. HPV16 is the focus in this study which is based on investigation of the effectiveness of conventional and novel compounds in cell models harbouring the HPV16 genome or the viral oncogenes, E6 and E7.

2.1.1 Classification and Types of HPV

Papillomaviruses (PVs) belong to the *Papillomaviridae* family and they are classified based on the nucleotide sequence of the conserved gene sequence, L1 capsid protein open reading frame (ORF) in the HPV genome. L1 was therefore used to construct the phylogenetic trees to indicate evolutionary relationship between the viral genomes of different species (Figure 2.1) (de Villiers et al., 2004; de Villiers, 2013). To date, the known 189 PVs are grouped into 29 genera, 24 of which are animal PVs and the remaining 5 genera are human PVs. Human

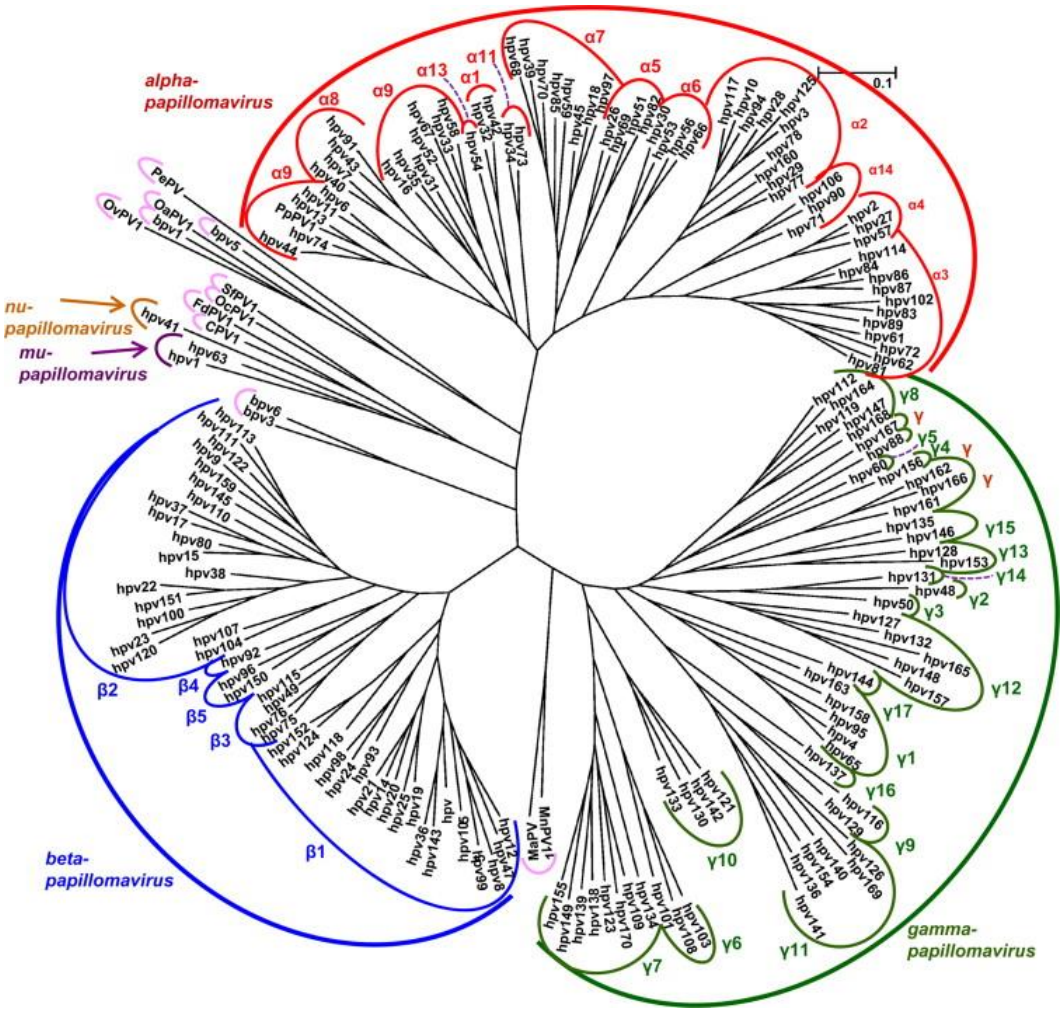

Figure 2.1 Phylogenetic tree of 170 human papillomavirus types categorised based on the sequence of the L1 open reading frame. The five major HPV genera that have been identified, are alpha- (α-), beta- (β-), gamma- (γ-), mu- (μ-) and nu- (ν) papillomavirus. The alpha group contains the most oncogenic viruses that are associated with cancer development. The commonly studied oncogenic virus in the alpha genus is HPV type-16. (Figure adapted from de Villiers, 2013)

papillomavirus (HPV) types are grouped into five major genus, namely alpha- (α-), beta- (β-), gamma- (γ-), mu- (μ-) and nu- (ν-) papillomavirus (Xue et al., 2012; Bzhalava et al., 2015). Members of the alpha genus predominantly infect the mucosal and cutaneous surfaces and are often associated with the development of both benign and malignant lesions (Burk et al., 2013). In addition, mucosal HPV types in the alpha genus can be subdivided into low-risk and high-risk HPV types based on their oncogenic potential. The low-risk HPV types, including HPV6 and HPV11 cause benign hyperplasia or warts with low malignant potential (Psyrri and DiMaio, 2008; Bzhalava et al., 2013), whereas the high-risk HPV types, most commonly HPV16, and HPV18 are associated with various epithelial cancers. Among the two high-risk HPVs, HPV16 has been known to be involved in approximately 57% of all cervical cancer cases, followed by HPV18 at 16% prevalence rate (Garbuglia, 2014). In addition, HPV16 also has been detected in head-and-neck cancer, particularly the oropharyngeal squamous cell carcinoma (OPSCC) with over 50% prevalence rate (Dufour et al., 2012; Stein et al., 2014; Gillison et al., 2015). Hence, most work has been carried out focusing on the oncogenic HPV, in particular HPV16, due to its clinical importance. The β-HPVs, e.g. HPV5 and HPV9 and γ-HPVs, e.g. HPV4 and HPV65, are commonly associated with benign and malignant cutaneous lesions in immunocompromised individuals suffering from epidermodyplasia verruciformis (EV) (de Villiers et al., 2004; Egawa et al., 2015). Likewise, μ-HPVs, e.g. HPV1 and HPV63 and v-HPV, represented by HPV41, are also reported to induce cutaneous lesions (Paradise et al., 2013; Garbuglia, 2014).

2.1.2 HPV16 Genome Organisation

All the HPVs share a common non-enveloped icosahedral structure despite their association with different epithelial diseases. HPVs are small, double-stranded DNA viruses with a circular genome approximately 8 kilobase pairs (kb) in size. The HPV genome encodes eight major proteins, organised into three different regions: (i) an early (E) region composed of seven open reading frames, E1, E2, E4, E5, E6, E7 and E8, that are involved in replication of the HPV genome and cellular transformation (Graham and Faizo, 2017); (ii) a late (L) region which encodes two major capsid proteins, L1 and L2, that are responsible for the assembly and transmission of the virus; and (iii) an upstream regulatory region (URR), also called noncoding long control region (LCR), which contains the late and early promoter sequences, P97 and P640, as well as *cis*-regulatory elements to regulate viral DNA transcription and replication (Tommasino, 2014; Morshed et al., 2014; Bravo and Félez-Sánchez, 2015; Graham and Faizo, 2017).

2.1.3 HPV Viral Life Cycle

HPV16 is the most extensively studied HPV. HPV16 is an epitheliotropic papillomavirus and the viral life cycle is strictly regulated by the epithelial differentiation programmes of the infected host cells (McBride, 2008; Kajitani et al., 2012; Kadaja et al., 2009; Bravo and Félez-Sánchez, 2015). In normal stratified squamous epithelium, the basal cells consist of self-renewable stem cells and transit

amplifying cells (TACs) that are committed progenitor cells which do not divide but withdraw from the cell cycle to undergo terminal differentiation. These cells progress to form the highly keratinised squamous cells that serve as the epithelial barrier that protects the body from the environment (Watt, 1998; Doorbar, 2005; Graham and Faizo, 2017). The virus is introduced into the epithelium via micro-abrasions and infection is initiated by targeting the proliferative-competent basal cells. Viral DNA replication involve three phases: (i) establishment of HPV infection at the proliferative basal keratinocytes; (ii) maintenance of low viral DNA copy number in the non-vegetative amplification phase; and (iii) amplification resulting in high viral DNA copy number in the vegetative amplification phase, followed by release of virions at the terminally differentiated epithelium layer (Figure 2.2) (McBride, 2008; Pyeon et al., 2009).

Upon initial infection, viral entry into the host cell is facilitated by the attachment of the virions to heparan sulfate proteoglycan (HSPG) present on the extracellular matrix (ECM) or the basal keratinocytes membrane (Culp et al., 2006; Horvath et al., 2010; Cerqueira et al., 2013). The binding to HSPG triggers conformational changes of the L1 and L2 viral capsid proteins. Subsequently virions are endocytosed into the host endosome via receptor-mediated endocytosis (Zhang et al., 2014; Digiuseppe et al., 2015). Upon entry, the acidic components of the endosome dissemble the viral capsid proteins, allowing viral DNA to escape from the endosome, with the help of the L2 minor capsid protein, into the host nucleus via the microtubule network (McBride, 2008; Deligeoroglou et al., 2013).

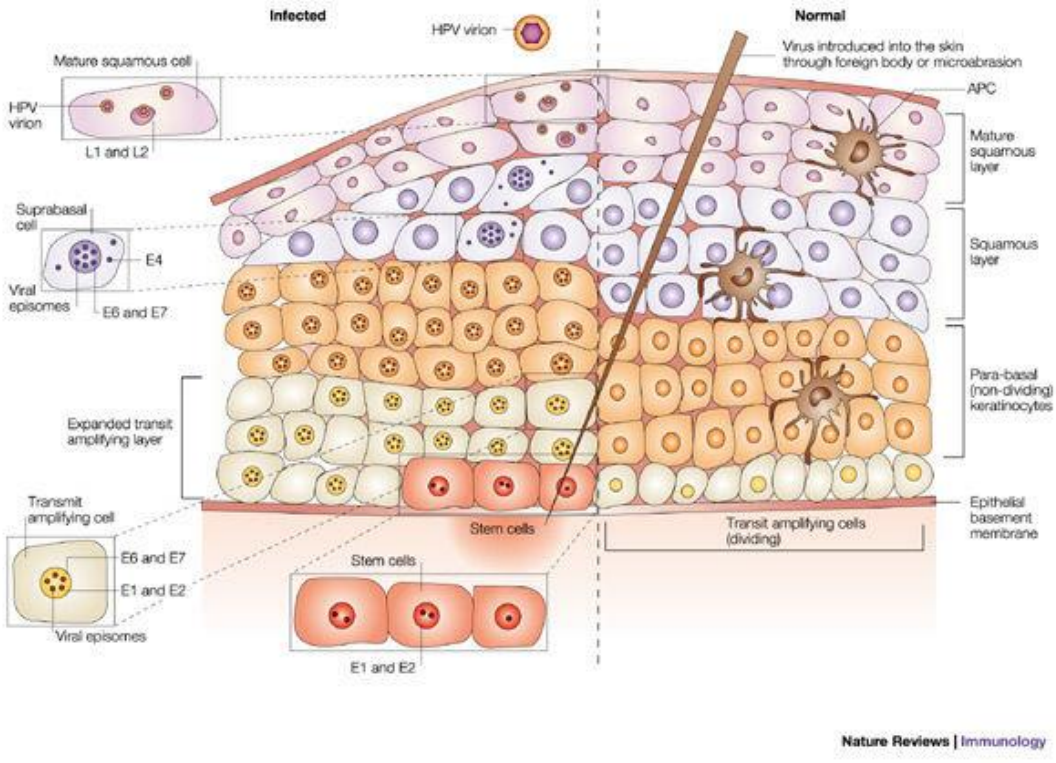

Figure 2.2 Normal and human papillomavirus-infected stratified cervical squamous epithelial cells. Under normal conditions, the highly proliferative stem cells, also known as transit-amplifying cells, divide along the epithelial membrane. The daughter cells mature going up to the parabasal epithelial layer and without further cell division (right panel). Through micro-abrasion, HPV reaches the dividing basal cells of the epithelium and expresses the viral early (E) proteins, E1, E2, E4, E6 and E7. The infected daughter cells that are rapidly dividing continue to expand and move to the upper epithelial layers, but expression of HPV proteins interferes with the differentiation programme of epithelial cells. Late (L) proteins, L1 and L2 of HPV are expressed sequentially with epithelial differentiation. Mature virions are generated only at the top layers of the epithelium (left panel). (Figure adapted from Frazer, 2004)

Viral DNA is maintained in an extrachromosomal or episomal form and viral genome replication is persistent and synchronised with the host DNA replication machinery system in a cell-cycle dependent manner (McBride, 2008). As the basal cells divide, infected daughter cells enter the suprabasal layer and exit cell cycle to differentiate. These infected cells remain active in the cell cycle due to the expression of E6 and E7 oncogenes which abrogates p53 and pRb activities, thereby enabling viral DNA amplification (Longworth and Laimins, 2004; Conway and Meyers, 2009; Stanley, 2012; Chang and Jeang, 2013). Expression of E6 and E7 is also upregulated at the productive phase of the viral life cycle to ensure the uncontrolled proliferation of infected cells (Kajitani et al., 2012). Subsequently, expression of the late genes, encoding the L1 and L2 capsid proteins is upregulated to allow for packaging the viral DNA into virion particles (Stanley, 2012). At the terminally differentiated epithelium layer, virion assembly occurs in which viral DNA is encapsidated by the capsid proteins into virions, and the virus progeny are released to infect other surrounding epithelial cells (McBride, 2008; Horvath et al., 2010; Bravo and Félez-Sánchez, 2015).

2.1.3.1 Early Event: Non-Vegetative Genome Amplification

In the early stage of HPV16 infection, the early P97 promoter that lies upstream of the E6 ORF in the LCR controls expression of the early viral genes including E1, E2, E4, E5, E6 and E7 in the undifferentiated basal cells (Zheng and Baker, 2006; Chang and Jeang, 2013). Although E1 protein is the primary

replication protein, HPV infection is initiated by the E2 transcription factor to load the E1 helicase onto the virus origin of replication (ori) which contains the binding site for the E1 protein (McBride, 2013). The E2 protein acts as a cofactor to enhance the transcription activity of E1 by first forming a E1/E2 complex (Miller and Stack, 2015) to further promote the recruitment of DNA replication proteins, including topoisomerase I (topo I), α-primase DNA polymerase, δ-polymerase, replication protein A (RPA), proliferating cell nuclear antigen (PCNA) and replication factor C to the viral origin of replication (Xue et al., 2012; Archambault and Melendy, 2013). Subsequently, the E1 protein undergoes conformational changes into a double-hexameric structure induced by ATP binding (Bergvall et al., 2013) destabilising E2, leading to E2 displacement (Sanders and Stenlund, 1998). The upregulation of the E2 protein represses expression of the E6 and E7 viral proteins, hence allowing the infected cells to escape from immune surveillance of the host cells and to maintain persistent viral genome amplification (Graham, 2010; Bodily and Laimins, 2011; Johansson and Schwartz, 2013).

Viral DNA copy number is relatively low (20 to 100 episomal copies) in the non-vegetative genome amplification phase and viral DNA is maintained in the episomal form (Longworth and Laimins, 2004; Moody and Laimins, 2010; Kajitani et al., 2012). Viral copy number varies in different epithelial lesions and at different sites of infection. Cell lines derived from cervical lesions have been reported to harbour episomal HPV16 DNA at around 200 copies per cell in the mitotically-active dividing basal cells (Chang and Jeang, 2013; Doorbar et al., 2015). The viral

episomes replicate once during every host-cell division, and E2 facilitates the segregation of HPV episomes into two daughter cells (Hoffmann et al., 2006; Feller et al., 2009). Maintenance of the viral genome in an episomal state during this phase is crucial for the establishment of the early viral life cycle. As the infected cells leave the basal cell layer and begin to differentiate, the E1 and E2 transcription signals switch from the early promoter, P97 to the late promoter, P670, in response to other cellular signals released by differentiation- specific transcription factors (Johansson and Schwartz, 2013).

2.1.3.2 Late Event: Vegetative Genome Amplification

In the vegetative- or differentiation-dependent genome amplification phase, the HPV16 late promoter, P670, located within the E7 ORF, is activated along with the E8 promoter located at the 5' end of the E1 ORF, upon receiving differentiation signals (Doorbar et al., 2012; Graham and Faizo, 2017). Activation of the P670 promoter induces upregulation of the E1, E2, E4 and E5 genes at the suprabasal epithelial layers (Johansson and Schwartz, 2013; Hong and Laimins, 2013; Graham and Faizo, 2017). In addition, accumulation of the E1 and E2 viral proteins in the nucleus also lead to increased amplification of viral DNA (Graham, 2010; Doorbar et al., 2015).

The viral DNA copy number increases from around 200 copies in the initial phase to thousands of viral DNA copies per cell in the productive life-cycle stage

(Kadaja et al., 2009; Graham, 2010; Pinidis et al., 2016). Studies showed that the HPV16-positive cells, W12E, carried an average of 1200 copies of HPV episomes per cell in early passage of the cells, but gradually reduced in viral copy number on prolonged culture, with evidence suggesting integration of the viral genome into the host chromosomes (Jeon et al., 1995; Garner-Hamrick and Fisher, 2002). High-risk HPV genomes have been found to integrate into the host cell chromosomal DNA over time through the L1 ORF and the integrated genome fragment still retains the functional viral origin of replication, co-existing with the HPV episomes (Kadaja et al., 2009). In many cases of cervical carcinoma, HPV16 genome is consistently found to be integrated into the host genome, and increased frequencies of genome integration are associated with disease progression (Kadaja et al., 2009; Williams et al., 2011). Experimental data further showed that HPV genome is present in episomal state in early low-grade lesions of cervical intraepithelial neoplasia (CIN) I and II, whereas integration of viral genome is often found in CIN III lesions and in invasive carcinoma, suggesting that HPV16 integration into host cells occurs at the late stage of carcinogenesis.

In addition, HPV integration commonly occurs in fragile sites of the human genome that are prone to chromosomal breakages (Münger et al., 2004; Liu et al., 2016; McBride and Warburton, 2017). The E2 ORF has been identified as the commonly disrupted HPV sequence during HPV integration; this results in elevated expression of E6 and E7 (Münger et al., 2004; Williams et al., 2011). However, it is now known that the HPV integration sites are broadly dispersed across the entire

viral genome (Liu et al., 2016; McBride and Warburton, 2017). Interestingly, the E6 and E7 ORFs are invariably retained in most of the HPV-associated cancer cases where HPV integration has occurred (Choo et al., 1987; zur Hausen, 2012). The upregulation of E6 and E7 expression accelerates the degradation of p53 and the retinoblastoma tumour suppressor gene (pRb) resulting in increased genomic instability and cell proliferation, thereby promoting cell transformation and immortalisation (Münger et al., 2004; Williams et al., 2011; Kajitani et al., 2012).

2.1.4 Functions of HPV16 Genes

Replication of the HPV genome in infected keratinocytes requires the action of various oncoproteins. The HPV16 E1 protein, a hexameric ATP-dependent DNA helicase, initiates viral replication and amplification of HPV episomes (Bergvall et al., 2013). The E1 protein stimulates topoisomerase I to unwind the double-stranded DNA helix structure thereby initiating DNA replication (Clower et al., 2006). Further, the E1 protein is crucial in increasing the copy number of the viral episomes upon viral infection, maintaining the viral DNA at a constant levels in the latently-infected basal cells as well as in promoting viral genome amplification during the productive phase of the viral life cycle (Kadaja et al., 2007; Bergvall et al., 2013).

The E2 protein has been characterised as an important DNA regulatory protein and is involved in initiation of viral DNA replication (McBride, 2013)

through its association with E1 protein. In addition, E2 protein is crucial in regulating the papillomavirus life cycle as it acts as a P97 promoter transcriptional activator or repressor of the HPV16 E6 and E7 (Soeda et al., 2006; Durzynska et al., 2017). Repression of oncogene expression occurs at the early stage of HPV infection. Such silencing leads to down-regulated E6/E7 expression and protects the infected cells against deleterious genomic instability (Francis et al., 2000; Bechtold et al., 2003; Durzynska et al., 2017). The E2 open reading frame (ORF) of cervical cancer cells is reported to be frequently disrupted in the event of HPV DNA integration at the vegetative phase of viral life cycle. Significantly, loss of E2 expression was found to result in overexpression of the E6 and E7 oncogenes, thereby conferring a growth advantage to the HPV-infected cells (Bechtold et al., 2003; Parish et al., 2006), which could contribute to the oncogenic process.

In HPV-infected cells, expression of HPV16 E4 protein has been shown to facilitate nuclear localisation of the E1 replication protein and contribute to increased viral genome amplification in the differentiation-dependent viral life cycle (Parish et al., 2006). Experimental data showed that the E4 protein is abundantly expressed at the differentiation-dependent stage of viral life cycle, accumulating at the upper epithelial layer (Egawa et al., 2017). Besides this, HPV16 E4 has been shown to induce G2 cell cycle arrest of the infected cells preventing entry into mitosis by sequestering cyclinB1/CDK1 into the cytoplasm and preventing the accumulation of cyclinB1/CDK1 complexes in the nucleus (Doorbar, 2013; Egawa et al., 2017). This limits viral cell cycle progression while enhancing

efficient viral DNA replication during the productive life cycle of the virus (Wang et al., 2009). Another important action of the E4 protein is perturbation of the network of cellular intermediate filaments leading to reorganisation of the cytokeratin network to facilitate virions release from the terminally differentiated epithelial cells (Khan et al., 2011; Doorbar, 2013).

The HPV16 E5 protein acts as an oncogene in cooperation with the E7 oncogene to enhance cellular transformation similar to the E6/E7 interaction (DiMaio and Mattoon, 2001; Maufort et al., 2010). The E5 protein also plays an important role at the early stage of HPV life cycle, down-regulating expression of antigen-presenting major histocompatibility complex (MHC) of the infected cells which helps the virus to escape from host immune recognition (Campo et al., 2010; Song et al., 2015; de Freitas et al., 2017). The E5 protein has also been shown to upregulate vascular endothelial growth factor (VEGF) via activation of several EGFR-dependent pathways to induce angiogenesis (Kim et al., 2006; Dimaio and Petti, 2013). Experimental data from several studies have suggested that HPV16 E5 synergises with the epidermal growth factor receptor (EGFR) signalling pathway to enhance cell cycle progression (Pedroza-Saavedra et al., 2010; Müller et al., 2015). The E5 protein is thought to interact with H^+-ATPase to abrogate the endosomal acidification process, which in turn inhibits the degradation of EGFR and increases the recycling of endocytic EGFR to the cell surface to promote keratinocyte proliferation (Zhang et al., 2005; Suprynowicz et al., 2010; Müller et al., 2015). However, the molecular mechanism on how HPV16 E5 affects EGFR

levels or signalling pathways remains to be fully elucidated. The role of HPV E6 and E7 oncoproteins in HPV-infected cells is discussed below.

2.1.4.1 The E6 Protein: Structure and Functions

The HPV E6 protein is a small polypeptides composed of approximately 150 amino acid residues, and contains two pairs of zinc-like finger, CXXC motifs (Mantovani and Banks, 2001; Howie et al., 2009; Tomaić, 2016). The CXXC are highly conserved in the HPV family and the integrity of the motifs is important to ensure normal E6 biological functions (Thomas et al., 1999; Mantovani and Banks, 2001). Proteins that are shown to be closely associated with E6 are E6-associatd protein (E6AP) and tumour suppressor protein, p53. High-risk HPV16 E6 proteins can efficiently interact with the LXXLL motif of E6AP, an E3-ubiquition ligase (Martinez-Zapien et al., 2016; Tomaić, 2016), which results in ubiquitination and degradation of p53. The p53 protein is a transcription factor that represents a major switch to halt cancer formation by promoting cell-cycle checkpoint arrest and apoptosis of the infected cells (Mantovani and Banks, 2001; Hoe et al., 2014). As a result of targeted degradation of p53 by the E6 oncoprotein, p53 function is greatly decreased, and p53-dependent growth arrest and apoptosis in response to viral replication are abolished (Mantovani and Banks, 2001).

Although the major anti-apoptotic activity of E6 is through degradation of the p53 protein, the HPV16 E6 protein has also been shown to target other pro-

apoptotic targets, such as the BAK protein, to inhibit apoptosis though the E6AP-dependent proteasome-mediated degradation pathway in the intrinsic apoptotic pathway (Garnett and Duerksen-Hughes, 2006; Jiang and Yue, 2014; Tomaić, 2016). In addition, the HPV16 E6 has also been shown to interact with trans membrane death receptors, including tumour necrosis factor receptor-1 (TNFR-1), to abolish the interaction between TNFR-1 and the TNFR-1-associated death domain (TRADD) adapter molecule, hence inhibiting the apoptosis (Howie et al., 2009; Jiang and Yue, 2014). Besides the tumour necrosis factor (TNF) pathway, it has also been shown that HPV16 E6 inhibits apoptosis by interacting with Fas-associated death domain (FADD), TNF-related apoptosis inducing ligand (TRAIL) receptor and procaspase 8 via the death effector domains (DEDs), thereby enhancing degradation of these proteins (Jiang and Yue, 2014; Tomaić, 2016).

The E6 protein of the high-risk HPV type-16 and 18 shares a highly conserved PDZ-binding motif (PDZ-BM) designated as XT-SXV (Mantovani and Banks, 2001; Howie et al., 2009) at its C-terminal region. This region of the E6 is known to bind with PDZ cellular proteins or PDZ ligands and plays an important role for the oncogenic action of the HPV16 E6 protein (Nguyen et al., 2003). The PDZ proteins are crucial in regulating cell polarity, control of cell-cell attachment and cell signalling (Pim et al., 2012; Mischo et al., 2013). Several PDZ proteins have been identified to be associated with E6 and subject them for degradation, including cell polarity regulators, human Dig (hDIg) (Halim et al., 2013; Brimer and Vande Pol, 2014), human Scribble (hSrib) as well as cell scaffolds regulators,

MAGI, which are membrane associated guanylate kinase homology proteins with an inverted domain structure (Howie et al., 2009; Yoshimatsu et al., 2017). HPV16 has also been shown to target PTPN3 and PTPN13, non-receptor tyrosine phosphatases, and subject them to E6AP-mediated degradation. Degradation of PTPN13, which normally acts as a tumour suppressor in several signalling pathways, has been shown to influence cancer initiation and progression (Vermeer et al., 2013; James and Roberts, 2016). Studies have revealed that the association of PDZ proteins with the PDZ-BM of E6 oncoprotein play a critical role in HPV16 episomal maintenance, as the loss of PDZ-BM leads to failure to maintain the HPV16 episomes and greatly reduces the transforming properties of HPV16 E6 in *in vivo* and *in vitro* experimental models (Kranjec and Banks, 2011; Nicolaides et al., 2011; Yoshimatsu et al., 2017) suggesting that one of the PDZ protein targets might play a role in stabilising the E6 protein and its expression (Brimer and Vande Pol, 2014; Ganti et al., 2015). Impairment of the PDZ proteins leads to disruption of cell polarity and cell-cell adhesion (Spanos et al., 2008; Jing et al., 2007; Moody and Laimins, 2010), subsequently enhancing cell proliferation, hence, promoting tumorigenesis in the infected cells.

Another striking feature of the E6 oncoprotein is the ability to activate telomerases to prevent the infected cells from entering cellular senescence (Mantovani and Banks, 2001; Tomaić, 2016). Telomerase activity is detected in 90% of HPV-positive cancers, and its activation is considered an important event in HPV-induced cellular immortalisation and tumorigenesis (Katzenellenbogen and

Rachel, 2017). Evidence show that HPV16 E6 prevents the shortening of the telomerase by inducing telomerase activity through transcriptional activation of the telomerase catalytic subunit of the hTERT gene in epithelial cells (Klingelhutz et al., 1996). The activation of hTERT is affected by both the E6 and E7 proteins (Katzenellenbogen and Rachel, 2017). In fact, activation of hTERT is dependent on the binding of E6-E6AP complex, to the hTERT promoter site, c-Myc (Liu et al., 2009). In addition, the E6/E6AP complex binds to transcriptional repressors of the hTERT promoter to trigger its degradation, leading to dissociation of the mSin3A/histone deacetylase 2 (mSin3A/HDAC) complex from the hTERT promoter, allowing the hTERT transcription to proceed (Günes et al., 2000; Horikawa et al., 2002; Liu et al., 2008; Xu et al., 2008; Katzenellenbogen and Rachel, 2017).

2.1.4.2 The E7 Protein: Structure and Functions

The E7 oncoprotein is a small acidic polypeptide with 98 to 105 amino acid residues, which contains a C-terminal zinc-finger-like binding domain (Zheng, 2010; Jiang and Yue, 2014; Tomaić, 2016). The E7 protein has three conserved regions (CR), CR1, CR2 and CR3. All these conserved regions play an important role in cellular transformation by triggering the proliferative signals of epithelial cells.

The transforming activity of HPV16 E7 is exerted by targeting

retinoblastoma tumour suppressor protein (pRb) and its family members, p130 and p170, for ubiquitin-based proteosomal degradation. This results in the elimination of the growth-suppressive activity of pRb which could play a role in cellular immortalisation (Morandell et al., 2012; Jiang and Yue, 2014; Rashid et al., 2015; Tomaić, 2016). The pRb protein associates with E2F transcription factor to form pRb-E2F that acts as a transcriptional repressor in regulating the G1-to-S phase transition. In HPV16-infected cells, binding of E7 to pRb also leads to disruption of the pRb-E2F complex (Hwang et al., 2002; Klingelhutz and Roman, 2012) and results in the release of E2F from the pRb-E2F complex. The free E2F then promotes E2F-induced transcription by interacting with the cyclinA/cyclin-dependent kinase 2 (CDK2) complex, leading to impaired cell-cycle arrest and enhanced G1/S-phase transition to promote viral DNA replication (Morandell et al., 2012; Rashid et al., 2015; Tomaić, 2016).

The HPV16 E7 protein has also been reported to directly bind and inactivate cyclin-dependent kinase inhibitors (CKIs), including $p21^{CIP1}$ and $p27^{KIP1}$, which have been implicated in regulating cell cycle withdrawal in differentiating keratinocytes (Funk et al., 1997; Jones et al., 1997; Zerfass-Thome et al., 1997). Moreover, the HPV16 E7 protein upregulates angiogenic inducers, vascular endothelial growth factor (VEGF) and interleukin-8 (IL-8) but, to a lesser extent, compared to the E6 protein. (Chen et al., 2007; Walker et al., 2011). VEGF and IL-8 are upregulated when the infected cells are progressing towards tumorigenicity; upregulation of these angiogenic factors by HPV16 E7 is suggested to be pRb-

independent (Walker et al., 2011).

2.2 Human Papillomavirus-associated Cancers

Human papillomavirus is the causative agent of various human epithelial cancers. HPV infection accounts for more than 50% of infection-linked cancers in females and about 5% in males (zur Hausen, 2009). HPV is associated with various clinical conditions that range from benign lesion to invasive cancer in both men and women (Burd, 2003; Bansal et al., 2016). HPV-associated cancers include cervical, head-and-neck, anal, penile and vulvovaginal cancers (Burd, 2003). Majority of HPV infections resolve spontaneously within 1 to 2 years as a result of an effective cell-mediated immune response. Persistent high-risk HPV infection, which occurs in a small fraction of individuals is a prerequisite for cancer development (Cubie, 2013; Ryser et al., 2015). HPV-associated intraepithelial neoplasia are named based on the infection sites: such as cervical intraepithelial neoplasia (CIN), penile intraepithelial neoplasia (PIN), vulva intraepithelial neoplasia (VIN) (Cubie, 2013).

2.2.1 Cervical carcinoma (CxCa)

Squamous carcinoma of the cervix is the third most common cancer in women worldwide with more than 500,000 cancer cases reported every year (Silverberg and Loffe, 2003; Alfaro et al., 2016; Bansal et al., 2016). Persistent infection of high-risk HPV, in particular HPV16 is the major risk factor for cervical

cancer development (Hoste et al., 2013; Alfaro et al., 2016). Other risk factors contributing to cervical cancer development include an active sexual lifestyle, having multiple sexual partners, frequent use of oral contraceptive and weak immune system due to pre-existing infection (Bansal et al., 2016). The naming system used in classification and grading the cervical cancer based on histopathology and cytology is shown in Figure 2.3.

Cervical precancerous lesions first arise in a cancer-susceptible region of the cervix known as the transformation zone (TZ) (Autier et al., 1996; Schiffman et al., 2007; Herfs et al., 2012). It is the junction between the two distinct epithelium linings of the cervix, the endocervical columnar epithelium and the cervical squamous epithelium. The TZ is a dynamic region as the anatomic location of TZ varies with age, and is influenced by hormonal changes in response to puberty, pregnancy and menopause stages (Hwang et al., 2009; Nucci and Oliva, 2009). The immature proliferating squamous epithelium at the transformation zone serves as reservoir for HPV latent infections and is considered the site of metaplastic change, a precursor for cancer development (López et al., 2012; Herfs et al., 2017).

2.2.2 Head-and-Neck Squamous Cell Carcinoma (HNSCC)

Head-and-neck squamous cell carcinoma (HNSCC) includes carcinoma in the oral and nasal cavities, the larynx, hypopharynx and oropharynx. HNSCC is the

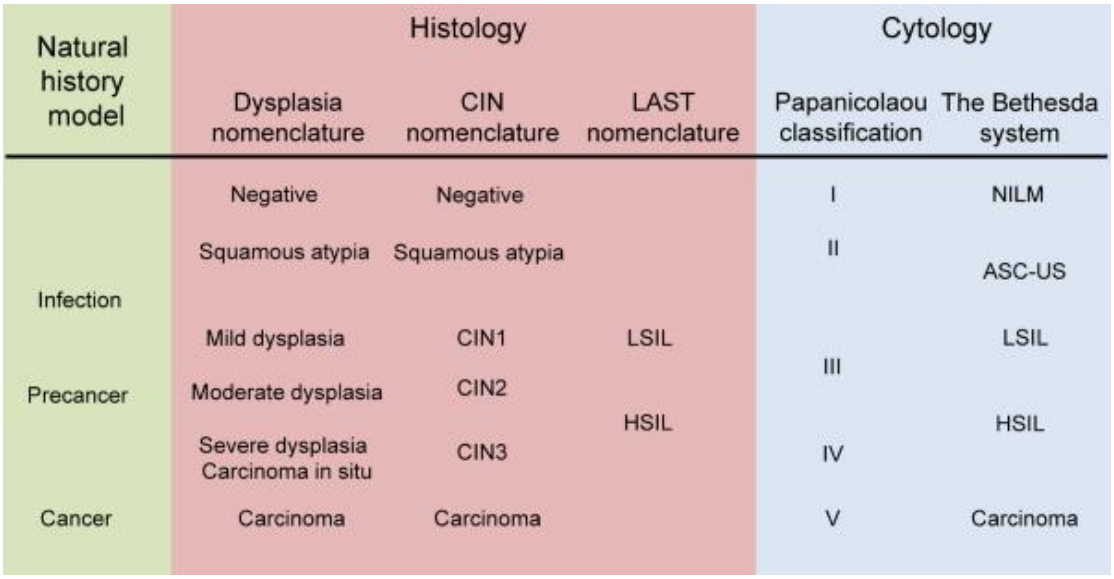

Figure 2.3 Terminology used in classification and grading of cervical cancer. The natural history of HPV-induced cancer formation involves three stages; (1) initial stage of HPV infection; (2) precancerous lesions formation; (3) cancer development. Nomenclature used for grading of cervical lesions include (1) dysplasia, (2) cervical intraepithelial neoplasia (CIN), and (3) LAST, lower anogenital squamous terminology standardisation. Two different classifications are used for cervical cytology, the Papanicolaou classification and the Bethesda system. LSIL, low-grade squamous intraepithelial lesion; HSIL, high-grade squamous intraepithelial lesion; NILM, negative for intraepithelial lesion / malignancy and ASC-US, atypical squamous cells of undetermined significance. (Figure adapted from Schiffman and Wentzensen, 2013)

sixth most common non-skin cancer globally (D'Souza and Dempsey, 2011; Spence et al., 2016). Majority of HNSCC are located in the oropharyngeal region which include the tonsils, soft palate or the back of the tongue (Spence et al., 2016), and such HNSCC is called oropharyngeal squamous cell carcinoma (OPSCC). Seventy to 80% of OPSCC cases are associated with HPV, particularly HPV16 (Spence et al., 2016). The major risk factors of OPSCC are tobacco exposure, alcohol consumption, and HPV infection. The association of HPV infection with OPSCC has significantly increased over the years (Pai and Westra, 2009; D'Souza and Dempsey, 2011). Other risk factors of HPV-positive OPSCC have been reported including multiple sexual partners, premarital sex, frequent oral-genital and oral-anal contact as well as other unsafe sexual activities (Pai and Westra, 2009; Lui and Grandis, 2012).

The stratified squamous epithelial lining of the oral cavity and the reticulated squamous epithelial lining of the tonsil are the preferred sites for HPV infection (Pai and Westra, 2009; Miniggio, 2016). HPV-positive OPSCC originates from the basement membrane of the tonsil reticulated squamous epithelium (Pai and Westra, 2009; Boscolo-Rizzo et al., 2013). The basement membrane is loosely-arranged naturally to facilitate the intimate contact between immune effector cells to the external environment. This is the preferred site for HPV infection which can occur in the absence of mechanical abrasion (Pai and Westra, 2009; Rautava and Syrjänen, 2012; Miniggio, 2016) which is in contrast to cervical cancer initiation, that requires micro-trauma to initiate the HPV infection.

2.2.3 Other HPV-related Diseases

HPV-associated vulvar, vaginal, anal and penile cancers are relatively uncommon compared to cervical cancer (Cubie, 2013). Vaginal cancer accounts for only 2% of the female genital-tract malignancies, and is frequently diagnosed in elderly or post-menopausal women (Hacker et al., 2015). Younger patients who develop vaginal cancer are likely to have HPV-positive cervical neoplasms (Hacker et al., 2015). The most common histological types of vaginal cancer is squamous cell carcinoma (SCC), which accounts for 80 to 90% of all documented cases (Shah et al., 2009; Hacker et al., 2015).

Vulvar cancer is frequently HPV16- or HPV18- positive, and often occurs in patients from 35 to 65 years of age (zur Hausen, 2009; Alkatout et al., 2015). Similar to vaginal cancer, vulvar squamous cell carcinoma is responsible for over 95% of malignant tumours of the vulva (Alkatout et al., 2015). Over 70% of anal cancer cases is associated with HPV16 infection, and it is more common in women than in men (Palefsky, 2010; Moscicki and Palefsky, 2011). However, homosexual men also show increased risk of anal cancer (zur Hausen, 2009; Palefsky, 2010). On the other hand, penile cancer is a rare malignancy and often occurs in men over 60 years of age (Moscicki and Palefsky, 2011). Human papillomavirus infection is associated with 42 to 48% of penile cancer cases and is predominantly linked to HPV types 16 and 18 (Shabbir et al., 2013). Multiple risk factors have been identified for penile cancer including poor hygiene, phimosis, active sexual activity

and smoking (Moscicki and Palefsky, 2011; Shabbir et al., 2013; Morrison, 2014)

2.3 Prevention, Current Treatments, and Challenges in HPV16-associated Cancers

The recognition of the high-risk HPV types, particularly HPV16 and 18 as the aetiological agents of cancers have led to the introduction of HPV vaccination as a preventive measure for the development of HPV-associated cancers (Basu et al., 2013; Yang et al., 2016). A number of prophylactic HPV vaccines have been developed and proven to have greater than 90% efficacy in preventing persistent HPV infections and cervical precancerous lesions (Basu et al., 2013). The bivalent and quadrivalent vaccines, Cervarix and Gardasil, respectively were approved in 2006, and target the L1 capsid protein of the virion of oncogenic HPV types 16 and 18. (Wang and Roden, 2013; Yang et al., 2016). Despite the high efficacy of the commercial HPV vaccines, several challenges remain and HPV-induced cervical cancer still remains a common cancer among women (Wang and Roden, 2013). The main limitation in the HPV vaccination programme is the unaffordability of the HPV vaccine for the low-income group. Furthermore, the vaccines are unlikely to benefit individuals with pre-existing HPV infections or who already have HPV16- and 18-induced cellular abnormalities (Monie et al., 2008; de Sanjose et al., 2013; White, 2014). Hence, early detection of cervical lesion by Pap smear screening remains an essential measure. However, false-positive results are relatively common in Pap smear tests which can lead to unnecessary treatment

(Hoste et al., 2013; Agorastos et al., 2015).

More recently, HPV testing has been introduced as part of the screening program. This allows the detection of HPV as well as genotyping of common high-risk HPV in those individuals who are positive for the virus infection. However, it is noted that a positive result is not conclusive evidence of positive HPV infection as the virus may be present in transient infections in women with an active sexual lifestyle (Coutlée et al., 2005; Hoste et al., 2013; Schlichte and Guidry, 2015).

The primary treatment strategy for individuals who have low-grade lesions of the epithelium (CIN 1 and 2) is surgery. In patients with high grade CIN and invasive cancers, surgery is followed by chemotherapy, radiotherapy or chemoradiotherapy (Petignat and Roy, 2007). The standard chemotherapy regimens used in cervical cancer treatment are the platinum drugs, cisplatin or carboplatin used in combination with other drugs, such as topotecan, fluorouracil or paclitaxel (Soumya and Arun, 2011; Tsuda et al., 2016; Long III et al., 2017). Such modalities of treatment are associated with numerous undesirable effects on the patients which underline the continued effort to look for alternative anti-cancer drugs or compounds and regimes.

2.4 In-Vitro Models for Studies of HPV-associated Cancers

It has been difficult to study and understand the HPV lifecycle due to the

requirement of a stratified epithelial differentiation system for the virus to complete its viral life cycle and virion production. The episomal form of the HPV DNA was first discovered in human epidermal keratinocyte culture infected with HPV-1 derived from plantar warts, revealing that viral DNA may maintain and replicate as stable episomes in monolayer cell cultures (Laporta and Taichman, 1982).

Commonly used epithelial keratinocyte culture systems involve the use of primary keratinocytes (Hawley-Nelson et al., 1989; Magaldi et al., 2012; Diao et al., 2015), immortalised keratinocytes, such as NIKS cells (Hawley-Nelson et al., 1989; Allen-Hoffmann et al., 2000), or cancer cell lines harbouring oncogenic HPV, such as CaSki, SiHa and HeLa cell lines (Choo et al., 1994; Xu et al., 2015). Although monolayer keratinocyte cell culture systems are useful models in studying the early events of HPV infection at the basal layer of the epithelium, they do not support the vegetative stage of HPV viral life cycle (Taichman et al., 1984). Further, due to the species- and tissue-restriction specificity of HPV viruses, only selected animal models such as mouse, rabbit, horse, primate, sheep, and ox are useful to study the HPV infections (Stanley et al., 1997).

The use of three-dimensional (3D) culture systems or organotypic raft culture have provided the basis to study the complete HPV life cycle and provide for efficient production of virus progeny in contrast to low HPV virion production in clinical lesions (Denise A Galloway, 2009; Ozbun and Patterson, 2014). These 3D raft cultures support HPV virus-host interactions in the differentiating stratified

epithelium layer which mimics the *in vivo* cellular architecture (Jackson et al., 2014; Anacker and Moody, 2012). This *ex vivo* system has enabled characterisation of gene expression at different stages of HPV infection (Lee et al., 2016; Frattini et al., 1997).

2.4.1 The Use of Normal Immortalized Keratinocytes, NIKS

The use of primary human keratinocyte to study HPV viral life cycle has been a great challenge due to the limited life span of the primary cells with less than 10 passages *in vitro* (Choi and Lee, 2015). When the primary cells enter senescence, they display an enlarged and flattened cell morphology indicating loss of replicative potential (Choi and Lee, 2015).

The establishment of a normal near-diploid immortalised keratinocyte (NIKS) culture by Allen-Hoffmann et al., 2000 has provided researchers with an alternative platform. NIKS cells, BC-1-Ep strain, originated from normal human neonatal foreskin, are immortalised by the hTERT gene *in vitro* (Allen-Hoffmann et al., 2000; Tomaić, 2016). Despite the presence of an extra iso-chromosome 8, NIKS cells remain non-tumourigenic in athymic nude mice and maintain anchorage-dependent growth characteristics, a feature which is usually lost in the cancer cells (Shin et al., 1975; Allen-Hoffmann et al., 2000; Mori et al., 2009; Choi and Lee, 2015). Furthermore, NIKS cells have been shown to not only maintain an unlimited life span up to passage 59 *in vitro*, but also to have cell-to-cell contact

inhibition similar to healthy primary keratinocyte cells. They also possess wild-type p53 along with its downstream effector proteins, p16 and pRb. NIKS cells require the presence of growth-arrested 3T3 feeder layer to provide cytokines or other growth factors to support its proliferation. The cell morphology is highly similar to primary human keratinocytes (Allen-Hoffmann et al., 2000; Llames et al., 2015).

This immortalised keratinocyte cell line is used to construct models which recapitulate two key steps in oncogenesis of HPV-associated cancers through introduction of the HPV16 full genome and the HPV16 oncogenes, E6, E7, or both E6 and E7. Cells that harbour the HPV genome in episomal form are used to represent the precancerous stage of the HPV-associated carcinogenesis process. Cells that harbour the E6 and E7 oncogenes singly or together represent the cancerous stage in which the virus genome is integrated into the host cells. These models were studied with respect to their chemosensitivity for standard cytotoxic drugs and selected compounds relative to unmodified parental cells.

2.5 Chemosensitivity of HPV-associated Tumours and Cell Lines

Over 90% of HPV-positive head-and-neck squamous cell carcinoma (HNSCC) and more than 52% of cervical cancer cases are attributed to high-risk HPV16. Interestingly, clinical data have shown that patients with HPV16-positive HNSCC have better prognosis than HPV-negative HNSCC patients (D'Souza et al.,

2007; Fakhry et al., 2008; Ang et al., 2010; Gillison et al., 2000). Patients with HPV-negative HNSCC were reported to associate with a history of heavy tobacco smoking, alcohol drinking, poor oral hygiene in the older age group (above 60 years old) but not any measures of sexual history (Gillison, 2008; McIlwain et al., 2014). In contrast to HPV-positive patients, patients were usually younger age (below 60 years old), correlated with less smoking and alcohol consumption (Grisar et al., 2018; Gillison, 2008).

Similar data were obtained in HPV-positive cervical cancer cases treated with cisplatin-based chemotherapy (Sultana et al., 2003) compared to HPV-negative cervical cancer patients. It is uncommon to have cancer with HPV negative phenotype as HPV infection is a necessary cause of cervical cancer. Previous studies reported that HPV-negative cervical cancer patients could relate with false-negative screening results due to low viral load or progressively loss of HPV DNA within the patient's tumour (Rodríguez-Carunchio et al., 2015). It has been shown that rare cervical cancer subtypes, adenocarcinomas were frequently associated with HPV-negativity but the reason behind is not clear (Rodríguez-Carunchio et al., 2015).

Besides, HPV-positive tumours in immunocompetent mice treated with cisplatin have also been shown to have increased chemosensitivity than in mice with HPV-negative tumours (Spanos et al., 2009). Other studies have also demonstrated that HPV-positive HNSCC cell lines and cervical cancer cells were

significantly more sensitive to cisplatin treatment than HPV-negative cell lines *in vitro* (Ziemann et al., 2015; Koivusalo and Hietanen, 2004). Many hypotheses have been proposed to explain these findings. One hypothesis is that the persistence of wild-type p53 in HPV-associated cancers allow induction of the p53-associated apoptosis pathway in response to DNA damage caused by cytotoxic agents (Koivusalo and Hietanen, 2004). However, the exact molecular mechanisms underlying HPV-associated chemosensitivity are not understood and remain to be elucidated.

2.6 Mechanisms of Cisplatin and Topotecan Action

2.6.1 Cisplatin and Mechanism of Action

The platinum-based chemotherapeutic agent, cisplatin, also known as cis-diamminediachloroplatinum(II) is the major chemotherapeutic agent for the treatment of HPV-associated cancers. Cisplatin displays strong anticancer activity against cervical and head-and-neck cancers (Pendleton and Grandis, 2013; Hutchinson, 2016). Cisplatin mediates its cytotoxic effects by interacting with purine bases of the DNA, thereby forming DNA adducts, leading to the activation of intrinsic and extrinsic apoptotic pathways (Figure 2.4) (Siddik, 2003; Dasari and Bernard Tchounwou, 2014). In the mitochondrial or intrinsic pathway, proapoptotic proteins, BAX and BAK are activated in response to DNA damage (Florea and Büsselberg, 2011; Dasari and Bernard Tchounwou, 2014) induced by cisplatin

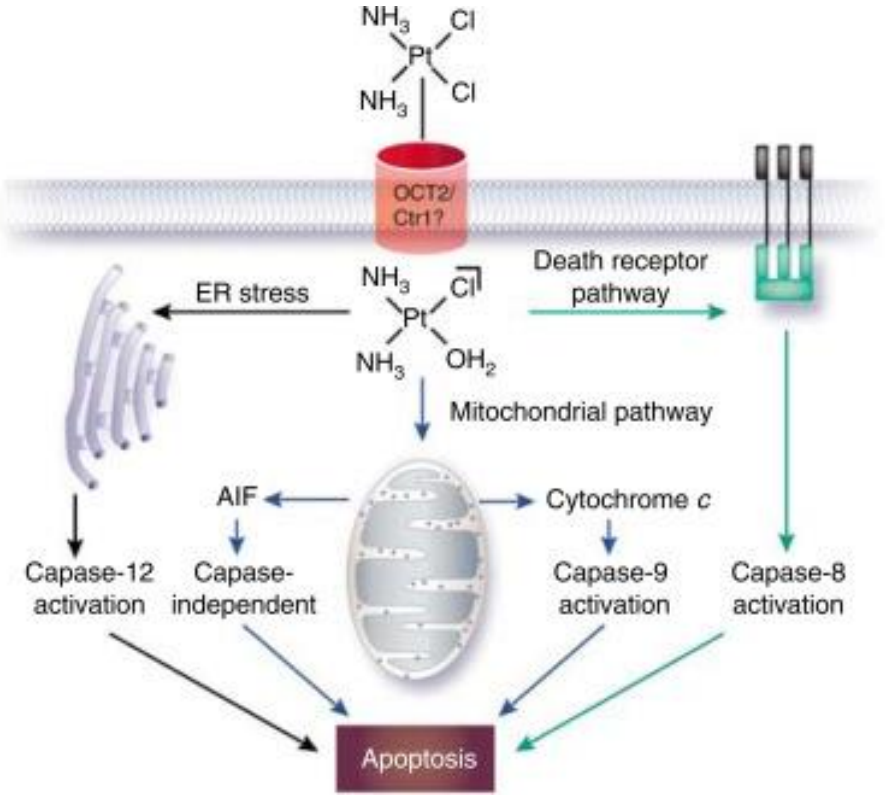

Figure 2.4 Mitochondrial (intrinsic) and death-receptor (extrinsic) apoptotic pathways activated by cisplatin. Cisplatin activates the intrinsic pathway (blue arrows) through the pro-apoptotic proteins, BAX and BAK (not shown). Subsequently, BAX and BAK permeabilise the mitochondrial membrane to release the antiapoptotic-inducing factor AIF and cytochrome C into the cytosol to execute the caspase-independent and caspase-9-dependent apoptosis pathways. Death receptors that reside on the plasma membrane activate the extrinsic pathway (green arrows) upon cisplatin treatment leading to the activation of caspase-8 to facilitate in apoptosis. Furthermore, cisplatin may also activate the endoplasmic reticulum (ER) stress pathway (grey arrows) to stimulate the activation of ER-specific caspase-12 in the execution of cellular apoptosis. (Figure adapted from Pabla and Dong, 2008)

action. The BAX and BAK proteins trigger permeabilisation of the mitochondrial membrane to release anti-apoptotic-inducing factor, AIF, hence resulting in the activation of the caspase cascade leading to apoptosis (Pabla and Dong, 2008; Florea and Büsselberg, 2011). In addition, cisplatin activates the extrinsic or death receptor-mediated pathway where ligands bind to the death receptors, such as tumour necrosis factor-α (TNF-α) receptor, or the Fas ligand (FasL) residing at the plasma membrane, to trigger the recruitment and activation of caspase-8, subsequently activating the downstream caspases to mediate cellular apoptosis (Pabla and Dong, 2008).

Cisplatin has been shown to downregulate E6 and E7 expression in HPV16-positive cells in cervical cancer and HNSCC models, allowing the reactivation of the p53 and pRb (Jung et al., 2012; Ziemann et al., 2015). Furthermore, cisplatin has also been proven to upregulate p53 allowing p53 to escape from E6-mediated p53 degradation, thereby enhancing p53-mediated apoptosis (Węsierska-Gądek et al., 2002; Liu et al., 2005; Fulda and Debatin, 2006).

2.6.2 Topotecan and Mechanism of Action

Topotecan is a semi-synthetic alkaloid compound that belongs to the campthothecin family. Topotecan has been approved for used as a single agent in treatment of patients with metastatic relapsed ovarian cancer, advanced and recurrent stages of cervical cancer (Coleman, 2002; Garst, 2007; Robati et al., 2008;

Lorusso et al., 2010). Topotecan is also used in conjunction with cisplatin for treatment of cervical cancer and these two drugs have non-overlapping toxic effects. This combination therapy improves treatment response and reduces drug resistance (Robati et al., 2008). Topotecan exerts its anticancer activity on dividing cells at the S-phase of the cell cycle by targeting and inhibiting the DNA topoisomerase I. DNA topoisomerase relaxes supercoiled DNA by introducing transient DNA breaks which allows replication fork progression and subsequently resealing these breaks. Topotecan specifically targets the cleavage complex, the enzyme's catalytic intermediate, thereby interfering with its function. These functions are important during transcription and DNA replication (Figure 2.5). As a consequence, topotecan treatment results in irreversible double-stranded DNA break and abrogates DNA replication, leading to apoptosis (Rasheed and Rubin, 2003; Garst, 2007; Robati et al., 2008). Topotecan-mediated S-phase arrest in cell cycle involves activation of DNA-damage response pathway, in which the mediator of the DNA-damage response (DDR), checkpoint kinase-1 (Chk1), is rapidly phosphorylated by ataxia telangiectasia and rad3-related, ATR. Subsequently, Chk1 phosphorylates the dual-specificity phosphatase, CDC25A, to abrogate the transition from G1 to S phase of the cell cycle (Cliby et al., 2002; Xiao et al., 2003). Topotecan has been shown to reduce E6 level and triggers the upregulation of p53 activity in SiHa, a HPV16-positive cell line (Koivusalo and Hietanen, 2004). The increase of p53 expression would be expected to enhance p53-induced apoptosis of DNA-damaged cells. However, the apoptosis triggered by topotecan was reported to be p53-independent

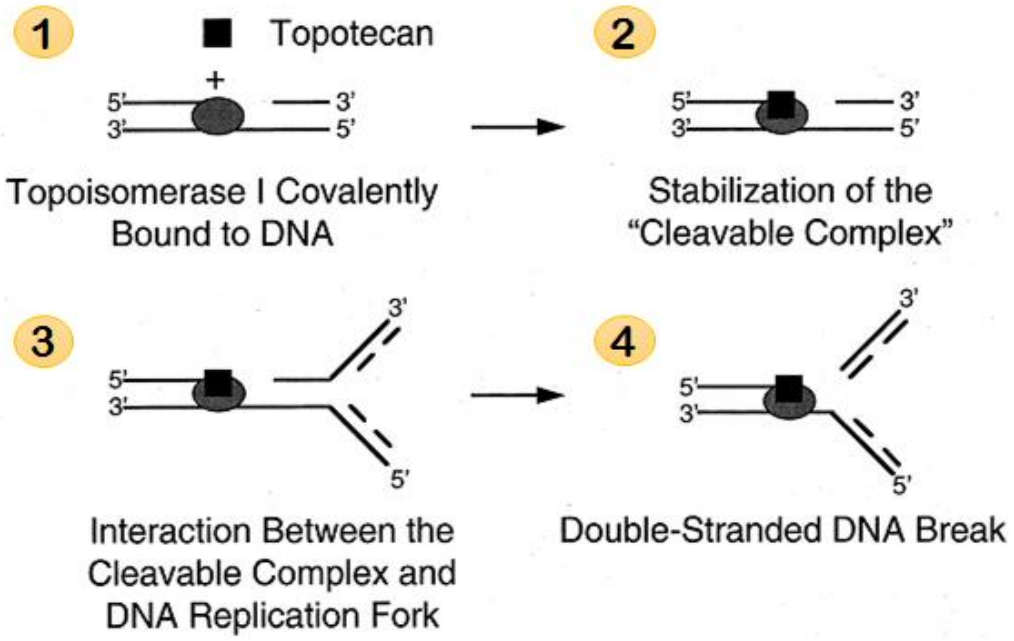

.

Figure 2.5 Mechanism of action of topotecan. Step 1. During DNA replication, DNA topoisomerase I binds to the DNA forming the reversible topoisomerase I (TOP)-DNA cleavable complex, the enzyme catalytic intermediate. This allows cleavage of supercoiled double-stranded DNA and DNA transcription to occur. Step 2. Topotecan stabilises the TOP-DNA cleavable complex by non-covalently binding to it. As a result, the cleavage reaction is abrogated and the re-ligation reaction is inhibited. Step 3. The TOP-DNA cleavable complex collides with the replication fork, resulting in irreversible arrest of the replication fork and accumulation of DNA damage. Step 4. Consequently, the reversible TOP-DNA cleavable complex is converted into an irreversible complex due to the formation of DNA double-stranded breakages (DSBs). (Figure adapted and modified from Takimono and Arbuck, et al., 1997)

2.7 The Use of Natural Flavonoid Compounds in Cancer Treatment

2.7.1 Eupatorin and Sinensetin

Both eupatorin and sinensetin are flavonoid compounds isolated from the leaves of the *orthosiphon stamineus* plant, which can be found in Southeast Asia countries, particularly in Malaysia and Indonesia (Awale et al., 2003; Akowuah et al., 2004; Loon et al., 2005). The *orthosiphon stamineus* plant is a traditional medicinal herb, which is used to treat jaundice, gallstone, diabetes, rheumatoid diseases and is traditionally well-known for its diuretic effects (Ameer et al., 2012).

Previous studies have demonstrated that eupatorin exerts anti-proliferative effects on different cancer cell lines, including breast adenocarcinoma MCF-7, various leukemia cell lines HL-60, MOLT-4 and K562 and multiple myeloma cell line RPMI8226 (Dolečková et al., 2012). Furthermore, eupatorin has also been shown to induce apoptosis in HeLa, an HPV18-positive cervical cancer cell line by stabilising the p53 tumour suppressor protein to promote the G2/M phase cell-cycle arrest (Lee et al., 2016). Besides, caspase-3 and -8 levels are found to be elevated upon eupatorin treatment, suggesting that upregulation of caspases-3 and -8 may be involved in executing cellular apoptosis (Dolečková et al., 2012; Lee et al., 2014).

On the other hand, sinensetin treatment has been shown to inhibit the AGS gastric cancer cell growth, induce apoptosis in a dose-dependent manner, and

trigger cell-cycle arrest at G2/M (Dong et al., 2000). Exposure of sinensetin on the AGS gastric cancer cells also demonstrated an increased expression of p53 and p21 proteins, suggesting that these two proteins are involved in sinensetin-induced apoptosis (Dong et al., 2000). However, studies on the cytotoxicity or anti-cancer effects of sinensetin are relatively limited.

In view of the reported anti-proliferative actions of these two flavonoid compounds, there were selected candidates for use in this study.

2.8 The Use of Synthetic Compounds in Cancer Treatment

2.8.1 Tribenzyltin Carboxylates (TC) 1 and 4

Tribenyltin carboxylates (TC) 1 and 4 are organotin (IV) compounds with carboxylate ligands. Organotin compounds are non-platinum-based compounds that display cytotoxicity effects *in vitro* against various cancer cell lines, including HeLa, leukemia cell line HL-60, lymph carcinoma B and T cell lines, nasopharyngeal carcinoma KB, and hepatocellular carcinoma Bel-7402 with higher potency than cisplatin (Hadjikakou and Hadjiliadis, 2009; Fani et al., 2015). In addition, despite its therapeutic success against various cancers, cisplatin causes significant side effects, such as accumulation of heavy metal ions leading to cellular toxicity, and intrinsic drug resistance, the last being a major reason for treatment failure (Zhang and Lippard, 2003; Alama et al., 2009; Arjmand et al., 2014). Indeed,

synthetic organotin compounds have been reported as promising alternative agents with improved specificity in killing cancer cells, reduced toxicity and minimal effects on normal cells (Arjmand et al., 2014).

Both the TC1 and TC4 compounds are novel halogenated tribenzyltin complexes, which have been tested in human breast cancer cell lines, MCF-7 and MDA-MB231 (Anasamy et al., 2017). Among of all the tested tribenzyltin complexes and triphenyltin analogues, the tribenzyltin complexes 9 (TC9) activity due to the presence of the isonicotinate ligand which enhances its cytotoxicity effects. This is followed by TC1 which was reported to display significant cytotoxicity effects in breast cancer cell lines. TC1 was shown to initiate apoptosis through upregulation of caspase-8 and -9 to drive both the intrinsic and extrinsic apoptosis pathways.

CHAPTER 3

MATERIALS AND METHODS

3.1 Cell Lines

Normal immortalised keratinocytes (NIKS), mouse embryonic fibroblast, (3T3-J2) and retrovirus packaging cell line (Phoenix) were all provided by Dr. Kenneth Raj (Human and Protection Agency, United Kingdom). HPV16-positive cervical cancer cell line, CaSki (CRL-1550, Manassas Virginia, USA) was purchased from American Type Culture Collection, ATCC. The usage of each cell line is stated in Table 3.1.

3.1.1 Normal Immortalised Keratinocytes, NIKS

NIKS cells were cultured on a layer of γ-irradiated 3T3-J2 cells as the feeder layer. Frozen NIKS cells were removed from the liquid nitrogen tank and immediately thawed in a 37 ^{o}C water bath for less than 1 min. The cryovial was wiped with 70% ethanol before transferring into an Airstream Class II Biological Safety Cabinet culture hood (ESCO, Singapore). The thawed cells were transferred into 9 mL of pre-warmed complete medium containing 3 parts DMEM and 1-part F12 supplemented with 5% (v/v) fetal bovine serum (FBS) (Gibco,

Table 3.1 Cell lines used in the study

Cell type	Name	Use
Mouse embryonic fibroblast	3T3-J2	Feeder support for NIKS cells
Normal human neonatal foreskin keratinocytes	NIKS (Normal immortalized keratinocytes)	For preparation of cell models expressing the HPV16 genome or HPV16 oncogenes (E6, E7 or E6E7)
Retrovirus packaging cell line	Phoenix	Recombinant retrovirus production
HPV16-positive cervical cancer cell line	CasKi	Positive control - E6 and E7 expression

Thermo Fisher Scientific, Massachusetts, USA), 24 µg/mL adenine (Sigma-Aldrich, Missouri, USA), 0.4 µg/mL hydrocortisone (Sigma-Aldrich), 5 µg/mL insulin (Gibco), 8.4 ng/mL cholera toxin (Sigma-Aldrich) and 1% of penicillin-streptomycin (Gibco) in a 15-mL tube (SPL, Gyeonggi-do, Korea). The tube was centrifuged at 1,500 rpm for 5 min in a benchtop centrifuge (Allegra® X-30 Series, Beckman Coulter, California, USA). The supernatant was discarded and the cell pellet was resuspended in 1 mL fresh complete medium. The cell suspension was pipetted into a 100-mm cell culture treated plate (SPL) containing 10 mL complete medium. Epidermal growth factor (EGF) (Peprotech, New Jersey, USA) was added to the fresh medium at a concentration of 10 ng/mL, and the cells were maintained in a 37 ^{o}C cell culture incubator (ESCO) with 5% of CO_2.

NIKS cells were split twice a week at a ratio of 1:3. During subculturing, spent medium was discarded and cells were washed once with 5 mL 1X Phosphate Buffered Saline (PBS) (Takara, Tokyo, Japan). A differential detachment method utilising 2 different concentrations of trypsin-EDTA solution was used to detach both the NIKS and the feeder cells. 3T3-J2 feeder cells were first detached by incubating with 3 mL pre-warmed 0.05% trypsin-EDTA (Gibco) for 1 min. The plates were then washed once with 5 mL 1X PBS, followed by detachment of NIKS by incubating with 3 mL pre-warmed 0.25% trypsin-EDTA (Gibco) for 5-8 min at 37 ^{o}C. The cells were examined under an Eclipse TS100 inverted microscope (Nikon, Tokyo, a Japan) to ensure 90% detachment and the trypsin action was inactivated by adding 6 mL complete medium. The supernatant containing the

NIKS cells were transferred to a 15-mL conical tube (SPL) and centrifuged at 1,500 rpm for 5 min to obtain cell pellet. Supernatant was discarded and the cell pellet was resuspended in 5 mL pre-warmed complete medium. The cells were stained with 0.4% trypan blue (Gibco) and the total cell number was determined by using a hemacytometer. Briefly, ten microlitre of the cell suspension was mixed with an equal amount of trypan blue and the cells were counted using an Eclipse TS100 inverted microscope at 200X magnifications. The cell concentration was determined using the formula below:

Cell concentration (cell/mL) =
(Average of cells per big square on hemacytometer) x (dilution factor) x (10^4)

Prior to seeding of the desired concentration of NIKS cells, 1 x 10^6 of feeder cells was plated on a new plate, followed by NIKS cells. Approximately 8 mL NIKS complete medium and EGF were added fresh into the plate. The NIKS culture medium supplemented with EGF was changed every two days, and the cultures were routinely examined under the microscope to check for possible contamination.

For cell cryopreservation, NIKS cells were harvested at 70-80% confluency and pelleted at 1,500 rpm for 5 min. The cell pellet was resuspended in a freezing medium containing 70% (v/v) NIKS complete medium, 20% FBS and 10% DMSO. The cell suspension was transferred to a NUNC® cryovial (Thermo Fisher Scientific) and stored at -80 ^oC in an ESCO Lexicon Ultra-low temperature freezer

(ESCO) overnight. The cryogenic vials were transferred to liquid nitrogen on the subsequent day for long term storage.

3.1.2 Mouse Embryonic Fibroblast Cell Line, 3T3-J2

3T3-J2 cells were irradiated for use as a feeder layer to support the growth of NIKS cells. A cryovial containing the 3T3-J2 cells was thawed and transferred into a 15-ml conical tube (SPL) containing 9 mL pre-warmed DMEM high-glucose medium supplemented with 10% FBS (Gibco) and 1% penicillin/streptomycin (Gibco). The thawed cells were centrifuged at 1,500 rpm for 5 min and the supernatant was discarded. Cell pellet was re-suspended in 1 mL pre-warmed complete medium and transferred into a 100-mm cell culture dish containing 9 mL complete medium, and maintained in a 37 ^{o}C cell culture incubator with 5% of CO_2.

3T3-J2 cells were subcultured three times a week at a ratio of 1:4 upon reaching 80% confluency. The 3T3-J2 subculturing procedure was similar to that of NIKS cells with cell detachment facilitated by using 3 mL pre-warmed 0.05% trypsin-EDTA solution (Gibco). 3T3-J2 cells were maintained at 1 x 10^6 seeding density.

For cryopreservation of the 3T3-J2 cells, cell pellets were suspended in a freezing medium containing 70% (v/v) 3T3-J2 complete medium with 20% FBS and 10% DMSO. The cell suspension was transferred into a cryovial which was

stored overnight at -80 ^{o}C and transferred to liquid nitrogen for long term storage the next day.

3.1.2.1 Irradiation of 3T3-J2 Cells to Serve as Feeder Layers

3T3-J2 cells at 80-90% confluency were harvested and irradiated at 80 Grays using a Caesium source from a gamma (γ) irradiator (Gammacell® 3000 Elan, Best Theratronics, Canada) located in Universiti Malaya Medical Centre (UMMC, Malaysia). Irradiated feeder cells were either used fresh by directly plating the 3T3-J2 feeder cells or cryopreserved for long-term storage prior to NIKS splitting. Irradiated feeder cells were pelleted at 1,500 rpm centrifugation for 5 min, and the cell pellet was resuspended in 35 mL complete medium. Cell count was performed using a hemacytometer. Excess irradiated feeder cells were cryopreserved at 4 x 10^6 cell density per vial using a freezing medium 90% (v/v) FBS with 10% DMSO and stored in liquid nitrogen until use.

3.1.3 HPV16-positive Cell Line, CaSki

CaSki cells were thawed and maintained in a complete medium containing 90% (v/v) RPMI 1640 supplemented with 10% FBS in a 37 ^{o}C, 5% CO_2 cell culture incubator. The cells were subcultured twice a week at a ratio of 1:5. To subculture, existing medium in a 100-mm plate was first removed and the cells were washed once with 3 mL 1X PBS. The wash solution was discarded and 3 mL 0.25% of

trypsin-EDTA was added. The plate was incubated for 5-8 min in a 37 ºC, 5% CO_2 incubator to aid cell detachment. The cells were examined under an Eclipse TS100 inverted microscope to ensure 90% cell detachment. Subsequently, 6 mL pre-warmed complete medium with serum was added to the detached cells and the cell suspension was collected in a 15-mL conical tube. The tube was centrifuged at 1,500 rpm for 5 min and the cell pellet was resuspended in 5 mL pre-warmed complete medium. The cells were evenly split into four 100-mm plate and 9 mL complete medium were added to each plate.

For cryopreservation of the CaSki cells, the cells were harvested with 0.25% trypsin-EDTA and suspended in a freezing medium containing 70% (v/v) CaSki complete medium and 20% FBS. DMSO (10%, v/v) was added into the cryovial and the suspension was pipetted up and down to achieve thorough mixing. The cryovial was transferred to a -80 ºC freezer (ESCO) overnight before transferring to liquid nitrogen the next day for long term storage.

3.1.4 Retrovirus Packaging Cell Line, Phoenix

Phoenix cells were thawed and cultured in a complete medium containing 90% (v/v) DMEM, 10% FBS, 1% 100X L-glutamine (Gibco) and 1% penicillin-streptomycin. Phoenix cells were subcultured at 80-90% confluency, generally twice a week at a ratio of 1:2. Medium changes were made every second day to

remove non-adherent cells. The cells were maintained in a 37 ^{o}C, 5% CO_2 incubator and examined daily to detect any contamination.

To cryopreserve the Phoenix cells, a freezing medium containing 70% (v/v) Phoenix-cell complete medium was added to the cell pellet, and the cells were resuspended evenly before being transferred to cryogenic vial. DMSO (10%, v/v) was added into the cryovial and the cells suspension was pipetted up and down to mix thoroughly. The vial was stored at -80 ^{o}C overnight before being transferred to liquid nitrogen for long term storage.

3.2 Plasmid Constructs and Primers

3.2.1 Plasmid DNA Constructs

Plasmids were provided by Dr. Kennenth Raj (HPA, UK) in a lyophilized form. The plasmids and their usage in generating the HPV16-precancerous and cancerous models are shown in Table 3.2. The plasmid map and other features are detailed in Appendix A-G.

3.2.2 Primers Used in the Study

Primer sequences used in the study are listed in Table 3.3. Primer synthesis service was provided by First Base Laboratories, Malaysia. Primer was delivered

Table 3.2 Plasmids used to generate experimental models

Name of plasmid	Inserted gene	Antibiotic marker	Usage
pcDNA6	None	Blasticidin	Empty vector (EV) control for the precancerous model
pSPW12	Full HPV16 genome (8 kb)	Blasticidin	For generation of HPV16 precancerous model using NIKS cells
pBABE-neo	None	Geneticin	Empty vector (EV) control for the cancerous models
pLXSN-HPV16 E6	HPV16-E6	Geneticin	For introduction of HPV16-E6, -E7 or E6E7, respectively into NIKS cells to generate the HPV16 cancerous models
pLXSN-HPV16 E7	HPV16-E7	Geneticin	
pLXSN-HPV16 E6E7	HPV16-E6E7	Geneticin	
pMX-GFP	Green fluorescence protein (GFP)	None	As the reporter gene to monitor transfection or transduction

Table 3.3 Primers used in mRNA RT-PCR

Gene	Primer Sequence (5' – 3')	Amplicon size (bp)
HPV16	**F:** TTATCA(T/A)ATGCCCA(T/C)TGTACCAT	188
	R: ATGTTAAT(A/T)(G/C)AGCC(A/T)CCAAAATT	
Blasticidin	**F**: GAT CGG AAA TGA GAA CAG GGG CA	154
	R: CAC ATA ACC AGA GGG CAG CA	
GFP	**F**: GAC GTA AAC GGC CAC AAG TT	188
	R: AAG TCG TGC TGC TTC ATG TG	
HPV16-E6	**F**: CGA CCC AGA AAG TTA CCA	117
	R: AGC AAA GTC ATA TAC CTC ACG	
HPV16-E7	**F**: CCG GAC AGA GCC CAT TAC AA	92
	R: CGA ATG TCT ACG TGT GTG CTT TG	
GADPH	**F:** ACA TCA TCC CTG CCT CTA	274
	R: TCA AAG GTG GAG GAG TGG	

in a lyophilized form and double-distilled water (ddH_2O) was added to generate a 100 µM stock solution. Primer was further diluted into working concentrations at 10 µM.

3.3 Preparation of Bacteria Culture Media and Antibiotic

3.3.1 Lysogeny (LB) Agar Plate

Lysogeny (LB) agar plate was used to culture *Escherichia coli* (*E. coli*), DH5-α strain. Formulation of the commercially available LB agar powder comprise 15 g/L agar, 10 g/L tryptone, 10 g/L sodium chloride (NaCl) and 5 g/L yeast extract (Sigma-Aldrich). To prepare 500 mL LB agar, 40 g LB powder was weighed and added into 500 mL double-distilled water (ddH_2O) in a 1-litre borosilicate bottle (Schott, Mainz, Germany). The bacterial medium was autoclaved at 121 ^oC for 15 min for sterilization purpose. The medium was cooled down to 55-60 ^oC and ampicillin (Sigma-Aldrich) was added at a concentration of 100 µg/mL. LB-ampicillin agar plates were prepared in an Airstream Laminar flow hood (ESCO). LB agar medium was swirled evenly and poured into sterile 100-mm petri dish at approximately 20 mL per plate.

The plates were allowed to solidify inside the laminar flow hood. The LB-ampicillin agar plates were stored at 4 ^oC in an inverted position to avoid water droplets on the agar surface.

3.3.2 Lysogeny (LB) Media

Lysogeny broth (LB) medium was used to propogate *E. coli*. LB medium was prepared by dissolving 7.5 g LB powder (Sigma-Aldrich) in 500 mL double-distilled water (ddH_2O) in a 1-litre borosilicate bottle (Schott). LB broth was autoclaved at 121 ^oC for 15 min and cooled down to 55-60 ^oC before use. Ampicillin (100 µg/ml) was added to LB broth and kept at room temperature prior to use.

3.3.3 Ampicillin Stock Solution

Plasmid vector used in this study contain the ampicillin resistance selective marker for selection on LB-ampicillin agar plate. Ampicillin stock preparations were performed in an Airstream Laminar flow hood (ESCO). Fifty microgram ampicillin (Sigma-Aldrich) was dissolved in 50 mL double-distilled water (ddH_2O) giving a final concentration of 1 mg/mL. The antibiotic solution was filtered using a 0.22-µm cellulose acetate syringe filter (Sartorius AG, Germany) and 1 mL aliquots were added to storage vials. The ampicillin aliquots were stored at -20 ^oC until use.

3.4 Preparation of Plasmids DNA

3.4.1 Transformation of *E. coli* with Plasmid DNA

One-Shot TOP10 chemically-competent *E. coli* (Invitrogen) were transformed with plasmid DNA according to the manufacturer's protocol. Transformed *E. coli* was plated on three different LB agar plates containing 50, 100 and 150 µg/ mL ampicillin (MP Biomedicals, California, USA). The three plates were inverted and incubated overnight for 16 h at 37 ^{o}C. Plates with single colonies were selected and analysed for the presence of the particular gene by colony polymerase chain reaction (PCR).

3.4.2 Identification of Positive Clones by Colony PCR

A total of five single colonies of transformed *E. coli* were picked from the agar plate using 200 µL pipette tips and dipped into a 200-µL tube containing the PCR master mixture. PCR reaction components were prepared according to Table 3.4. The PCR reagents included 10X PCR buffer with 20 mM of $MgCl_2$, 10 mM dNTPs mix, 5U/µL Taq polymerase and 25 mM $MgCl_2$ supplied in the kit (Thermo Scientific). PCR was performed using Applied Biosystems (ABI) Veriti Thermal Cycler (Thermo Fisher Scientific) using the PCR cycling profile shown in Table 3.5. The amplification conditions were as follows - initial denaturation at 95 ^{o}C for 5 min, followed by 30 cycles of denaturation at 95 ^{o}C for 30 sec,

Table 3.4 PCR components for colony PCR

Reagents	Stock conc^{n}	Working conc^{n}	Per reaction (µl)
PCR buffer with 20mM of $MgCl_2$	10 X	1 X	1.0
dNTPs mix	10 mM	200 µM	0.4
Taq polymerase	5 U/µL	0.5 U	0.1
$MgCl_2$	25 mM	2.0 µM	1.6
Forward primer	10 µM	0.5 µM	1.0
Reverse primer	10 µM	0.5 µM	1.0
ddH_2O	-	-	13.9
DNA Template	-	-	Single colony
Total			20

Table 3.5 PCR cycling profile for colony PCR

Step			Time	Temperature (ºC)
Initial denaturation			5 min	95
Denaturation	Repeated for 30 cycles		30 sec	95
Annealing			30 sec	60 - 66
Extension			1 min	72
Final extension			30 sec	72
Cooling			∞	25

annealing at (60 – 66 ^{o}C) for 30 sec, extension at 72 ^{o}C for 1 min and final extension at 72 ^{o}C for 30 sec.

3.4.3 Agarose Gel Electrophoresis

Colony PCR products were subjected to agarose gel electrophoresis to determine the presence of plasmid DNA. Agarose gel was prepared by dissolving 0.15 g agarose powder (Seakem® LE Agarose, Lonza, Switzerland) with 30 mL 1X Tris-acetate-EDTA (TAE) buffer (First Base Laboratories). The mixture was heated with gentle stirring until the agarose powder was fully dissolved. One microlitre 3X GelRed nucleic acid stain (Biotium, California, USA) was then added and the mixture immediately poured onto the gel casting unit. The gel was allowed to solidify and placed submerged into a gel tank containing 1X TAE running buffer with its level at approximately 1.5 mm above the agarose gel. Five microlitre PCR product was mixed with 1 µL 6X gel loading dye (Thermo Scientific) and loaded into the wells of the agarose gel. GeneRuler 100-bp DNA ladder (Thermo Scientific) was used for size estimation of the PCR products. The gel was run at 65 V for 60 min and visualised under a 302-nm UV light using the BioSpectrum Imaging System (UVP, California, USA).

3.4.4 Expansion Culture of Transformed *E. coli* Clones

After identification, individual colonies containing transformed clones

harbouring the desired plasmid were dipped into 5 mL of LB broth containing 100 µg/mL of ampicillin (Sigma-Aldrich) and incubated overnight in a shaking incubator (IKA-Works, Staufen im Breisgau, Germany) with vigorous shaking. About 1 mL overnight culture was transferred to 250 mL LB broth containing 100 µg/mL of ampicillin for bulk production. Bacterial glycerol stock was prepared by mixing 700 µL bacterial culture with 300 µL of 100% (v/v) glycerol in a 1.5-mL microcentrifuge tube and stored at -80 ^{o}C as the stock.

3.4.5 Plasmid DNA Extraction

Plasmids DNA was extracted from *E. coli* culture using two commercial kits. For small-scale (maximum of 5 mL bacterial broth) plasmid extraction, QIAprep® Spin Miniprep Kit (Qiagen, Germany) was used. For larger-scale culture (250 mL – 300 mL of bacterial broth), PureLink® HiPure Plasmid Maxiprep Kit (Invitrogen) was used. The plasmid extraction procedure was carried out according to the manufacturer's protocols.

For small-scale plasmid extraction, 5 mL bacterial broth was pelleted by centrifuging at 4000 *xg* for 10 min. Pelleted bacterial cells were resuspended in 250 µL resuspension buffer containing RNAse in a 1.5-mL microcentrifuge tube. Bacterial pellet was resuspended evenly to avoid cell clumping. Next, 250 µL of lysis buffer was added and the suspension was mixed gently by inverting the tube five times until a clear solution was observed. Lysis reactions were stopped by

adding 350 µL neutralization buffer into the solution and immediately mixed homogenously by inverting the tube 5 times. The microcentrifuge tube was centrifuged at 17,900 *xg* for 10 min using a Sigma® 1-14 table-top centrifuge (Sigma-Aldrich). The supernatant was transferred to a QIAprep spin column and centrifuged for 1 min. The spin column was washed once with washing buffer and centrifuged twice for 1 min each time to remove residual washing buffer. Plasmid DNA trapped inside the spin column was eluted by placing the spin column in a clean 1.5-mL microcentrifuge tube and 50 µL pre-warmed elution buffer at 55^{o}C was added to the center of the spin column. The column was allowed to stand for 1 min and centrifuged at 17,900 *xg* for 1 min. Plasmid DNA was quantified using Implen® UV/Vis NanoPhotometer™ P300 (Implen, Munich, Germany) and stored at -20 ^{o}C.

For large scale plasmid extraction, 300 mL transformed *E. coli* was placed into several 50-mL conical tubes and centrifuged at 4000 *xg* for 10 min to sediment the bacterial cells. Bacterial pellet was pooled into one 50-mL conical tube and resuspended homogenously using resuspension buffer containing RNase A. Lysis buffer was added to the suspension and the capped tube was inverted for mixing. The mixture was then incubated at room temperature for 5 min. Lysis buffer was neutralized by adding precipitation buffer and mixed by inverting the tube until the lysate was homogenous. Next, the mixture was centrifuged at 12,000 *xg* for 10 min at room temperature and the supernatant was loaded into the equilibrated column. The supernatant was allowed to flow through the column by gravity. The plasmid

DNA remained trapped in the column. The column was washed twice using wash buffer and the DNA was eluted using elution buffer and collected with a sterile 50-mL conical tube placed under the column. Eluted plasmid DNA was precipitated by adding isopropanol to the eluent. The eluent was centrifuged at 12,000 *xg* for 30 min at 4 °C. The DNA pellet was washed in 70% ethanol and centrifuged at 12,000 *xg* for 5 min at 4 °C. The supernatant was discarded and the pellet was air-dried for 15 min before being resuspended in 200 µL TE buffer. Concentration and purity of each plasmid DNA were determined using Implen® UV/Vis NanoPhotometer™ P300 (Implen, Munich, Germany). The plasmid DNA obtained was aliquoted at around 50 µL each in a 1.5-mL microcentrifuge tube. Plasmid stocks were stored at -20 ^{o}C.

3.4.6 Preparation of Re-circularised HPV16 DNA

Full HPV16 genome was excised from the pSPW12 plasmid by restriction enzyme digestion, and re-circularised by ligation for use in transfection of NIKS. For digestion of HPV16 DNA, pSPW12 plasmid (5 µg) was first incubated with 2 µL fast-digest BamHI restriction enzyme (Thermo Scientific) for 5 min at 37 ^{o}C. The enzyme activity was inactivated by incubating at 75 ^{o}C for 20 min. The ligation reaction mixture was prepared as shown in Table 3.6.

The ligation reaction was carried out by placing the reaction tube in a floater and incubated in a 16 ^{o}C water bath overnight. The reaction mixture was purified

Table 3.6 Ligation reaction mixture set-up for preparation of circular HPV16

Component	Volume (µL)
Digested DNA	15
DNase, RNase free water	882.5
10X T4 DNA Ligase buffer (NEB, USA)	100
T4 DNA Ligase (NEB, USA)	2.5
Total volume	1000

and concentrated using binding, washing and elution buffers. These three buffers are all included in QIAprep® Spin Miniprep Kit (Qiagen, Germany). The mixture was first loaded together with 10 mL binding buffer into a QIAprep spin column and the column was centrifuged at 13,000 *xg* for 30 sec using a Sigma® 1-14 table-top centrifuge (Sigma-Aldrich). Following this, the column was washed once with 750 µL washing buffer and centrifuged twice at top speed for 1 min to remove most of the washing buffer. Elution buffer was next added to the column which was allowed to stand for 1 min. The column was then spun at top speed for1 min to elute the genomic DNA. DNA integrity was assessed by taking 3 µL eluted DNA mixed with 1 µL 6X loading dye and run on a 1% agarose gel (1% w/v agarose in TBE). The gel was pre-stained with 1 µL 3X GelRed nucleic acid stain (Biotium) and the KAPA™ Universal DNA ladder (Kapa Biosystems, USA) was used for size estimation. The gel was run for 60 min at 80 V. Successful re-circularisation of HPV16 genome should give a supercoiled band at about 8 kb (kilobase pairs) as shown in Figure 3.1.

3.5 Establishment of HPV16 Precancerous Models: NIKS-HPV16$_{EPI}$

3.5.1 Co-transfection of Re-Circularised Full HPV16 Genome and pcDNA into NIKS

A day prior to transfection, NIKS cells were plated in a 6-well plate at a density of 7 x 10^5 cells together with 3 x 10^5 feeder cells. The plate was incubated

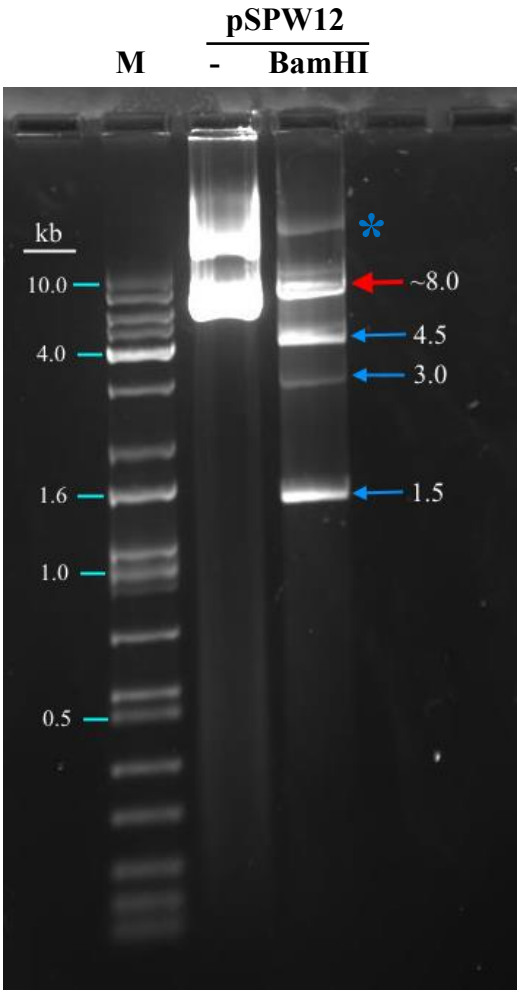

Figure 3.1 Identification of HPV16-full genome fragment by restriction enzyme digestion. Lane 1, DNA marker; lane 2, undigested pSPW12; lane 3, BamHI-digested pSPW12. The full 8-kb HPV16 genome fragment at 8 kb location is indicated by the red arrow; other vector-derived BamHI fragments are indicated by the blue arrows; the blue asterisk indicates the >10-kb band, which was probably an undigested, or incompletely-digested, pSPW12 DNA fragment.

overnight at 37 ^{o}C with 5% CO_2 until 80% confluency. Existing medium in each well was aspirated off and 2 mL fresh complete medium were added into the wells. Transfection was carried out using Lipofectamine® 3000 (Invitrogen). Transfection mixtures containing the appropriate reagents were prepared according to the manufacturer's protocol (Table 3.7).

Three sets of controls were set up for the transfection exercise. They include a reagent (parental cell) control, a vector control and an efficiency control. For each of the controls and for the transfection with HPV, two sets of tubes labelled as A and B were prepared separately. As shown in the Table 3.7, component A comprised 7.5µL Lipofectamine® 3000 diluted in 125µL of DMEM. In the case of component B, pcDNA6 and pMX-GFP were added to DMEM and P3000^{TM} for the vector control and the transfection/efficiency control respectively, while HPV DNA was added together with pcDNA6 (which contain the blasticidin resistance gene) for the transfection mix. The negative (i.e. reagent control) contained all the reagents with the exclusion of DNA. Components A and B were mixed together in equal volume (125 µL each) to form the DNA-lipid complexes. The reaction mixes were then allowed to incubate at room temperature for 5 minutes before being added to the NIKS cells. The cells were incubated at 37 ^{o}C with 5% CO_2.The cells were cultured until about 80% confluency and were then treated with blasticidin (Gibco) at 8 µg/ml, with the exception of the transfection/efficiency control. The culture medium was replenished every two days and blasticidin added to the appropriate plates until all the cells in the negative control plate are dead.

Table 3.7 Preparation of transfection mixes using Lipofectamine® 3000

Component	Reagent	Tube 1 (Parental Control)	Tube 2 (Vector Control)	Tube 3 (Co-transfection Tube)	Tube 4 (Transfection/ Efficiency Control)
A	DMEM (µL)	125	125	125	125
	Lipofectamine® 3000 (µL)	7.5	7.5	7.5	7.5
Component	**Reagent**	**Tube 1**	**Tube 2**	**Tube 3**	**Tube 4**
B	DNA Amount (µg)	Nil -	pcDNA6 2.5	HPV16 genome + pcDNA6 2.5+1.5	pMX-GFP 2.5
	DMEM (µL)	125	125	125	125
	P3000^{TM} Reagent (µL)	7.5	7.5	7.5	7.5

Procedure

1. Prepare components A and B as above
2. Add 125µL of component A to 125µL of component B for each tube (→ DNA lipid complex)
3. Incubate the tubes for 5 minutes at room temperature
4. Add the equilibrated transfection mixes (DNA lipid complex) to the NIKS cells

The success of the transfection and its efficiency was gauged by examining the fluorescence signal (green) of the cells treated with the pMX-GFP transfection mix at 24 hours. The signals were monitored thereafter at 48 and 72 hours. This was done using the Zeiss Imager (A1 Fluorescence Microscope, Carl Zeiss, Germany). Positive signals at 24 hours indicate successful transfection, and the relative number of cells positive for the signal a measure of the efficiency of transfection. These results are taken to imply overall success in transfection for the other plasmids. An increase in the signals over time is an indication of active replication of the pMX-GFP transfected cells. Simultaneously, cell growth was followed by examining the plates using phase contrast microscopy.

The live transfected cells were trypsinised and transferred to a new 100-mm culture dish for expansion of cell colonies. The expanded transfected cells were either cryopreserved or used directly in subsequent experiments. Transfected cells harbouring the HPV16 were maintained using NIKS complete medium and the medium was changed every second day. Transfected cells were morphologically similar to the parental NIKS cells but showed higher growth rates based on microscopic observation. They were subcultured at 80-90% confluency in 100-mm culture plates.

3.6 Establishment of HPV16 Cancerous Models: NIKS-HPV16$_{INT}$

3.6.1 Production of Recombinant Retroviruses

A day prior to transfection, Phoenix cells were plated in a 6-well plate at a density of 1 x 10^6 cells per well with 2 mL complete medium. The plate was incubated overnight at 37 ^oC in a 5% CO_2 incubator to 80% confluency. Medium was aspirated off and 1.8 mL fresh complete medium was added into each well. Transfection mixtures containing calcium phosphate, $CaCl_2$ (Sigma-Aldrich), plasmid DNA and sterile water were prepared according to Table 3.8.

Eighty-three microlitres of 2X HEPES buffered saline, HBS (Sigma-Aldrich) were added in a drop wise manner to the transfection mixtures (tubes 1-5) while vortexing vigorously. The DNA/HBS mixture was immediately pipetted onto the Phoenix cells gently in a drop wise manner to avoid disturbing the cells. The cells were incubated at 37 ^oC in a 5% CO_2 incubator.

The culture medium was aspirated off and replenished with fresh complete medium every 24 h. The retrovirus-containing medium at 72 h was filtered using a 0.45-µm PVDF syringe filter (Sartorius AG) and the filtrate was collected in a 15-mL conical tube. The filtrate containing the retroviruses at 72 h was used immediately to infect NIKS cells. GPF signal in cells transfected with pMX-GFP was observed at 24-h intervals using a Zeiss Imager A.1 Fluorescence Microscope

Table 3.8 Production of recombinant retroviruses reparation of transfection mixture using the calcium phosphate

Tube	Plasmid	Plasmid DNA (µg)	2.5M $CaCl_2$ (µL)	ddH_2O (µL)	Total volume (µL)
1	pBABE-neo	3.3	8.3	Varies (according to initial plasmid concentration)	83
2	pLXSN-HPV16 E6	3.3	8.3		83
3	pLXSN-HPV16 E7	3.3	8.3		83
4	pLXSN-HPV16 E6/E7	3.3	8.3		83
5	pMX-GFP	3.3	8.3		83
6	None (negative control)	Nil	8.3	74.7	83

(Carl Zeiss, Germany) as a means to assess the transfection efficiency.

3.6.2 Retroviral Transduction of NIKS cells

NIKS cells were plated a day prior to transduction at a density of 7 x 10^5 cells together with 3 x 10^5 feeder cells in a 6-well plate. The plate was incubated overnight at 37 ^oC in a 5% CO_2 incubator prior to transduction. At around 70% confluency, the medium was removed and replaced with the filtrate containing the retroviruses. Polybrene (Sigma-Aldrich) was added at a final concentration of 8 µg/mL. The plate was centrifuged at 32 ^oC, 2000 *xg* for 1 h and incubated overnight at 37 ^oC in a 5% CO_2 incubator.

Medium in the 6-well plate was replenished with fresh complete medium every 24-h. At 96 h, transduced cells harbouring different HPV16 oncogenes and the negative control (parental) cells were trysinised and transferred to new cell culture-treated 60-mm dishes together with 5 x 10^5 feeder cells. Transduced cells were grown to 80% confluency and treated with the antibiotic geneticin (G418) (Gibco) at 500 µg/mL concentration. Medium was replenished every two days together with 500 µg/mL geneticin until the cells in the negative plate were completely dead. The surviving transduced NIKS cells were trypsinised and transferred to a new 100-mm cell culture plate for expansion of the cell colonies. The expanded transduced cells were either cryopreserved or used directly for subsequent applications. Transduced cells were maintained in NIKS complete

medium with medium changes every second day. Transduced cells were morphologically similar to the parental NIKS cells but with higher growth rates based on assessment. They were subcultured to 80-90% confluence in a 100-mm culture dish. GFP signal of the transduced NIKS was observed under a Zeiss Imager Fluorescence Microscope (Carl Zeiss, Germany) as a means to monitor the success of transfection and its efficiency.

3.7 Characterization of the HPV16 Modified Cell Lines

3.7.1 Assessment of Gene Expression

3.7.1.1 Total Ribonucleic Acid (RNA) Extraction

Cells harbouring the HPV16 genome and HPV16 E6, E7 or E6E7 oncogenes from passage 5 to 30 each were harvested for total RNA extraction. Pellets of approximately 1 x 10^6 of transduced cells were lysed in 1 mL Trizol® Reagent (Invitrogen). The cell mixture containing the Trizol reagent was homogenised by pipetting up and down several times and incubated at room temperature for 5 min.

Lysed cells were centrifuged at 12,000 *xg* for 10 min at 4 ^{o}C and the supernatant was transferred to a clean 1.5-mL microcentrifuge tube. Chloroform (0.2 mL) was added to the RNA supernatant and the mixture was vortexed

vigorously for 15 sec. The mixture was incubated for 3 min at room temperature prior to centrifugation at 12,000 *xg* for 15 min at 4 ^{o}C. After centrifugation, the mixture was separated into 3 distinct layers with a lower red phenol-chloroform phase, an interphase and a colourless upper aqueous phase. RNA was carefully aspirated out from the aqueous phase using a 200-µL pipettor into a clean 1.5-mL microcentrifuge tube without disturbing the interphase layer. RNA was precipitated with 0.5 mL 100% isopropanol (Nacalai Tesque, Kyoto, Japan) and incubated at room temperature for 10 min. The RNA-isopropanol mixture was centrifuged at 12,000 *xg* for 10 min at 4 ^{o}C. The supernatant was removed and the RNA pellet was washed by adding 1 mL 75% ethanol (Nacalai Tesque). The RNA-ethanol mixture was vortex briefly prior to centrifugation at 7500 *xg* for 5 min at 4 ^{o}C. Supernatant was discarded and the washing step was repeated by adding 1 mL absolute ethanol (Nacalai Tesque) onto the RNA pellet. Supernatant was removed and the RNA pellet was air-dried in an Airstream Laminar flow hood (ESCO) for 10 min. The dried RNA pellet was dissolved in 20 µL DEPC-treated double-distilled water (ddH_2O) and gently pipetted up and down several times to ensure that the RNA pellet was completely dissolved. RiboLock RNase Inhibitor (40U/ µL) was added to the extracted RNA to inhibit RNase activities. RNA concentration was measured in a NanoPhotometer UV/Vis spectrophotometer (Implen, Germany). A260/A280 reading of 1.8 – 2.0 indicated pure RNA sample.

RNA integrity assessment was performed by mixing 1 µL RNA solution with 1 µL 6X loading dye and analysed on a 1% agarose gel (1% w/v agarose in

DEPC-treated TBE). The gel was pre-stained with 1 µL 3X GelRed nucleic acid stain (Biotium) and the KAPA™ Universal DNA ladder (Kapa Biosystems, USA) was used for size estimation. Gel electrophoresis was carried out for 60 min at 80 V. Intact total RNA gave clear 28S and 18S ribosomal bands on the agarose gel.

3.7.1.2 Conversion of RNA into cDNA

RNA was converted into cDNA before subjected to standard polymerase chain reaction. cDNA conversion involved a two-step reaction in a Veriti Thermal Cycler (Life Technologies, USA).

For the synthesis of cDNA, components including 100 µM Oligo$(dT)_{18}$ primers (Thermo Scientific), DEPC-treated water (Thermo Scientific) and the RNA template were thawed on ice and centrifuged briefly to collect the contents at the bottom of the tube. RNA templates were made up to 1,000 ng in 10 µL and all the components were prepared as shown in Table 3.9. The mixtures were centrifuged briefly, incubated at 65 ^{o}C for 5 min and placed on ice. The reverse transcription master mix was prepared by thawing 5X reaction buffer (Thermo Scientific), 40 U/µL RiboLock RNase Inhibitor (Thermo Scientific), 10 mM dNTPs mix (Thermo Scientific) and 200 U/µL RevertAid Reverse Transcriptase (Thermo Scientific) on ice. The reaction mixture was prepared as stated in Table 3.10. The mixture was incubated at 42 ^{o}C for 60 min and the reaction was immediately terminated by

Table 3.9 Reverse-transcription reaction mixture (Step 1).

Component	Volume (µL)
RNA template	10
Oligo(dT)$_{18}$ primers (100 µM)	1
DEPC-treated water	1.5
Total	12.5

Table 3.10 Reverse-transcription reaction mixture (Step 2).

Component	Concentration	Volume (µL)
5X Reaction buffer	-	4.0
RiboLock RNase Inhibitor (40 U/µL)	20 U	0.5
dNTPs mix (10 mM each)	1 mM	2.0
RevertAid Reverse Transcriptase (200 U/µL)	200 U	1.0
RNA template (from Table 3.9)	-	12.5
Total volume	-	20

heating at 70 ºC for 10 min. The cDNA products were kept at -20 ºC for long term storage, or used directly in PCR experiments.

3.7.1.3 Polymerase Chain Reaction (PCR)

To determine the presence of E6 and/or E7 in the HPV16 precancerous or cancerous models cDNA products were first subjected to PCR. The PCR reaction mixture was prepared as shown in Table 3.11. PCR was performed in a Veriti Thermal Cycler (Applied Biosystems, USA), and the PCR cycling profile used was as shown in Table 3.5, Section 3.4.2, page 57.

PCR products were analysed by 2% agarose gel electrophoresis. The agarose gel (2%) was prepared by dissolving 0.6 g agarose powder (Seakem® LE Agarose, Lonza, Swithzerland) in 30 mL 1X Tris-acetate-EDTA (TAE) buffer (First Base Laboratories, Malaysia). The mixture was heated with gentle stirring until the agarose powder was fully dissolved. One microlitre 3X GelRed nucleic acid stain (Biotium, California, USA) was then added and the mixture immediately poured onto the gel casting unit. The gel was allowed to solidify and placed submerged into a gel tank containing 1X TAE running buffer with its level at approximately 1.5 mm above the agarose gel. Five microlitre PCR product was mixed with 1 µL 6X gel loading dye (Thermo Scientific) and loaded into the wells of the agarose gel. GeneRuler 100-bp DNA ladder (Thermo Scientific) was used for size estimation of the PCR products. The gel was run at 65 V for 60 min and visualised under a 302-nm UV light using the BioSpectrum Imaging System (UVP, California, USA).

Table 3.11 PCR reaction mixture

Reagents	**Stock concentration**	**Working concentration**	**Per reaction (µl)**
PCR buffer with 20mM of $MgCl_2$	10x	1 X	1.0
dNTPs mix	10 mM	200 µM	0.4
Taq polymerase	5 U/ µL	0.5 U	0.1
$MgCl_2$	25 mM	2.0 µM	1.6
Forward primer	10 µM	0.5 µM	1.0
Reverse primer	10 µM	0.5 µM	1.0
ddH_2O	-	-	13.9
cDNA Template	600 ng/µL	30 ng	1
Total	-	-	20

3.7.2 Analysis of Protein Expression by Western Blot

3.7.2.1Buffers and Solutions

Buffers and solutions used in western blot assay were prepared accordingly as stated in Table 3.12.

3.7.2.2 Protein Lysate Preparation

Protein lysates from NIKS and the HPV16 modified cells (precancerous and cancerous moels) at passage 5 to 30 were prepared. All the steps were performed on ice to avoid protein degradation. Cells were harvested according to standard sub-culturing technique using 0.25 % Trypsin-EDTA and cell pellets were collected in a 1.5-mL microcentrifuge tube. Cell pellets were washed once with 1X PBS and the cells were immediately lysed using 150 µL RIPA lysis buffer (Nacalai Tesque). The cells were suspended by pipetting up and down using a 200-µL pipette and kept on ice for 15 min. Tubes containing the cell lysate were centrifuged at 12,000 rpm for 15 min at 4 ^{o}C using a pre-cooled Kubota table top refrigerated microcentrifuge, Model 3500 (Kubota, Osaka, Japan). The supernatant containing the protein lysate was transferred into a new microcentrifuge tube and was labelled accordingly. The protein lysates were stored in a -80 ^{o}C freezer for long-term storage or subjected to Bradford Assay quantification.

Table 3.12 Preparation of buffers and solutions

Buffer and solution	Methods of preparation
0.5 M Tris, pH 6.8	6 g Tris base (MP Biomedicals) was dissolved in 80 mL distilled water and adjusted to pH 6.8 using 3M of hydrochloric acid (HCl) (Calbiochem, Merck KGaA, Germany). The solution was filtered through a 0.45-µm syringe filter (Sartorius AG) and stored at 4 ^{o}C.
1.5 M Tris, pH 8.8	18.15 g Tris base was dissolved in 80 mL distilled water and adjusted to pH 8.8 using 3M HCl. The solution was filtered through a 0.45-µm syringe filter and stored at 4 ^{o}C.
10% (w/v) Sodium Dodecyl Sulphate (SDS) solution	10 g SDS (Nacalai Tesque) was dissolved in 90 mL distilled water. The solution was topped up to 100 mL when SDS was dissolved completely. Solution was stored at 4 ^{o}C.
10% Ammonium Persulfate (APS)	APS was prepared freshly before use. An amount of 0.1 g APS (Thermo Scientific) was dissolved in 1 mL distilled water.
10X SDS-PAGE running buffer: 25 mM Tris, 190 mM glycine and 0.1% SDS	12.1 g Tris base, 57.6 g glycine (Merck KGaA, Germany) and 2 g SDS were dissolved in 2 L distilled water. The buffer was stored at 4 ^{o}C.

Table 3.12 Continued

Buffer and solution	Methods of preparation
10X Tris-Buffered Saline (TBS): 0.5 M Tris, 1.5 M NaCl	60.6 g Tris base and 87.66 g NaCl (Omnipur, Merck KGaA, Germany) were dissolved in 800 mL distilled water. The buffer was adjusted to pH 7.5 using 3 M HCl. The final volume was topped up to 1 L with distilled water and stored at 4 ^{o}C.
1X Transfer buffer: 25 mM Tris, 190 mM glycine, 20 % methanol	3.03 g Tris base and 14.4 g glycine were dissolved in 500 mL distilled water and 200 mL methanol (Sigma-Aldrich) were added into the solution. The volume was topped up to 1 L with distilled water and stored at room temperature.
Washing buffer (TBST) 1X TBS, 0.05 % Tween-20	1X Tris-buffered saline buffer was prepared by adding 100 mL of 10X concentrated TBS to 900 mL distilled water, followed by 500 µL Tween-20 (Biorad, USA). The solution was mixed well and stored at room temperature.
Blocking buffer: TBST with 5 % of milk	40 mL 1X TBST was used to dissolve 2 g non-fat dry milk powder (Bio Basis Inc., Canada) which was stirred to mix well. Blocking buffer was prepared fresh before use.
Medium Stripping buffer	1.5 g glycine, 0.1 g SDS and 1 mL Tween-20 were dissolved in 50 mL distilled water. 6 M HCl was used to adjust the solution to pH 2.2 and the buffer was stored at room temperature.

3.7.2.3 Protein Quantification

Protein quantification was performed by using the Quick Start Bradford Protein Assay (Bio-Rad, California, USA). A protein standard ranging from 125 – 2000 µg/mL was generated by dilution of bovine serum albumin (BSA). The protein assay was performed in triplicates. Diluted protein standards (5 µL each) and unknown samples at 1 in 10 dilutions were pipetted into a 96-well plate accordingly. Two hundred fifty microliters of the 1X dye reagent pre-thawed to room temperature was next added to each well. The plate was swirled gently by hand and incubated in the dark for 15 min. The reactions were read in the Infinite M200 Microplate Reader (Tecan, Männedorf, Switzerland) set at absorbance 595 nm. A standard curve was generated by plotting the 595-nm absorbance readings at the y-axis versus the protein concentration in µg/mL at the x-axis. The final concentrations of the unknown protein samples were adjusted by multiplying the dilution factor used.

3.7.2.4 Protein Separation by SDS-polyacrylamide Gel Electrophoresis (SDS-PAGE)

Extracted protein samples were separated on sodium dodecyl sulfate-polyacrylamide gel electrophoresis (SDS-PAGE). SDS-polyacrylamide gel was casted using the Mini-PROTEAN® Tetra Cell System (Bio-rad).

A 12 % separating gel was prepared and the gel casting reagents were

added in sequence as follows - 3.3 mL distilled water, 2.5 mL 1.5 M Tris (pH 8.8), 4.0 mL 30 % (w/v) Bis/Acrylamide (Bio-rad), 100 µL 10% SDS, 100 µL 10 % APS and 10 µL Tetramethylethylenediamine (TEMED) (Calbiochem). All components were mixed well and the mixture was pipetted into the gel caster gently. The separating gel was immediately overlaid with 100 µL isopropanol (Nacalai Tesque) to allow all air bubbles to be removed, thereby ensuring that the separating gel has a smooth surface. Isopropanol was rinsed off by flushing with distilled water when the gel had polymerised after 30 – 45 min. the residual water was wiped away using Kimwipes.

Next, 5% stacking gel was prepared. The gel casting reagents were added in sequence as follows - 1.9 mL distilled water, 1 mL 0.5 M Tris (pH 6.8), 0.67 mL 30% (w/v) Bis/Acrylamide, 30 µL 10% SDS, 30 µL 10% APS and 3.3 µL TEMED. The stacking gel solution was mixed well and slowly added on top of the polymerised separating gel until the top of the short plate was reached. A 10-well 1.0-mm gel comb was inserted between the glass plates and stacking gel was allowed to polymerise for 30 – 45 min.

After polymerisation of the stacking gel, the gel cassette was placed into the clamping frame of the electrode assembly, which was then placed into the Mini-PROTEAN Tetra Tank on a flat surface. The gel comb was gently removed and the wells were flushed with 1X SDS-PAGE running buffer. The chamber between the electrode assemble was filled up with 1X running buffer until it overflows to the outer chamber (tank). The tank was filled up with 1X running buffer (approximately 550 mL for running 2 gels). Twenty microlitres

of protein lysates was mixed with 5 µL of 5X lane marker reducing sample buffer (Thermo Scientific) to give a final concentration of 50 µg/mL. The mixture was heated at 95 ºC for 10 min in a heating block (Stuart Scientific, Staffordshire, UK) to denature the protein. Denatured protein samples and 10 µL Precision Plus Protein™ WesternC™ Standards (Bio-Rad) were carefully loaded into the wells. Electrophoresis was performed at 120 V for 90 min.

3.7.2.5 Wet Transfer of Proteins from Gel to Nitrocellulose Membrane

Prior to performing the wet transfer, 1 piece of 0.2-µm nitrocellulose membrane (Thermo Scientific) and 2 pieces of thick western blotting filter paper (Thermo Scientific) were cut to size (10-cm width and 6-cm length) according to the dimension of the gel. The membrane, filter papers, and fibre pads were pre-equilibrated in 1X transfer buffer pieces for 10 – 15 min.

The SDS-PAGE gel was considered complete when the protein marker dye indicator approached the bottom of the separating gel. The gel cassette was then removed from the electrophoresis apparatus. Stacking gel was removed and the separating gel was ready for wet transfer. When all the necessary components were completely soaked in 1X transfer buffer, the gel sandwich was arranged inside a tray containing transfer buffer in the following sequence: (i) a piece of pre-equilibrated fiber pad on the black side of the cassette, (ii) a piece of pre-equilibrated filter paper, (iii) polyacrylamide gel, (iv) pre-equilibrated membrane on top of the gel, and (v) a piece of pre-equilibrated fiber pad. A glass roller was used to gently push out air bubbles in between the layers.

The blotting sandwich cassette was closed with the white latch and placed into the electrode module. The transfer tank was filled up with 1X transfer buffer to the blotting mark level. A magnetic stirrer was placed into the electrode module and the transfer tank was placed onto a stir plate. The stirring speed was adjusted to maximum to maintain an even temperature and ion distribution in the tank.

The nitrocellulose membrane was removed and the gel orientation was labelled on the membrane using a pencil. The membrane was gently washed once with distilled water for 5 min on the bench rocker (Stuart). The membrane was stained with Pierce Reversible Protein Stain Kits (Thermo Scientific) to determine the transfer efficiency before continuing with primary antibody staining. The membrane was destained using a destaining solution and distilled water. The membrane was then ready for blocking.

3.7.2.6 Blocking of Nitrocellulose Membrane

The nitrocellulose membrane was blocked using 5% of milk to prevent non-specific binding of antibodies. Ten mL of blocking buffer was used to soak the membrane for 1 h at room temperature with gentle rocking on a bench rocker. The membrane was then washed three times with washing buffer (Table 3.12) for 5 min each with gentle rocking.

3.7.2.7 Reaction with Primary and Secondary Antibodies

The nitrocellulose membrane was probed with 5 mL primary antibody

against HPV16 E6 (C1P5, Abcam, Cambridge, UK) diluted 1:400 using washing buffer. The membrane was incubated at 4 ^{o}C overnight with gentle rocking. Subsequently, the membrane was repeatedly washed three times with 10 mL washing buffer for 5 min each with gentle rocking. The membrane was probed with 5 mL HRP-conjugated rabbit anti-mouse IgG (H+L) secondary antibodies (Thermo Scientific) diluted 1:10,000 using washing buffer. Secondary antibody incubation was for 1 h with gentle rocking. Lastly, the membrane was washed three times with 10 mL washing buffer for 5 min each with gentle rocking before proceeding to chemiluminescence detection.

Other target proteins including HPV16 E7 (289-13013, Abcam) and housekeeping gene, β-actin (BA3R, Thermo Scientific) were also detected using a similar procedure. β-Actin was used to normalise the protein levels loaded.

3.7.2.8 Chemiluminescence Detection

Chemiluninescence detection was carried out by using an enhanced chemiluminescent (ECL) substrate for detection of the horseradish peroxidase (HRP) conjugate of the secondary antibodies. The ECL substrate was prepared by mixing ECL reagents 1 and 2 provided in the SuperSignal® West Pico Chemiluminecent Substrate (Thermo Scientific) in a 1:1 ratio. The washed membrane from the previous step was placed on a sheet of transparent plastic paper and the ECL substrate mixture was added onto the membrane. The blot was drained of excess reagent and was then exposed to the CCD camera of the

BioSpectrum Imaging System (Ultra-Violet Products Ltd, California, USA) for 15 min to capture the western blot images.

3.7.2.9 Membrane Stripping and Reprobing

Once a western blot image was acquired, the membrane was washed once with 10 mL washing buffer. A 10-mL mild stripping buffer (Table 3.12) was used to remove the primary and secondary antibodies on the membrane. The membrane was incubated at room temperature with gentle rocking for 10 min and the stripping step was repeated once more. The membrane was washed once in 10 mL of 1X PBS and twice in 10 mL washing buffer with gentle rocking for 5 min each. The stripped membrane was drained of excess washing buffer and was subjected to the membrane blocking procedure (Section 3.7.2.6, page 84), followed by staining with primary and secondary antibodies (Section 3.7.2.7, page 84) and chemiluminescence detection (Section 3.7.2.8, page 85).

3.7.3 Southern Blot Analysis for Assessment of the Integration Status of the HPV16 Genome

Southern blot analysis was performed by Lofstrand Labs Ltd. (Gaithersburg, Maryland, USA). Total DNA was extracted from (i) transduced NIKS cells harbouring the HPV16 genome at different passages spanning passage 5 to 30, (ii) negative control NIKS harbouring pcDNA6 at passage 12, and (iii) the positive control pSPW12 plasmid and sent in dry ice for analysis. Transduced NIKS cells harbouring HPV16 genome or pcDNA6 were both

extracted by using Qiagen® blood and cell culture DNA midi kit (Qiagen, Germany). The DNA extraction procedure was carried out according to the manufacturer's protocols.

Pellets of approximately 1 x 10^7 of transduced cells were washed twice with 1 mL cold PBS (4 ^oC) and pelleted by centrifuging at 1,500 *xg* for 10 min at 4 ^oC. Cell pellets were lysed in 2 mL pre-equilibrated lysis buffer at 4^oC, mixed gently by inverting the tube five times and incubated on ice for 10 min in a 5 mL-microcentrifuge tube. The mixture was centrifuged at 1,300 *xg* for 15min at 4^oC, and supernatant was discarded. The lysis step was repeated by addition of 1 mL lysis buffer and 3 mL ice-cold distilled water to the cell pellet. The mixture was vortexed vigorously prior to centrifugation at 1,300 *xg* for 15 min at 4 ^oC and the supernatant was discarded. The cell pellet was washed once with 5 mL washing buffer followed by vortexing for 30 secs at maximum speed. Ninety-five microlitres proteinase K was next added to denature the protein. The mixture was incubated at 50 ^oC for 60 min until a clear solution was observed which indicates complete denaturation of the protein. Next, the mixture was vortexed at maximum speed for 10 sec and loaded into the equilibrated column. The mixture is allowed to flow through the column by gravity. The genomic DNA will remain trapped in the column. The column was washed twice using 7.5 mL washing buffer and the genomic DNA was eluted using 5 mL elution buffer by placing a clean 50-mL conical tube under the column. Eluted genomic DNA was precipitated by adding 3.5 mL isopropanol to the eluent and immediately mixed well by inverting the tube twenty times. The eluent was centrifuged at 8,000 *xg* for 20 min at 4 ^oC. The DNA pellet was

washed in 2 mL cold 70% ethanol, vortexed briefly and centrifuged at 8,000 *xg* for 10 min at 4 ^{o}C. The supernatant was carefully discarded and the DNA pellet was dissolved in 200 µL TE buffer at 55 ^{o}C for 2 h. Concentration and purity of genomic DNA were determined as described in Section 3.4.5, page 59.

3.7.3.1 Restriction Enzyme Digestion and Gel Electrophoresis

Briefly, total DNA from the pcDNA6 cells and NIKS harbouring the HPV16 genomic was digested with BamHI at 37 ^{o}C for 30 min. The digested DNA was electrophoresed in a 0.8 % agarose gel. The agarose gel was depurinated in 0.25 M HCl and DNA was denatured in 0.5 M NaOH.

3.7.3.2 Probe Preparation and Labelling

pSPW12 was digested with BamHI followed by electrophoresis in a 1.0 % agarose gel. The desired band was excised from the GelRed (Biotium) stained gel under UV-light, and DNA was extracted using the DNA Gel Extraction Kit (Norgen Biotek Corp., Thorold, Canada). The derived DNA fragment was then labeled with ^{32}P-dCTP for use as the hybridisation probe.

3.7.3.3 Southern Blot Transfer

Digested DNA was neutralised in 0.5 M tris HCl prior to transferring to the nylon membrane. The membrane was prehybridised at 65 ^{o}C for 30 min in hybridisation buffer for 4 h before addition of ^{32}P-dCTP-labelled HPV DNA probe.

3.7.3.4 Hybridisation and Autoradiography

Hybridization of DNA in the nylon membrane with a specific HPV16 probe was performed for 16 h followed by three times of washing in sodium phosphate buffer (pH 7.2) with 1% of SDS. The radioactive labelled target sequences were visualised by autoradiography.

3.8 Cell Proliferation Analysis by MTT Assay

Growth curves of NIKS, HPV16 precancerous and cancerous cells were determined to ensure that exponential growth was achieved during the 4-day incubation period. Cell proliferation was measured by the uptake of 3-[4,5-MTT (dimethylthiazol-2-yl]-2,5-diphenyl tetrazolium bromide) by the cells. The number viable cells were indicated by the amount of MTT uptake.

Cells were seeded at different seeding densities into a 96-well plate together with 5 x 10^4 feeder cells and 200 µL medium per well. The plate was incubated for 4 days (24 to 96 h) and the cell proliferation capacity was determined on a daily basis. Twenty microlitres filter-sterilized MTT solution (5 mg/ mL) were added and the cells incubated at 37 ^oC for 4 h prior to measure the absorbance at 570 nm. The existing medium was removed and 200 µL sterile DMSO was added to dissolve the purple formazan crystals formed within the cells. The plate was agitated gently for 10 min and A_{570} readings were taken using the i-control™ software provided by Infinite M200 PROMicroplate Reader (Tecan, Männedorf, Switzerland). Growth curves were generated by

plotting the absorbance against the incubation time. The MTT assays were performed in three independent experiments in triplicates.

3.9 Susceptibility of HPV-modified Cell Lines to Standard Chemotherapeutic Agents

3.9.1 Assessment of Cytotoxicity

Cisplatin or cis-Diamineplatinum(II) dichloride (Sigma-Aldrich) and Topotecan hydrochloride hydrate (Sigma-Aldrich) were the standard chemotherapeutic agents used in this study. Effects of these agents on the HPV16 precancerous and cancerous models were assessed using the MTT assay.

Three days prior to drug treatment, 3T3-J2 feeder cells were seeded into a 96-well plate at a seeding density of 0.5 x 10^4 cells/well and allowed to adhere for 24 h. Feeder cells were inactivated with 8 µg/mL of Mitomycin-C (MMC) (Calbiochem) for 2 h. The feeder cells were washed twice with 100 µL 1X PBS per well to remove residual MMC. NIKS and the HPV16-modified cells (precancerous and cancerous models) at 80% confluency were trypsinised and seeded into 96-well plate at a seeding density of 1 x 10^4 cells/well 2 h prior to drug treatment. Cisplatin was freshly prepared by dissolving 5 mg cisplatin in 1 mL DMSO. The final concentrations of cisplatin used for testing were 0.28, 0.56, 1.13 and 2.25 µM, while that for the topotecan were 0.07, 0.14, 0.27 and 0.55 µM. One hundred microliters of drug were added to the cells together with 100 µL of complete medium.

The cells were incubated for 72 h and 20 µL 5 mg/mL MTT solution was then added into each well. The 96-well plates were incubated at 37 ^{o}C for 4 h. The plates were centrifuged at 2000 *xg* and the medium containing the MTT solution were discarded. Two hundred microliter DMSO was added to dissolve the formazan crystals taken up by the cells. Absorbance readings were taken at 570 nm using the i-control™ software provided by Infinite M200 PRO Microplate Reader (Tecan, Männedorf, Switzerland). Cytotoxic effects of the standard chemotherapeutic drugs were determined by computing the IC_{50} value, which is the drug concentration that causes 50% growth inhibition of targeted cells. A dose-response curve was constructed by using percentage of cell viability (%) against various cisplatin or topotecan concentrations. The percentage of cell viability was calculated using the formula below:

Percentage of viability, % =

$$\frac{\text{Average absorbance of (treated cells – feeder cells – blank)}}{\text{Average absorbance of (DMSO control cells – feeder cells – blank)}} \times 100$$

The curve was plotted using Microsoft® Excel, version 2010 (Microsoft Corporation, Redmond, Washington, USA). The IC_{50} values were calculated from the e-exponential regression equation, $y = Ae^{Bx}$ obtained from the dose-response curve. The IC_{50} values of the NIKS cells from each set of replicates were normalised to 1.0 and the relative fold change in IC_{50} was calculated by divided the IC_{50} values of the normalised parental cells with that of the HPV16 precancerous and cancerous models. The formula used is shown below:

Fold-change in IC_{50} =

$$\frac{\text{Average } IC_{50} \text{ of parental NIKS cells}}{\text{Average } IC_{50} \text{ HPV16 models or empty vector controls}}$$

The significant difference between the control and the HPV16 precancerous and cancerous models was analysed by paired Student's *t*-test (*p<0.05; **p<0.01; ***p<0.001). Data were from three independent experiments performed in triplicates.

3.10 Treatment of Cells with Natural and Synthetic Compounds

3.10.1 Determination of Cytotoxic Effects of Natural and Synthetic Compounds by MTT

The natural flavone compounds, eupatorin and sinensetin, were provided by Dr. Kenny Voon Gah Leong, Department of Medical Sciences, International Medical University (IMU), Malaysia. A total of 5 concentrations were used for eupatorin - 4.54, 9.08, 18.15, 36.30 and 72.61 µM; sinensetin concentrations were 4.20, 8.39, 16.78, 33.57 and 67.14 µM.

Small synthetic compound, tribenzyltin carboxylates 1 (TC1) and tribenzyltin carboxylates 4 (TC4) were provided by Dr. Kiew Lik Voon, Faculty of Medicine, Universiti Malaya (UM), Malaysia. Concentrations tested with TC1 were 0.06, 0.13, 0.25, 0.50 and 1.00 µM; TC4 were tested at 0.03, 0.06, 0.13, 0.25, 0.50 µM. The structures of the novel and synthetic compounds are shown in Appendix H.

Cells treated with the natural and synthetic compounds were incubated for 72 h and A_{570} readings were taken. Dose-response curves, relative fold-changes compared to the parental cells were determined as described in Section 3.9.1, page 90. The assay was performed in three independent experiments with triplicates.

CHAPTER 4

RESULTS

The main objective of this study was to establish an HPV-associated cell-based model by employing a normal immortalised keratinocyte (NIKS) cell line. NIKS cells were modified to harbour (i) the HPV16 whole genome (episomes) to represent the precancerous stage in the carcinogenesis of HPV-associated neoplasms, and (ii) HPV16 oncogenes, E6, E7 or E6E7, to represent the potentially cancerous stage. These HPV16 models were then examined by testing with two standard chemotherapeutic agents, cisplatin and topotecan to verify the reported increased chemo-sensitivity of HPV-positive cells compared to cells that do not harbour that HPV genome or oncogenes. Following this, the HPV16 models were further tested on two natural compounds, eupatorin and sinensetin, and two novel synthetic compounds, tribenzyltin carboxylates 1 (TC1) and 4 (TC4), for their potential cytotoxic effects on HPV16-associated cells in relation to unmodified parental cells.

4.1 Study Design

This study was divided into three parts to achieve the objectives (Figure 4.1):

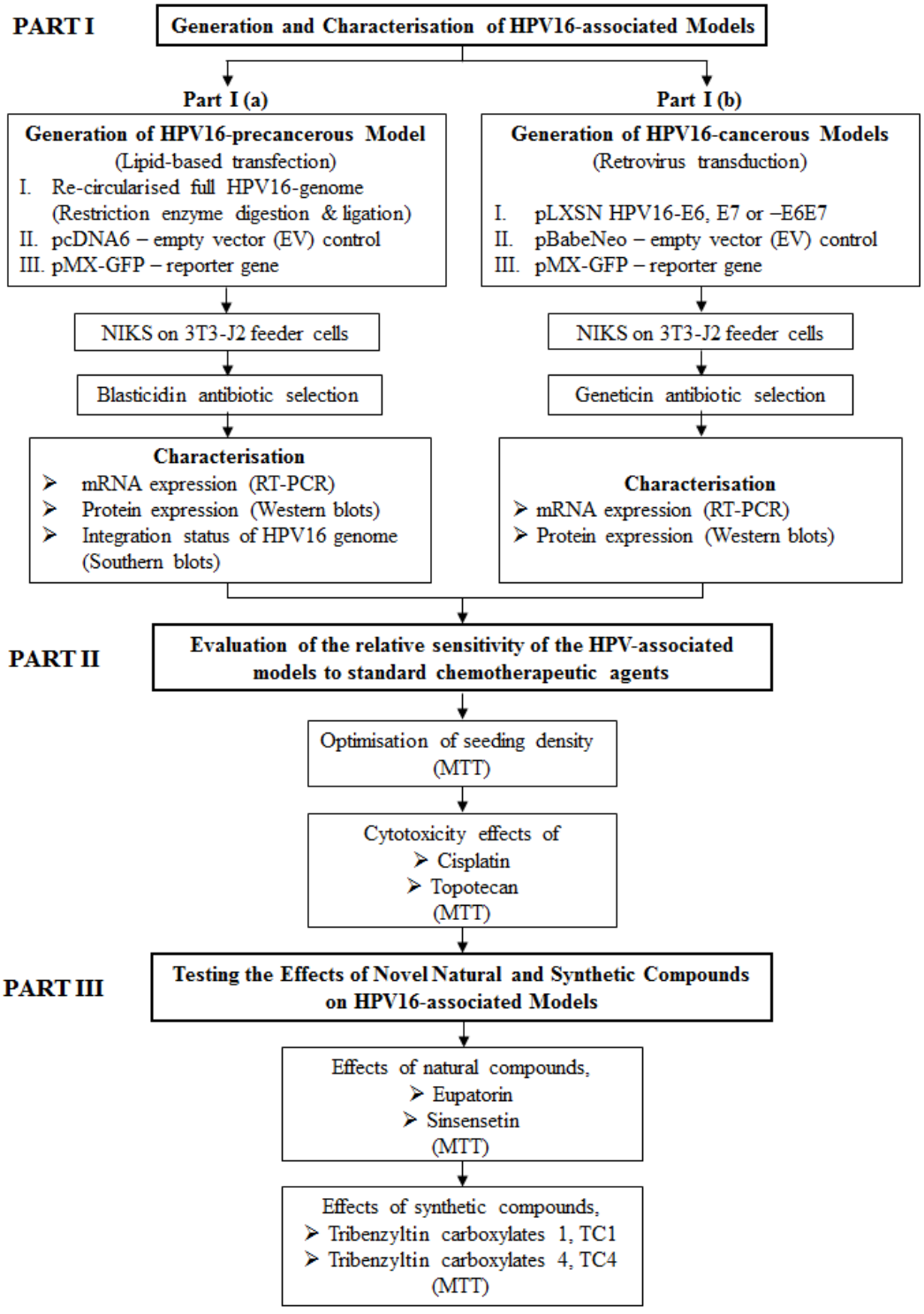

Figure 4.1 Overview of the study design. The study was divided into three main parts.

Part I:

Generation and characterisation of the HPV16-associated models

Part II:

Verification of the reported increased sensitivity of HPV-associated tumours relative to non-HPV associated tumours using the HPV16- models by testing with two standard chemo-therapeutic agents

Part III:

Testing the effects of novel natural and synthetic compounds on the HPV16-associated models.

Part I:

Generation and Characterisation of HPV16-Associated Models

Part I(a): HPV16 "Precancerous" Models (NIKS-HPV16$_{EPI}$)

4.2 Generation of the "Precancerous" Model

The HPV16 precancerous model was generated by re-circularising the HPV16-full genome excised from the pSPW12 plasmid and used subsequently to co-transfect NIKS cells together with pcDNA6, an empty vector (EV) which carry a blasticidin resistance gene. To confirm the presence of the HPV16 genome in the pSPW12 plasmid, it was digested with BamHI and electrophoresed on 1% agarose gel, which is expected to produce four fragments of distinct sizes. An 8-kb band indicates the presence of the HPV16 genome; vector-derived BamHI-digested fragments would include bands of 1.5 kb, 3.0

kb and 4.5 kb. A fifth fragment of ≥10-kb represents partially or undigested pSPW12 DNA. As demonstrated in Figure 3.1, Chapter 3, Section 3.5.1, all expected bands were present.

NIKS cell transfected with pMX-GFP were used for determining the success of transfection as well as an indication of transfection efficiency. The presence of signals (green fluorescence) in the transfected cells was indicative of successful transfection of the cells by pMX-GFP (Figure 4.2A, lower panel), and by inference successful transfection of the cells by the other plasmids (viz. pcDNA6 singly and in combination with the re-circularised HPV16 genome). In addition, the relative proportion of cells displaying the green signal provides a rough indication of the transfection efficiency. Increasing fluorescence signals were observed over time (24 to 72 hours, Figure 4.2A). This together with the results of phase microscopic examination of the cultured cells indicates proliferation of the transfected cells.

The negative control, in which DNA was omitted in the transfection mix, was set up to assess the effect if any of the transfection reagent on the cell viability. Results demonstrated in Figure 4.2B shows that there was no obvious effect on cell proliferation.

Cells successfully transfected with the empty vector (pcDNA6) as well as the co-transfected cells (HPV16 genome + pcDNA6) were selected by blasticidin. Figure 4.3 demonstrates that NIKS cells which harboured the pcDNA empty vector control, or co-transfected with pcDNA6 and the HPV16

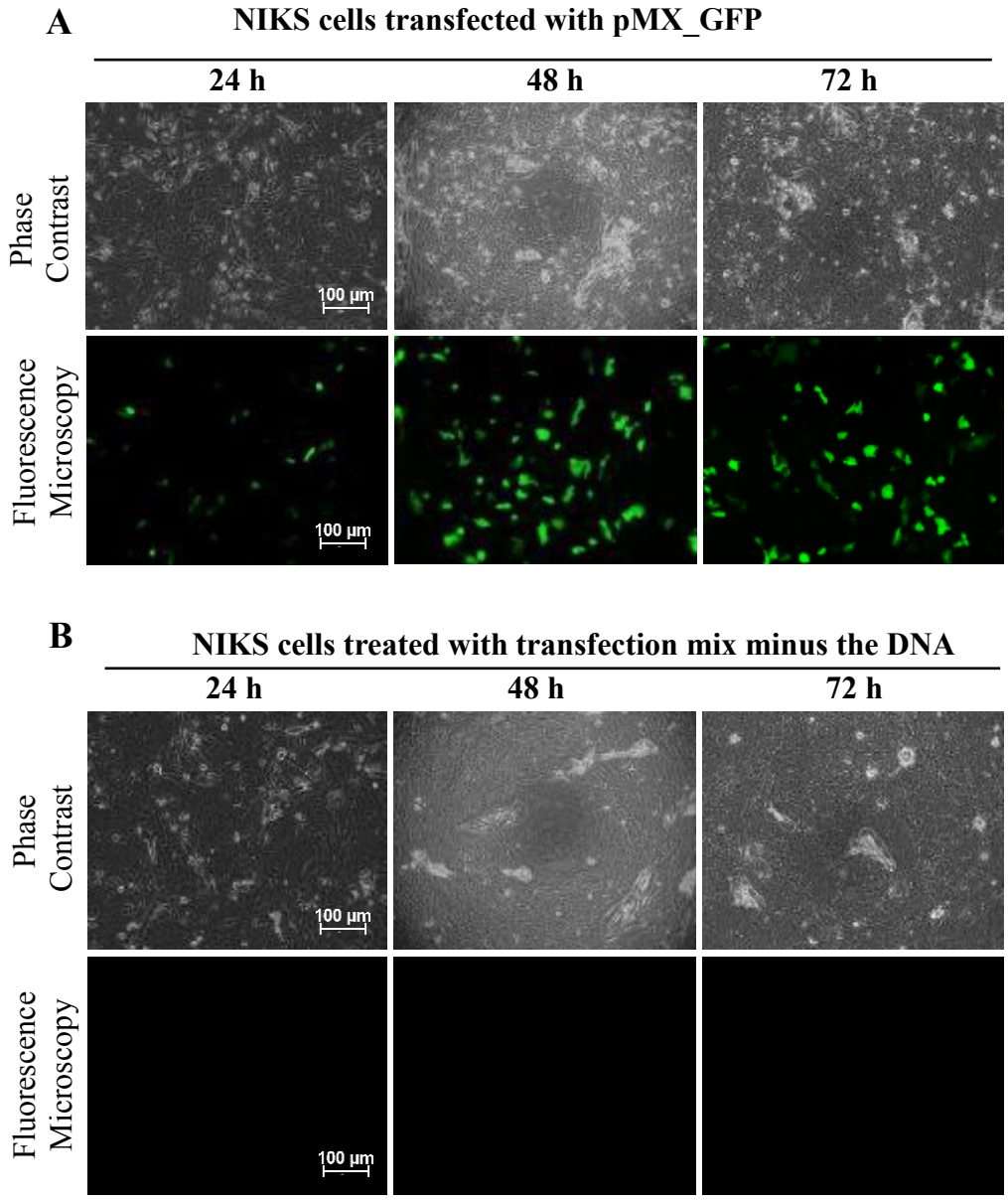

Negative cells were treated with the "blank" transfection mix

Figure 4.2 Microscopic images of NIKS cells. (A) NIKS cells transfected by the lipid-based method were monitored from 24 to 72 hours. (B) Fluorescent images of negative cells exclude the background auto-fluorescence. All images were photographed at 100X magnification.

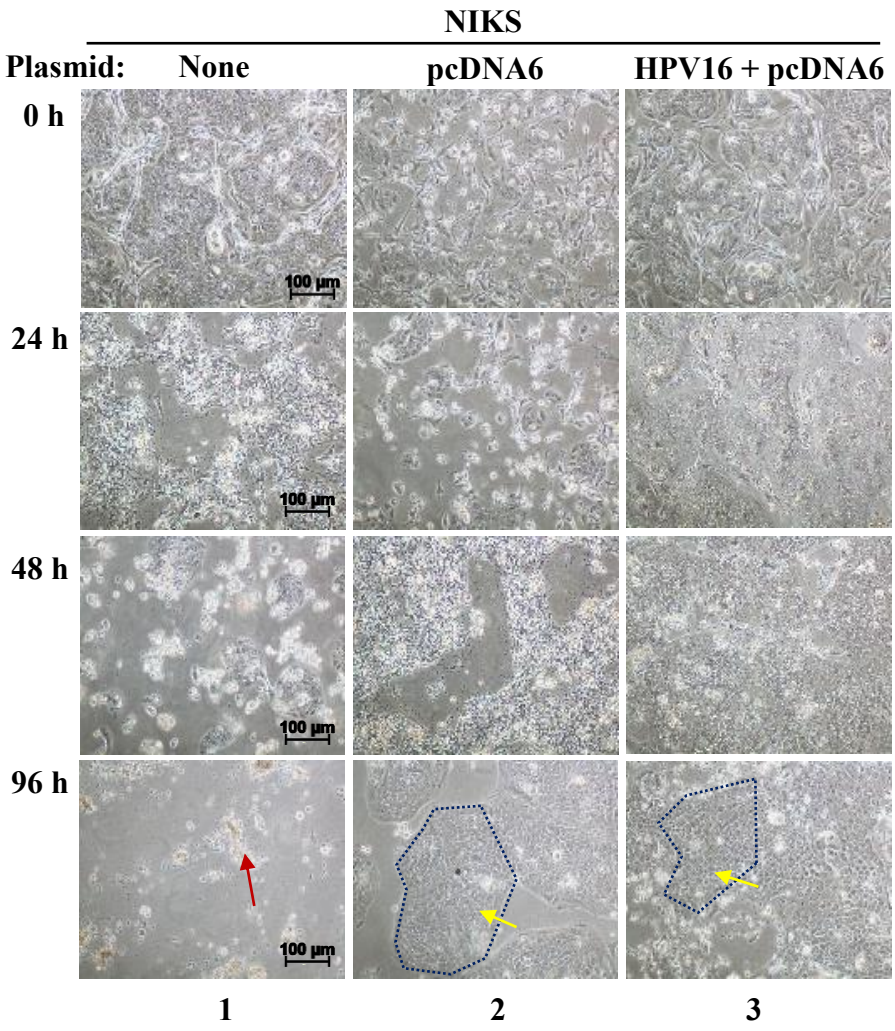

Figure 4.3 Morphology of blasticidin-treated HPV16 modified NIKS cells. After transfection, the cells were monitored for 96 h. Non-transfected parental NIKS cells (negative control) (column 1); NIKS transfected with pcDNA6 alone (column 2), or co-transfected with the HPV16 full genome (column 3). The parental NIKS cells were dead at 96 h as indicated by the formation of aggregated cells (red arrow). pcDNA6-transfected cells survived the blasticidin selection as indicated by the formation of distinct colonies of tightly-packed cells (circled by irregular blue-dashes). The negative control plate containing cells were dead at 96 h. Cell debris is indicated by yellow arrows. All images were taken at 100X magnification.

genome survived the blasticidin selection. The negative control plate containing the non-transfected parental cells were detached and aggregated at 96 h as they were not able to survive in the presence of blasticidin. Transfected cells with the full HPV16 genome were morphologically similar to the parental cells with tightly packed cells. However, HPV16-harbouring cells showed higher proliferative capacity. Taken together, the results indicated that NIKS cells were successfully modified to harbour the HPV16 genome.

4.3 Characteristics of the Transfected Cells

The purpose of the study was to generate a NIKS cell model to carry HPV16 episomes to represent the precancerous stage of HPV16-associated neoplasms. Therefore, it is essential to confirm that the HPV16 genome is maintained in the episomal form. This was demonstrated by Southern analysis of cells from passage 5 through to 30. Cells from these passages were also studied with respect to the E6 and E7 transcription and expression status as detailed in Section 4.3.1 and 4.3.2 below.

4.3.1 HPV16 Genome Integration Status

Southern blot analysis was carried out to investigate the HPV16 integration status in NIKS cells transfected with the HPV16 genome (Figure 4.4). HPV16 DNA was maintained in an episomal state indicated by the presence of 8-kb bands in cells from passage (P) 5 to 21 and genome integration appeared to have occurred thereafter up to passage 26 and 30. Multiple forms

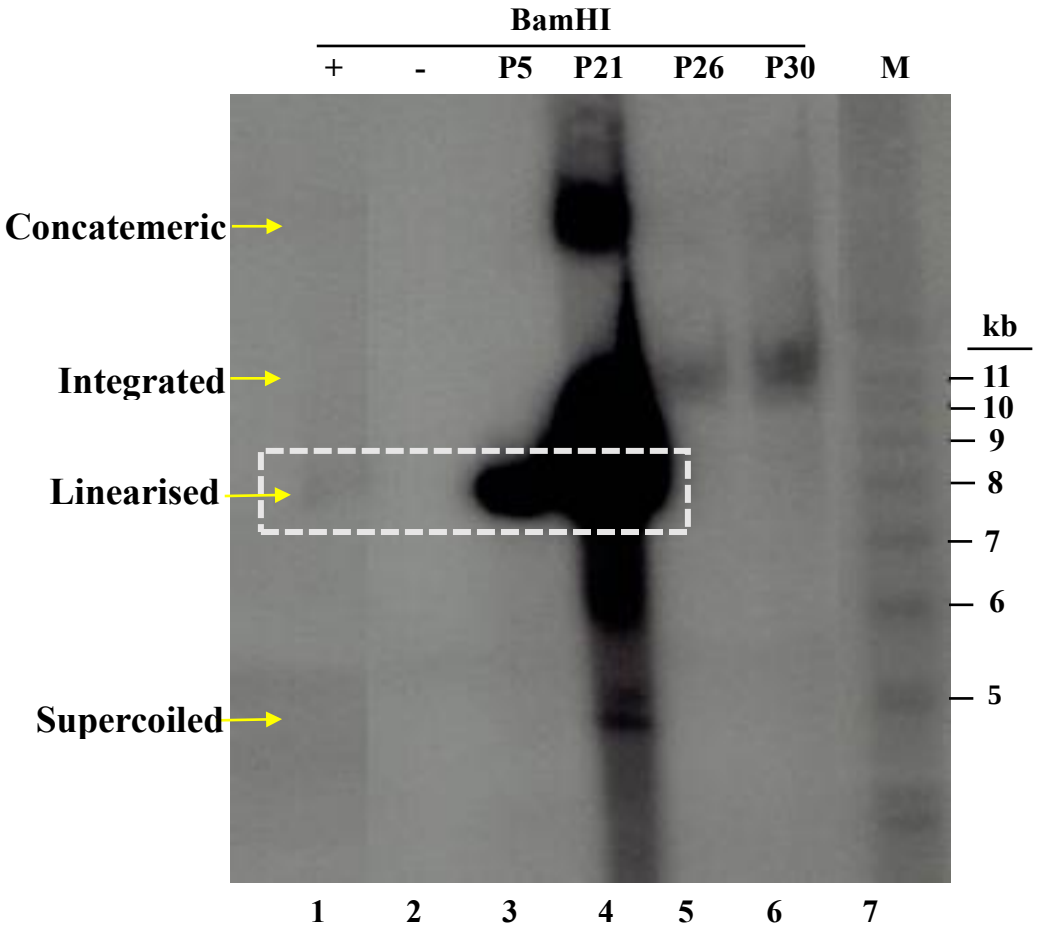

Figure 4.4 Southern blot analysis of NIKS cells transfected with HPV16 genome. Total genomic DNA from NIKS transfected with the full HPV16 genome at passage (P) 5, 21, 26 and 30 (lanes 3-6), was subjected to BamHI digestion before Southern blot analysis using a 32^{P}-labelled HPV16 probe. Lane 1, positive control, re-circularised HPV16 genome; lane 2, negative control, NIKS transfected with pcDNA digested with BamHI; (single-cut). DNA ladder are indicated in kilobases (kb) in lane 7. White dotted box indicates the 8-kb bands. The various HPV16 DNA forms are indicated by yellow arrows. Non-integrated but linearised HPV16 at P5 and P21 was 8 kb; integrated HPV16 at P26 and P30 was > 10 kb.

of the HPV16 DNA were identified: linearised HPV16 DNA was detected at P5; concatenated and supercoiled forms were found in addition at P21. In summary, HPV16 transfected cells at P5 to P21 maintained the HPV16 in episomes, and these cells were used in the subsequent experiments as the drug-testing models.

4.3.2 E6 and E7 mRNA Transcription Status

To detect the HPV16 E6 and/or E7 mRNA expression in the HPV16-transfected NIKS cells, RT-PCR was performed by using the total mRNA extracted from the transfected cells from P5 to P30. As shown in Figure 4.5A, the expected bands were observed in the 117-bp region for E6 and the 92-bp region for E7 indicating transcription of the genes by the HPV16 in NIKS cells. The loading control, GADPH as expected produced a band at 274 bp; in addition, there were no positive signals observed in the lane without HPV16 template. HPV16-E6 and E7 genes were invariably expressed in all the cell passages 5 to 30 regardless of the status of the HPV16 genome. Refer to Section 4.3.1 regarding the episomal versus the integration status of the HPV.

4.3.3 E6 and E7 Protein Expression Status

To confirm the HPV16 E6 and E7 protein expression in the HPV16-transfected NIKS cells, western blot analysis using HPV16 E6 or E7 antibodies was carried out on cells lysates of HPV16-transfected NIKS cells from P5 to 30. HPV16 E6 and E7 proteins were found to be expressed in all the passages (Figure 4.5B). The HPV16 E6 protein was detected at 17 kDa and E7 protein at

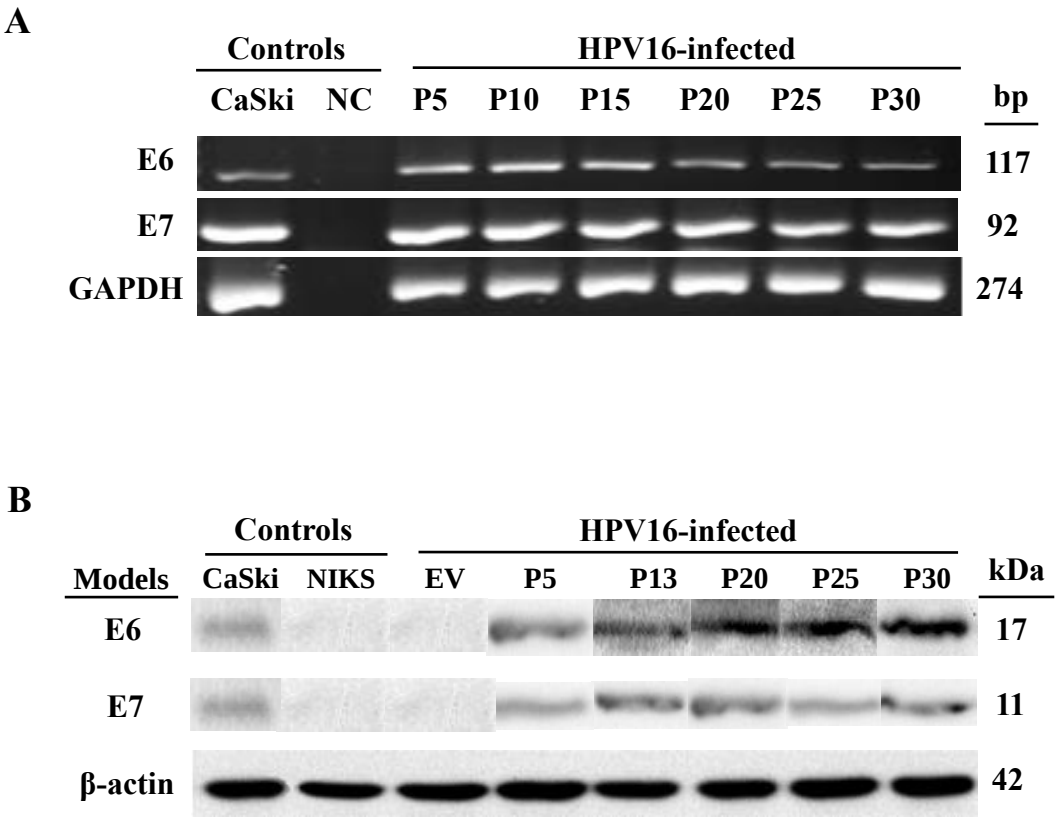

Figure 4.5 Expression of E6 and E7 in NIKS cells transfected with the HPV16 genome from passage (P) 5 to 30. (A) E6 and E7 mRNA expression detected by RT-PCR. NC, negative control without template; GADPH was used as a loading control. The agarose gel pictures are attached in Appendix I – K. (B) E6 and E7 protein levels detected by anti-E6 or -E7 antibodies in western blot analysis. β-actin was used as a loading control, and CaSki as HPV16 positive control. EV, empty vector control.

11 kDa. The β-actin loading control was detected at 42 kDa. No signal was detected in the parental cells (NIKS) and NIKS transfected with the empty vector, (pcDNA6) cells. The E6 proteins were expressed with increasing band intensity but E7 proteins at similar levels. These results indicate that the HPV16 precancerous model was successfully generated by lipofectamine transient transfection. The transfected NIKS cells carrying the HPV16 episomes expressed the E6 and E7 oncogenes at both the mRNA and protein levels.

Part I(b): HPV16 "Cancerous" Models (NIKS-HPV16$_{INT}$)

4.4 Production of E6, E7 or E6E7 Retroviruses

To generate the HPV16 cancerous models, HPV16 E6, E7 or E6/E7 genes were inserted into the genome of the NIKS cells. This was achieved by retroviruses infection. The recombinant retroviruses harbouring HPV16 E6, E7 or E6E7 retrovirus were produced by transfecting Phoenix cells, and using GFP transfection as the control to indicate successful transfection and the efficiency of transfection (Figure 4.6A). When the green fluorescence protein (GFP) signals were monitored over time, the fluorescence intensity was found to gradually increase from 24 to 72 h post-transfection, indicating the active cellular proliferation of the transfected cells over this period of time. Fluorescent signal was absent in the negative-control well (Figure 4.6B). The brightest GFP signal was achieved at 72 h.

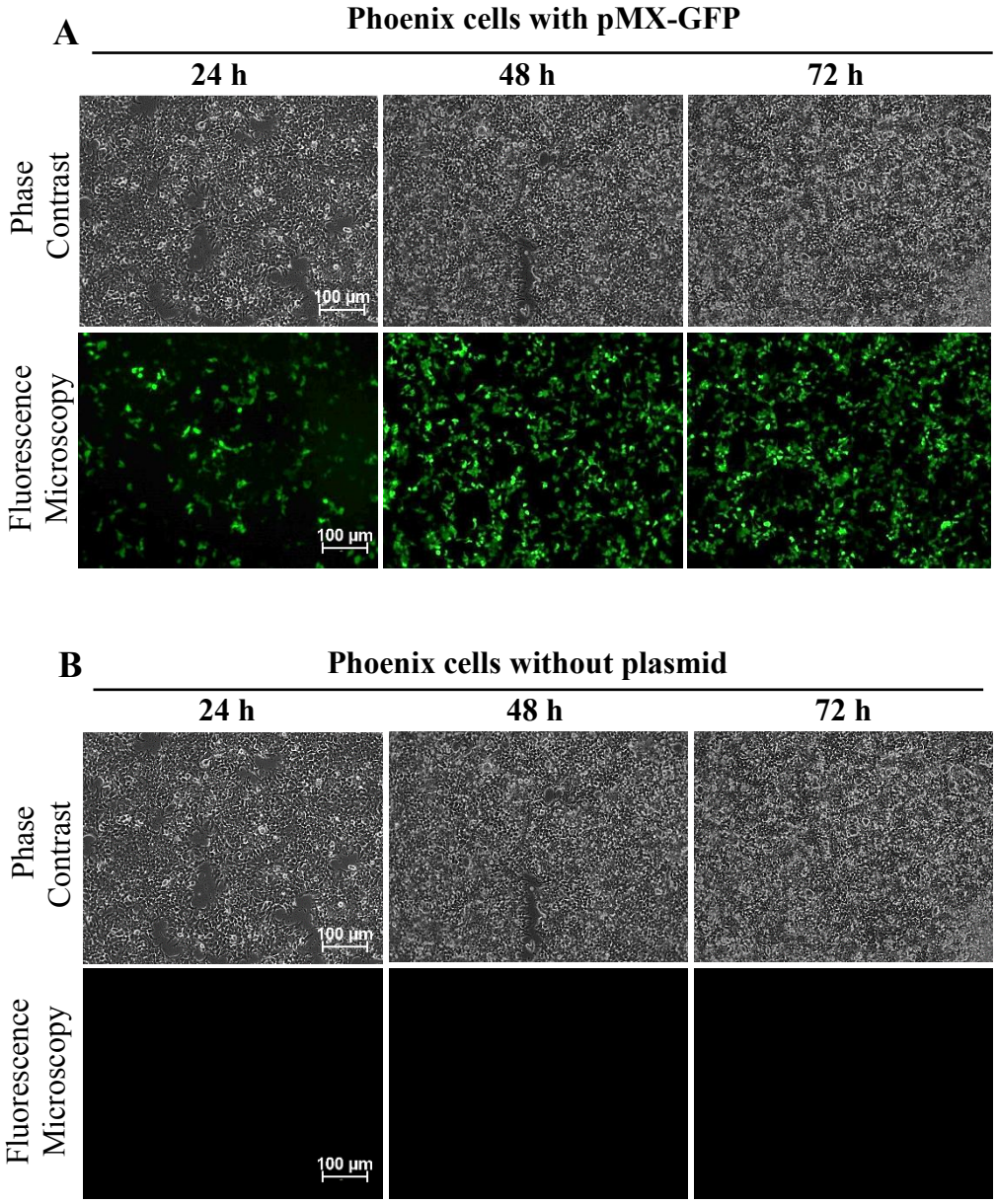

Negative cells were treated with the "blank" transfection mix

Figure 4.6 Morphology and GFP-staining of transfected Phoenix cells. Transfection was carried out by the calcium-phosphate method and the cells were monitored for 72 h. (A) Phoenix cells transfected with the pMX-GFP plasmid, which served as a positive control. (B) Transfection of Phoenix without pMX-GFP as negative control. All images were taken at 100X magnification.

4.5 Generation of the Cancerous Models

To introduce HPV16 E6, E7 or E6/E7 genes into the NIKS cells, retroviruses harbouring individual HPV16-oncogenes were collected from the transfected Phoenix cells and were used to further transduce the NIKS cells. Similarly, NIKS cells were transduced with the GFP-harbouring virus as the positive control to indicate positive transduction as well as its efficiency. Fluorescence intensity increased from 24 to 72 h in the GFP transduction plates (Figure 4.7A), whereas fluorescence was absent in the negative-control plates (Figure 4.7B).

The transduced cells underwent geneticin selection to pick out the authentic positive clones (Figure 4.8). NIKS cells harbouring pBABE-neo, an empty vector control, or vectors that carried the HPV16 E6, E7 or E6E7 genes expressed the neomycin-resistance gene and survived the geneticin selection. In the negative-control plate, NIKS cells were dead and cell detachment was observed at 96 h. As shown in Figure 4.8, the surviving transduced cells appeared as distinct cell colonies of tightly packed cells (circled in blue-dashes). Dead cells and cell debris are indicated by red and yellow arrows respectively. Transduced cells appeared to have a similar morphology to the parental cells, with round edges but at higher proliferative capacity. Taken together, HPV16 cancerous models, which harboured the HPV16 E6 and/or E7 oncogenes, were successfully generated using the NIKS cells.

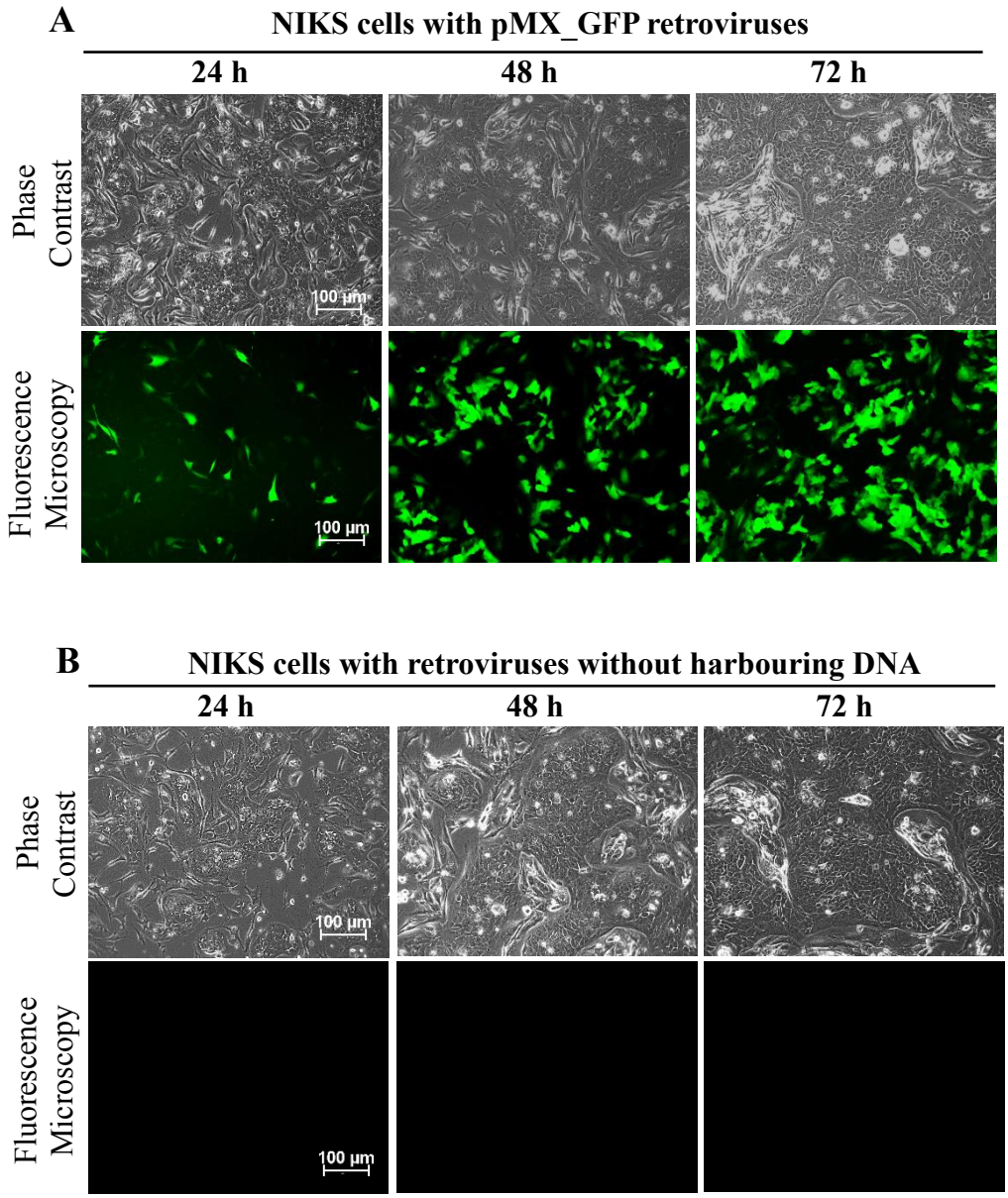

Figure 4.7 Post-transduction of NIKS cells from 24 to 72 h. (A) NIKS cells transduced with the pMX-GFP retrovirus as a positive control. (B) Transduction of Phoenix without pMX-GFP retrovirus as a negative control. All images were taken at 100X magnification.

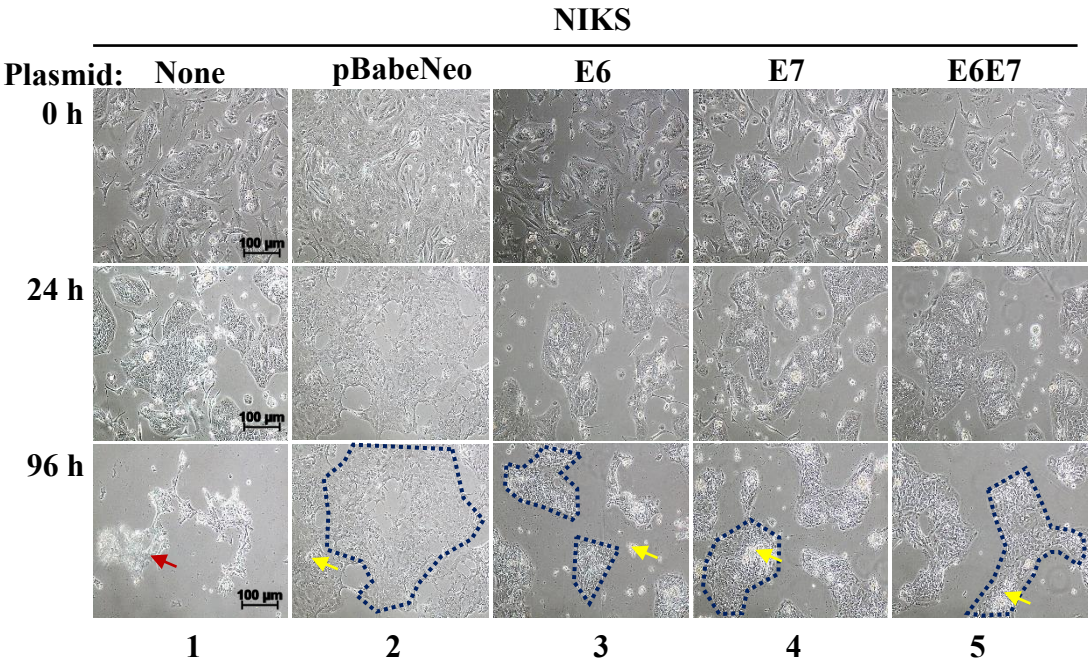

Figure 4.8 Geneticin treatment of the HPV16-cancerous model. Shown in the figure are: non-transfected parental NIKS (column 1); NIKS transduced with pBabeNeo, the empty vector control (column 2), HPV16-E6 (column 3), HPV16-E7 (column 4) or HPV16-E6E7 (column 5). Morphology changes of the cells were monitored for 72 h. Dead NIKS cells at 96 h are indicated by formation of aggregated cells (red arrow). Cells that survived the geneticin selection are indicated by the formation of distinct colonies of tightly-packed cells (irregular blue-dashed circle). Cell debris is indicated by yellow arrows. All images were taken at 100X magnification.

4.6 Characteristics of Transduced Cells

4.6.1 E6 and E7 mRNA Transcription Status

To detect the HPV16 E6, E7, or E6E7 mRNA expression in the HPV16-transduced NIKS cells, RT-PCR was performed by using the total mRNA extracted from the transduced cells from P5 to P30. HPV16 E6, E7 or E6/E7 mRNA was found to be stably expressed in all the passages (Figure 4.9A). The E6E7 co-expression was shown by the simultaneous presence of E6 PCR bands at 117 bp and E7 bands at 92 bp (Figure 4.9A) indicating that both E6 and E7 genes were transcribed in the transduced NIKS cells up to passage 30. Similar results were observed in the NIKS cells harbouring the E6 or E7 gene alone.

4.6.2 E6 and E7 Protein Expression Status

To confirm the expression of E6 and E7 proteins in the HPV16-transduced NIKS cells, western blot analysis of the E6 and E7 proteins was carried using cell lysates prepared from HPV16-transduced NIKS cells from P5 to 30. The E6 protein bands were detected at 17 kDa and E7 at 11 kDa, the β-actin protein was used as the loading control. The HPV16 E6 and E7 proteins were expressed in all the passages (Figure 4.9B) and no signal was detected in the parental NIKS cells and the empty vector (EV) control cells transfected with pBABE-neo. The HPV16 E6 transduced cells at passage (P) 20 to 30 showed increasing intensity of the E6 protein band; a similar observation was present for E7 of the HPV16 E7-transduced cells probed with an E7 antibody (Figure

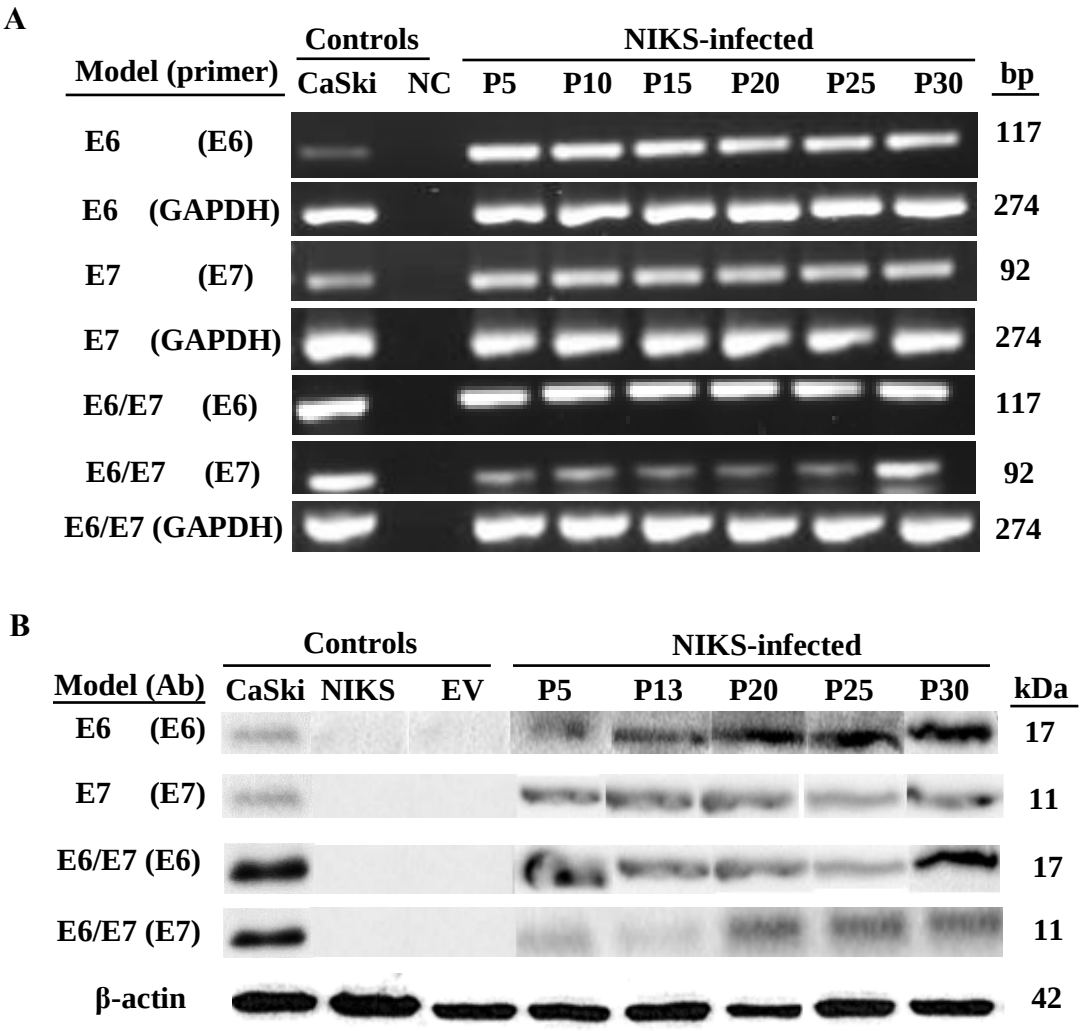

Figure 4.9 Expression of E6 and E7 mRNA and protein in NIKS transduced with HPV16 E6, E7 or E6/E7 genes. Cells were monitored from passage (P) 5 to 30 post-transduction. (A) E6 and E7 mRNA transcription detected by RT-PCR using the indicated primers. NC, negative control without template. GADPH was used as a loading control. The agarose gel pictures are attached in Appendix L - R. (B) E6 and E7 protein expression detected by western blot analysis using the indicated antibodies (Ab). β-actin was used as a loading control; Caski was used as HPV16-positive control. EV, empty vector control.

4.9B, first and fourth rows). In contrast, HPV16 E7-transduced cells probed with an E7 antibody showed uniform E7 protein expression in all the passages (Figure 4.9B, second row). An increase in the protein band intensity in the HPV16 E6E7-transduced cells detected with an E6 antibody at P30 (Figure 4.9B, third row) was also observed. In brief, HPV16 cancerous models were successfully generated using the calcium-phosphate direct transfection method. NIKS cells were able to stably express the E6, E7 or E6/E7 genes at the mRNA and protein levels in the culture up to 30 passages.

Part II:

Verification of the Reported Increased Chemosensitivity of HPV-associated Tumours Compared to Non-HPV associated Tumours using the HPV16 models

4.7 Optimal Seeding Densities of the Cell Lines

To determine the optimal cell seeding densities of NIKS cells in the HPV16 models, the respective cells were seeded at different initial seeding density and cell viability was assessed every 24-h for four-days. The cell-growth kinetics of the HPV16 precancerous models is shown in Figure 4.10 and the cancerous models in Figure 4.11. The growth curves of the NIKS cells revealed that cells seeded at lower seeding densities ($0.5 – 1.0 \times 10^4$ cells/ well) proliferated at slower rate compared to other cell seeding densities tested, but the cells maintain exponential growth up to day 4 of the culture for both precancerous and the cancerous models. In contrast, cells seeded at higher

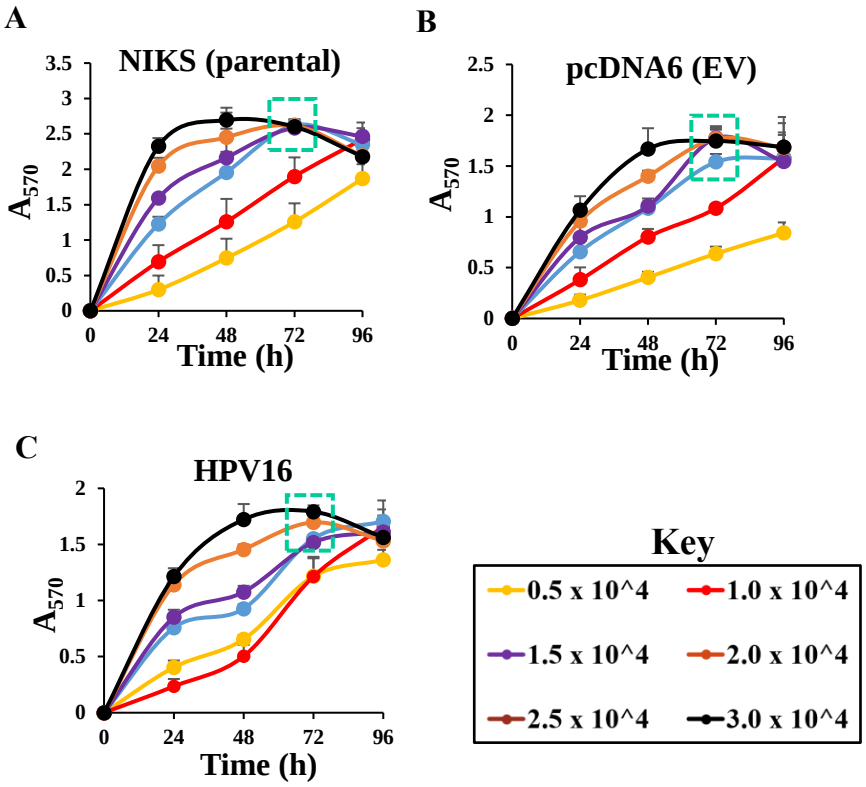

Figure 4.10 Cell proliferation of the HPV16 precancerous model. (A) Non-transduced NIKS cells; (B) NIKS cells transduced with pcDNA6; (C) NIKS cells transduced with the HPV16 genome. The post-seeded cells were incubated for 96 h, and absorbance values at 570 nm (A_{570}) were read for each time point. The different seeding cell densities are indicated by different colour lines. The saturation cell densities are marked by the boxes (dashed lines). Data were from three independent experiments performed in triplicate.

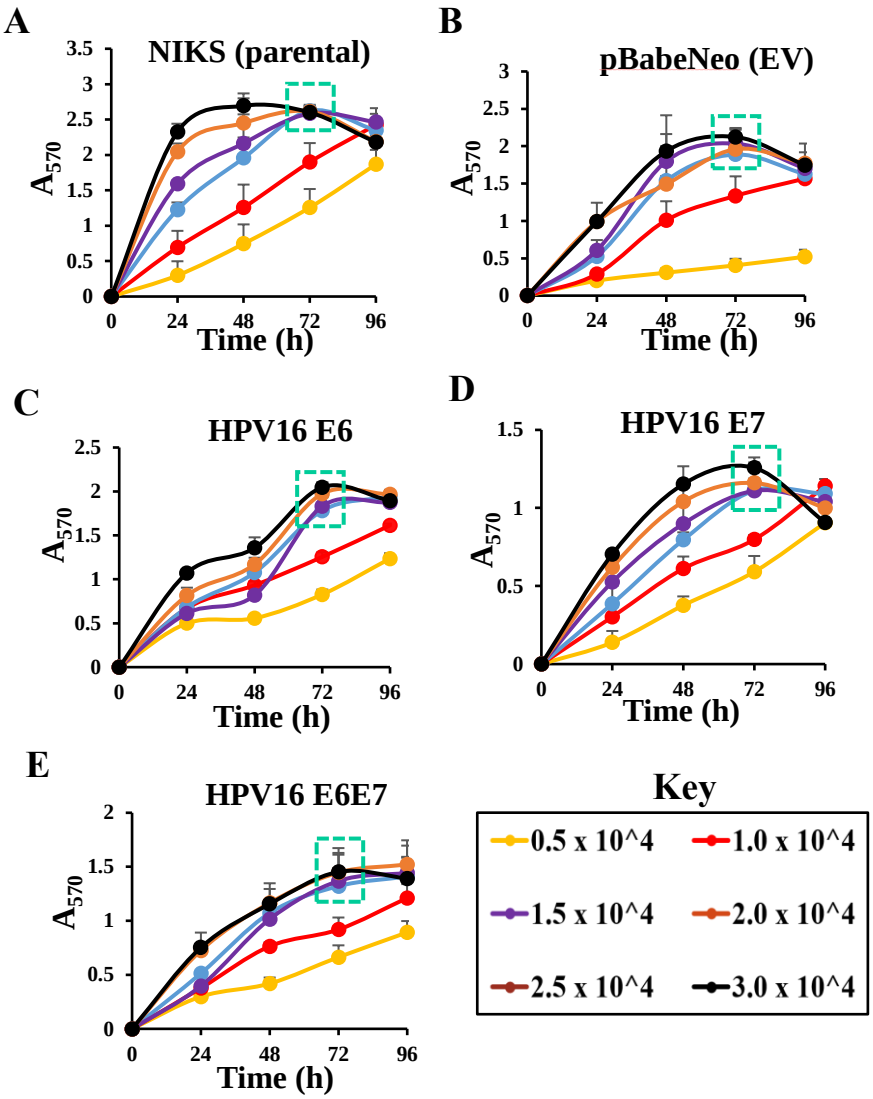

Figure 4.11 Cell proliferation of the HPV16 cancerous models. (A) Non-transduced NIKS cells; NIKS cells transduced with (B) pBabeNeo; (C) HPV16-E6; (D) HPV16-E7 or (E) HPV16-E6E7. The post-seeded cells were incubated for 96 h, and absorbance values at 570 nm (A_{570}) were read. The different seeding cell densities are indicated by different colour lines. The saturation cell densities are marked by the boxes (dashed lines). Data were from three independent experiments performed in triplicates.

seeding densities (1.5 – 3.0 x 10^4 cells/ well) achieved cell saturation at 72 h as indicated in both Figures 4.10 and 4.11. Subsequently, cell viability was reduced at 96 h. Similar growth-curve profiles were observed in both the HPV16 precancerous and cancerous models (Figures 4.10 & 4.11). Cell-cell interactions at the 1 x 10^4 cells/well seeding density appeared to be better compared to 0.5 x 10^4 cells/well based on microscopic observations. Therefore, cell seeding density at 1 x 10^4 cells/well was used in subsequent experiments.

4.8 Cytotoxic Effects of Cisplatin

To study the relationship between the effects of standard chemotherapeutic agents on the HPV16-associated models and to determine whether the reported increased sensitivity of HPV-associated neoplasms compared to non-HPV associated neoplasms can be verified *in vitro*, cytotoxicity profiles of the HPV16 models were established. The cell models were treated with increasing concentrations of cisplatin (Figures 4.12A & 4.12B) and the cell viabilities related to the HPV negative controls were monitored post-treatment.

Cisplatin treatment resulted in significant effects on the cell viability of the HPV16 models in a dose-dependent manner (Figures 4.12A & 4.12B, top panels). The half-maximal inhibition concentration (IC_{50}) values of cisplatin for the HPV16 precancerous model was 5.612 ± 0.268 µM whereas that for the cancerous models, were 4.360 ± 0.462, 4.134 ± 0.334 and 4.566 ± 0.362 µM respectively for cells harbouring the E6, E7 and E6E7 (Table 4.1).

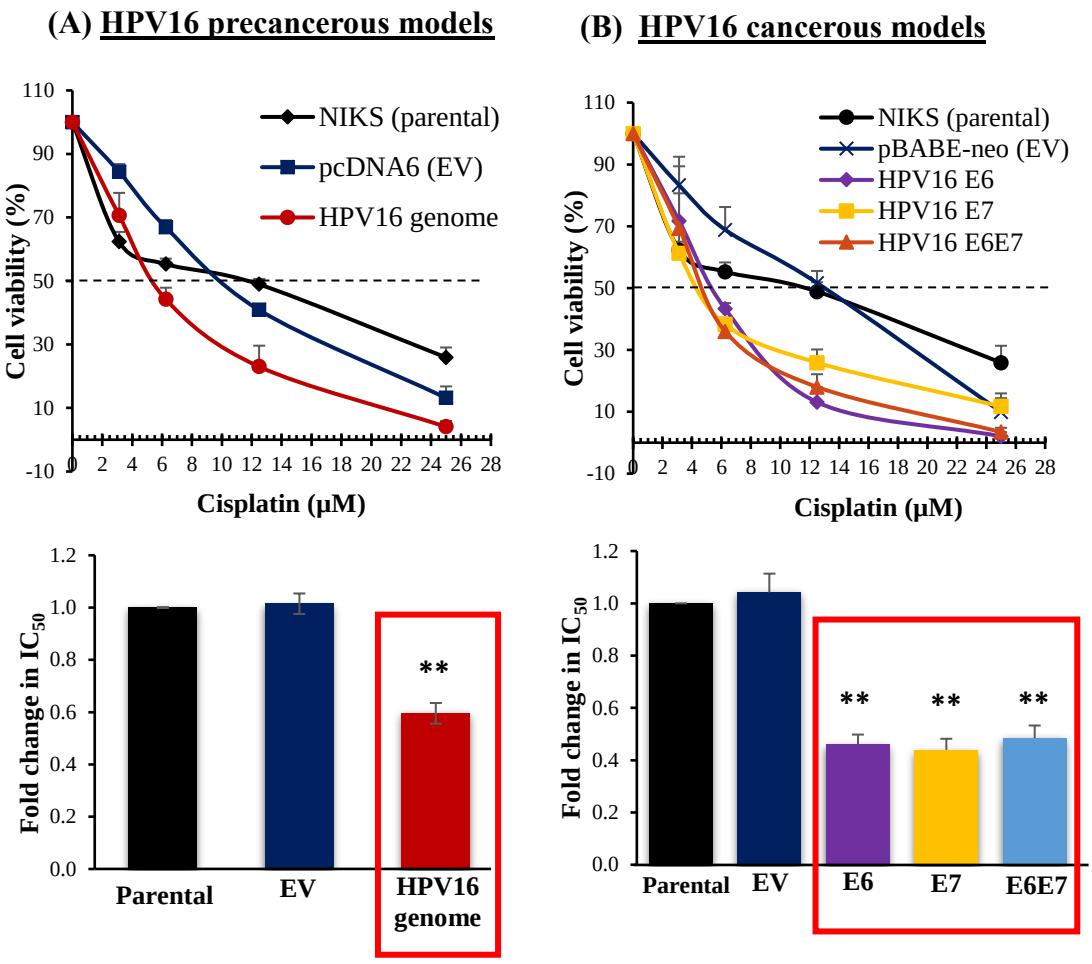

Figure 4.12 Cisplatin-induced inhibition of cell growth on the HPV models.

(A) HPV16 precancerous models; (B) HPV16 cancerous models. Dose-response curves (top panel) were generated from the parental NIKS cells and HPV16 models by determining cell viability with exposure to various concentrations of cisplatin (0.281 – 2.250 μM) at 72 h post-drug treatment. Fold-change bar charts (bottom panel) were derived from NIKS, normalised to 1.0, compared with the HPV16-models. Results are expressed as means ± standard error of means (SEM) of three independent experiments performed in triplicates. *$p \leq 0.05$ and **$p \leq 0.01$ vs. parental, NIKS.

Table 4.1 Cytotoxic effects of cisplatin and topotecan on the HPV16 models

		Precancerous		Cancerous			
	NIKS	pcDNA6	HPV16 genome	pBABE-neo	HPV16 E6	HPV16 E7	HPV16-E6E7
Cisplatin							
IC_{50} ± SEM (μM)	9.454 ± 0.211	9.594 ± 0.431	5.612 ± 0.268	9.713 ± 0.541	4.360 ± 0.462	4.134 ± 0.334	4.566 ± 0.362
Fold change in IC_{50}	1.0	1.0	**1.7 ****	1.0	**2.2 ****	**2.3 ****	**2.1 ****
Topotecan							
IC_{50} ± SEM (μM)	0.456 ± 0.015	0.445 ± 0.010	0.329 ± 0.005	0.473 ± 0.012	0.197 ± 0.023	0.030 ± 0.003	0.241 ± 0.023
Fold change in IC_{50}	1.0	1.0	**1.4***	1.0	**2.3 ****	**15.2 *****	**1.9 ***

The cytotoxic effects were determined by MTT. pcDNA6 and pBABE-neo were empty vector controls; IC_{50}, half-maximal inhibitory concentration; SEM, standard error of means. The numbers shown in bold are fold-change in IC_{50} of HPV16 models, respectively. Data shown are cumulative data of three independent experiments performed in triplicates. *$p \leq 0.05$, **$p \leq 0.01$ and ***$p \leq 0.001$ were derived from comparison of data between the parental NIKS cells vs. the HPV16-models.

Cisplatin treatment yielded statistically significant growth inhibition on all the HPV16 models (Figures 4.12A & 4.12B, bottom panels highlighted with red boxes). NIKS cells harbouring the E7 gene were most sensitive to cisplatin treatment with a 2.3-fold decrease in IC_{50} compared to parental cells, followed by NIKS cells harbouring the E6 and E6E7 with 2.2-fold and 2.1-fold decreases, respectively (Table 4.1). Among the HPV16 models, NIKS cells carrying the full HPV16 genome was least sensitive to cisplatin treatment with only a 1.7-fold decrease in IC_{50} compared to the parental cells.

The calculated fold changes were consistently greater in the HPV16 models indicating that cisplatin was more cytotoxic towards HPV16-positive cells than the HPV16-negative parental cells, consistent with previous clinical observations (Thomas et al., 2016; Ziemann et al., 2015; Das et al., 2014). The cisplatin sensitivity of the HPV16-associated models observed in this study was higher when either the E6 or the E7 gene was present alone, compared to when E6E7 were co-expressed.

4.9 Cytotoxic Effects of Topotecan

Next, another standard chemotherapeutic agent, topotecan, was used to further confirm the chemosensitivity of the HPV16-containing cells. The dose-response curves following topotecan treatment showed that topotecan inhibited the proliferation of HPV16 model cells in a dose-dependent manner (Figures 4.13A &

4.13B, top panels). Topotecan treatment exerted the greatest growth inhibition on NIKS cells harbouring the E7 gene with IC_{50} at 0.030 ± 0.003 µM compared to that of the parental cells at 0.456 ± 0.015 µM (Table 4.1). Comparatively inhibition of the NIKS cells carrying E6, E6E7 and the full HPV16 genome was much lower with IC_{50} values of 0.197 ± 0.012 µM, 0.241 ± 0.023 µM and 0.329 ± 0.005 µM, respectively compared to the parental cells (0.456 ± 0.015 µM).

The HPV16 precancerous and cancerous models were significantly more sensitive to topotecan treatment than the parental cells (red boxes, Figures 4.13A & 4.13B, bottom panels). HPV16 genome-containing NIKS (precancerous model) cells were more sensitive to topotecan treatment with a 1.4-fold decreased in IC_{50} compared to the parental cells (Table 4.1). On the other hand, in the cancerous models, NIKS cells harbouring the E7 genes showed very high sensitivity towards topotecan treatment with 15.2-fold decrease in IC_{50} compared to the parental cells, followed by E6 and E6E7-containing NIKS cells which showed 2.3-fold and 1.9-fold decrease indicating rather modest sensitivity to topotecan treatment.

Therefore, the HPV16 models were more sensitive to topotecan compared to the parental cells with significant reduction in cell viability after topotecan treatment. Similar to the cisplatin treatment, NIKS cells harbouring the HPV16 E6 or E7 gene alone possessed higher topotecan sensitivity compared to NIKS cells co-expressing E6 and E7.

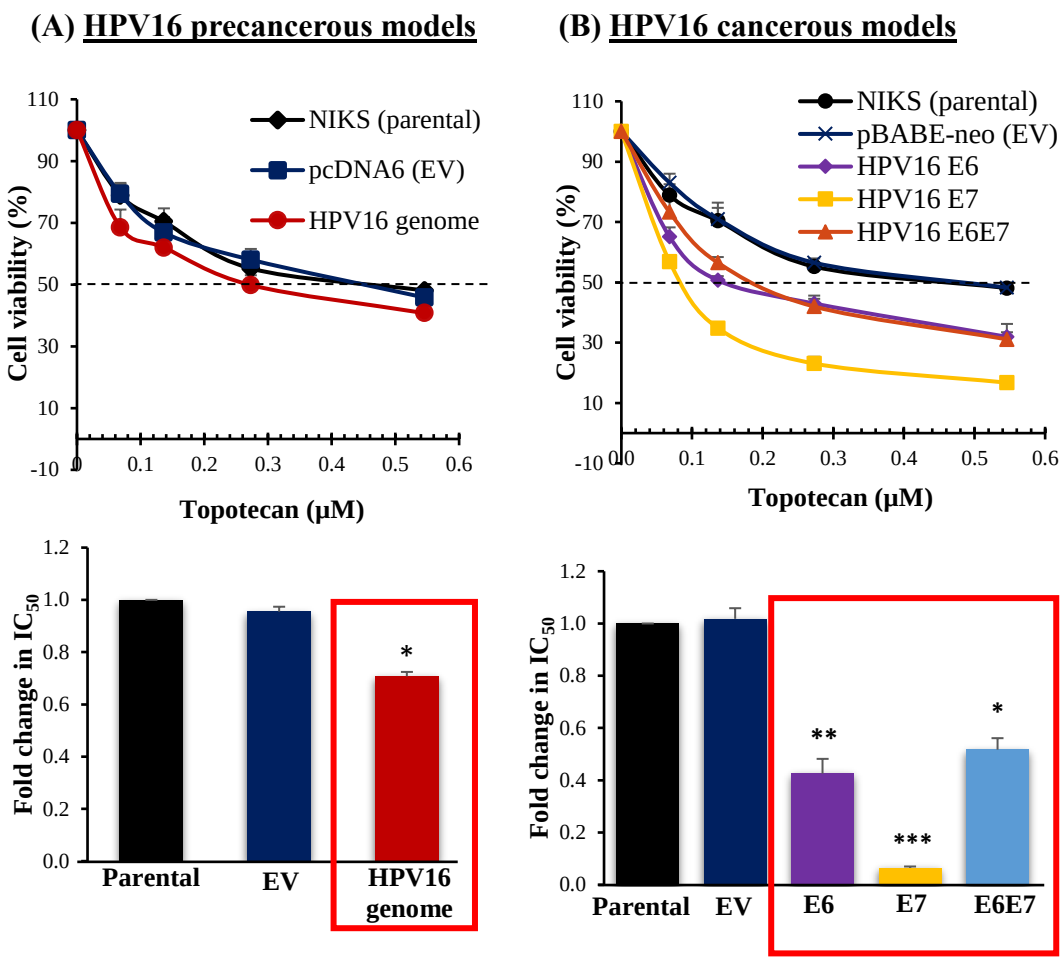

Figure 4.13 Topotecan-induced inhibition cell growth inhibition on the HPV models. (A) HPV16 precancerous models; (B) HPV16 cancerous models. Dose-response curves (top panel) were generated from the parental NIKS cells and HPV16 models by determining cell viability with exposure to various concentrations of topotecan (0.014 – 0.114 µM) at 72 h post-drug treatment. *$p \leq 0.05$, **$p \leq 0.01$ and ***$p \leq 0.001$ vs. parental, NIKS. See also legends to figure 4.12.

Part III:

Effects of Selective Novel Natural and Synthetic Compounds on the HPV16-associated Cell Lines

4.10 Effects of Eupatorin

To examine the potential cytotoxic effects of the natural flavonoid compound, eupatorin, on the HPV16 models, MTT assay was performed after the cells were treated with various concentrations of eupatorin. Eupatorin treatment also reduced cell viability in a dose-dependent manner (Figures 4.14A & 4.14B, top panels). Eupatorin treatment displayed the highest and significant anti-proliferative activity on NIKS cells expressing the E7 gene followed by E6 gene, with IC_{50} values of 6.411 ± 0.595 µM and 14.743 ± 1.744 µM, respectively compared to the parental cells at 24.573 ± 1.190 µM (Table 4.2). Both the E6E7 and HPV16 genome containing NIKS cells showed similar IC_{50} values at 21.216 ± 1.175 µM and 20.666 ± 1.357 µM, respectively.

For comparison, the sensitivity of each HPV16 models was expressed in fold change in IC_{50} values as shown in Figure 4.14A to 4.14B, bottom panels, and cells that showed statistical significance are highlighted in red boxes. The precancerous models, NIKS cells harbouring the HPV16 genome was not sensitive towards eupatorin treatment with a 1.2-fold decrease in IC_{50} compared to the parental cells, which is statistically not significant. A similar result was obtained

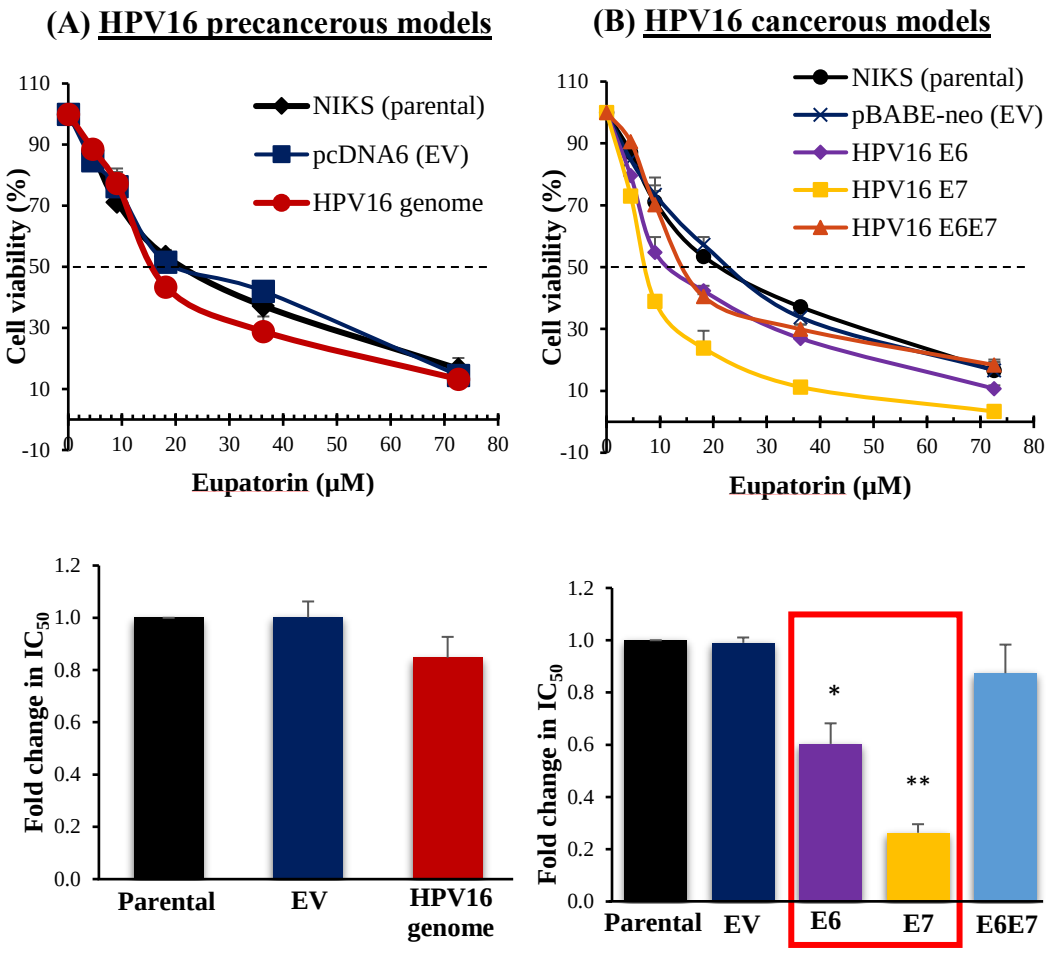

Figure 4.14 Effects of eupatorin on cell growth of the HPV models. (A) HPV16 precancerous models; (B) HPV16 cancerous models. Dose-response curves (top panel) were generated from the parental NIKS cells and HPV16 models by determining cell viability following exposure of eupatorin at different concentrations (0.538 – 8.608 µM) at 72 h post-drug treatment. Fold-change bar charts (bottom panel) were derived from NIKS, normalised to 1.0, compared with the HPV16-models. Results are expressed as means ± standard error of means (SEM) of three independent experiments performed in triplicates. *$p \leq 0.05$ and **$p \leq 0.01$ vs. parental.

Table 4.2 Effects of the natural compounds, eupatorin and sinensetin on the HPV16 models

		Precancerous		Cancerous			
	NIKS	pcDNA6	HPV16 genome	pBABE-neo	HPV16 E6	HPV16 E7	HPV16 E6E7
Eupatorin							
IC_{50} ± SEM (μM)	24.573 ± 1.190	24.459 ± 0.362	20.666 ± 1.357	24.282 ± 0.725	14.743 ± 1.744	6.411 ± 0.595	21.216 ± 1.715
Fold change in IC_{50}	1.0	1.0	**1.2**	1.0	**1.7 ***	**3.8 ****	**1.2**
Sinensetin							
IC_{50} ± SEM (μM)	30.373 ± 0.272	29.820 ± 0.974	29.563 ± 0.981	29.794 ± 1.674	20.469 ± 0.553	21.765 ± 1.551	30.562 ± 0.694
Fold change in IC_{50}	1.0	1.0	**1.0**	1.0	**1.5 ***	**1.4**	**1.0**

See footnote to Table 4.1 above.

for the NIKS cells carrying the E6E7 genes (cancerous model). The NIKS cells expressing only the E7 gene displayed the highest eupatorin sensitivity at 3.8-fold decrease in IC_{50} compared to the parental cells, followed by E6-containing cells at 1.7-fold decrease in IC_{50}. Hence, eupatorin significantly induced growth inhibition on NIKS cells expressing E6 or E7 alone, but not the E6E7-expressing NIKS cells.

4.11 Effects of Sinensetin

Likewise, to determine the potential cytotoxic effects of another flavonoid compound, sinensetin on the HPV16 models, the cells were treated with increasing concentrations of sinensetin for 72 h followed by MTT assay. Sinensetin inhibited the growth of both the precancerous and cancerous HPV16 models in a dose-dependent manner (Figure 4.15A & 4.15B, top panel). The IC_{50} values are shown in Table 4.2.

In the HPV16 precancerous model, sinensetin failed to induce growth inhibition. The IC_{50} value of the cell models carrying the HPV16 genome (29.563 ± 0.981 μM) was close to that of the parental cells (30.373 ± 0.272 μM) (Table 4.2). There was no decrease in IC_{50} of precancerous model cells harbouring the HPV16 genome compared to the parental cells indicating that the cells were not susceptible to sinensetin treatment (Figure 4.15A, bottom panel). On the other hand, in the HPV16 cancerous models, NIKS cells harbouring E6 or E7 gene alone were more susceptible to sinensetin treatment with the IC_{50} values of 20.469 ± 0.553 μM and

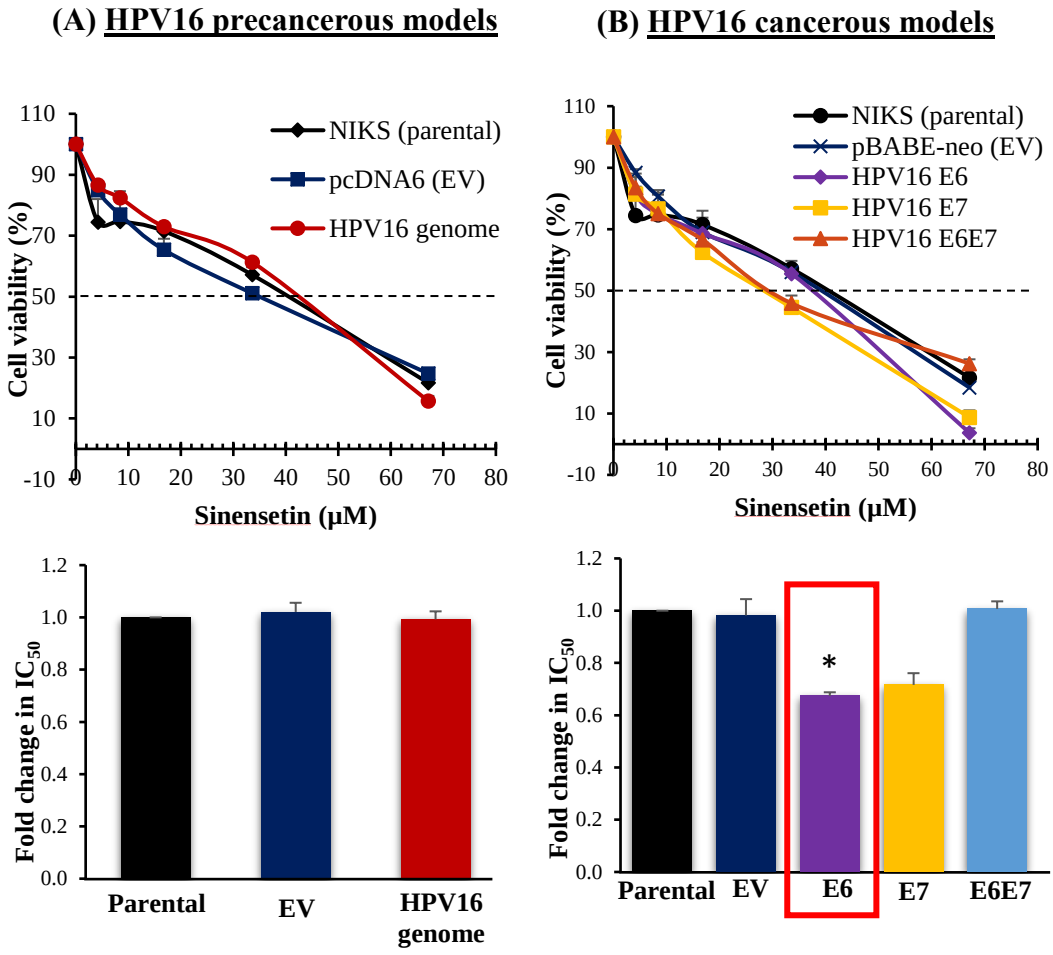

Figure 4.15 Effects of sinensetin on cell growth of the HPV models. (A) HPV16 precancerous models; (B) HPV16 cancerous models. Dose-response curves (top panel) were generated from the parental NIKS cells and HPV16 models by determining cell viability against exposure of various sinensetin concentrations (0.582 – 9.309 μM) at 72 h post-drug treatment. See also legends to figure 4.14.

21.765 ± 1.551 μM, respectively (Table 4.2). The cells harbouring the E6 gene were significantly sensitive to sinensetin treatment with a 1.5-fold decrease in the IC_{50} (red box in Figure 4.15B, bottom panel), but the effect was insignificant on the E7 gene model with only a 1.4-fold decrease in the IC_{50} (Table 4.2).

Similar to the precancerous model, NIKS cells that co-expressed the E6E7 genes were not sensitive to sinensetin treatment (IC_{50} =30.562 ± 0.694 μM), and there was no decrease in the IC_{50} values compared to that of the parental cells. Sinensetin treatment on all the HPV16 models was insignificant in inducing growth inhibition on the HPV16 models tested except for NIKS cells expressing the HPV16 E6 gene. The data indicates that sinensetin do not have preferential cytotoxic effect for NIKS cells that harbour HPV over parental cells.

4.12 Effects of Tribenzytin Carboxylates 1 (TC1)

Cytotoxicity activity of the synthetic compound, tribenzyltin carboxylates 1 (TC1) was determined by using different doses of TC1 on the HPV16 models. TC1 induced cell cytotoxicity in a dose-dependent manner (Figures 4.16A & 4.16B, top panels). The IC_{50} values of each of the HPV16 models treated with TC1 are summarised in Table 4.3.

The TC1 compound was able to inhibit cell proliferation significantly on the precancerous model: NIKS cells carrying the HPV16 genome were lower in

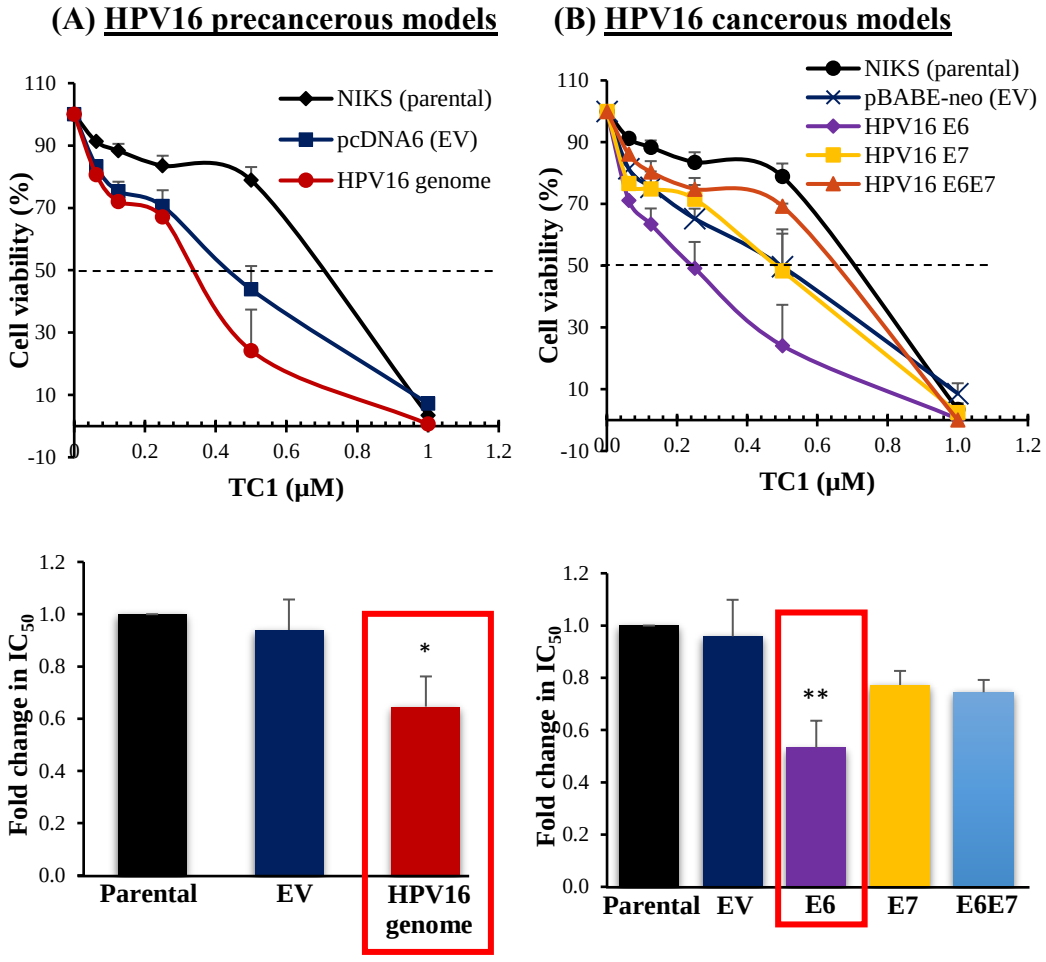

Figure 4.16 Effects of tribenzyltin carboxylates 1 (TC1) on cell growth of the HPV models. (A) HPV16 precancerous models; (B) HPV16 cancerous models. Dose-response curves (top panel) were generated from the parental NIKS cells and HPV16 models by determining cell viability against exposure of various TC1 concentrations (0.625 – 1.000 μM) at 72 h post-drug treatment. Fold-change graphs (bottom panel) were derived from NIKS, normalised to 1.0, compared with the HPV16-models. Results are expressed as means ± standard error of means (SEM) of three independent experiments performed in triplicates. *$p \leq 0.05$ and **$p \leq 0.01$ vs. parental, NIKS.

Table 4.3 Effects of novel synthetic compounds, tribenzyltin carboxylates 1 (TC1) and 4 (TC4), on HPV16 models

		Precancerous		**Cancerous**			
	NIKS	pcDNA6	HPV16-full genome	pBabeNeo	HPV16-E6	HPV16-E7	HPV16-E6E7
TC1							
IC_{50} ± SEM (μM)	0.353 ± 0.035	0.325 ± 0.020	0.220 ± 0.022	0.329 ± 0.021	0.181 ± 0.022	0.271 ± 0.023	0.260 ± 0.008
Fold change ± SEM	1.0	1.1	**1.6 ***	1.1	**2.0 ****	**1.3**	**1.4**
TC4							
IC_{50} ± SEM (μM)	0.199 ± 0.026	0.183 ± 0.034	0.142 ± 0.016	0.199 ± 0.025	0.150 ± 0.012	0.159 ± 0.014	0.226 ± 0.013
Fold change ± SEM	1.0	1.1	**1.4**	1.0	**1.3**	**1.3**	**0.9**

See footnote to Table 4.1 above.

IC_{50} value compared to the parental cells (0.220 ± 0.022 µM vs. 0.353 ± 0.035 µM), $p \leq 0.05$ (Table 4.3). There was a 1.6-fold decrease in IC_{50} between the precancerous model and the parental cells (Figure 4.16A, bottom panel & Table 4.3). For the cancerous models, TC1 also induced significant growth inhibition on NIKS cells expressing only the HPV16 E6 gene with IC_{50} of 0.181 ± 0.022 µM, a 2.0-fold decrease vs. the parental cells, $p \leq 0.01$, but TC1 showed weak and insignificant growth inhibition on the other NIKS cells transduced with HPV16 E6E7 or E7 gene alone, with IC_{50} of 0.260 ± 0.008 µM (1.4-fold decrease) and 0.271 ± 0.023 µM (1.3-fold decrease), respectively (Figure 4.16B, bottom panel and Table 4.3).

The results suggest that TC1 may be a potent inhibitor at the precancerous stages of HPV16-associated cancers. This observation is supported by a previous study (Anasamy et al., 2017), in which TC1 was used to treat breast cancer cells.

4.13 Effects of Tribenzytin Carboxylates 4 (TC4)

Similar to the previous TC1 assay, tribenzyltin carboxylates 4 (TC4) was also used in increasing concentrations to evaluate its anti-proliferative activity on the HPV16 models. TC4 also displayed a dose-dependent growth inhibition effects (Figure 4.17A & 4.17B, top panels). There was a marked decrease of cell viability of NIKS containing episomal HPV16 genome, or expressing the E6 gene compared to the parental cells (Figure 4.17A, top panel). The IC_{50} values are shown in Table 4.3.

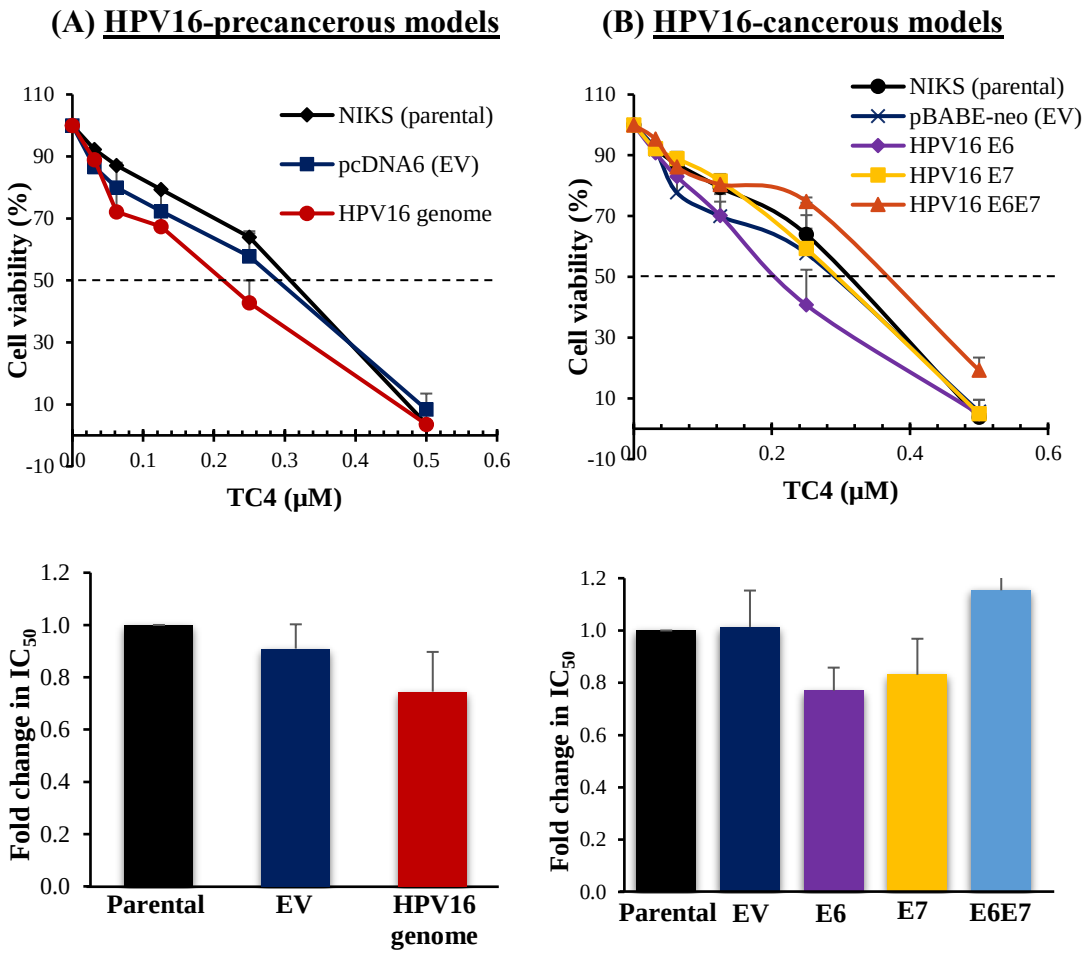

Figure 4.17 Tribenzyltin carboxylates 4 (TC4) effects on cell growth of the HPV models. (A) HPV16 precancerous models; (B) HPV16 cancerous models. Dose-response curves (top panel) were generated from the parental NIKS cells and HPV16-models by determining cell viability against exposure of various TC4 concentration (0.313 – 0.500 µM) at 72 h post-drug treatment. See also legends to figure 4.17.

The TC4 induced weak growth inhibition in all the HPV16 models. The precancerous model, NIKS cells carrying the HPV16 genome was slightly susceptible to TC4 treatment with IC_{50} at 0.142 ± 0.016 µM relative to that of the parental cells at 0.199 ± 0.026 µM (Figure 4.17A, bottom panel and Table 4.3). The fold-change in IC_{50} between the precancerous model and parental cells (1.4-fold decrease vs. parental) was insignificant (Table 4.3).

In the cancerous models, the IC_{50} of NIKS expressing the E6 or E7 alone largely similar to each other at 0.150 ± 0.012 µM and 0.159 ± 0.014 µM, respectively; they showed similar 1.3-fold-change compared to the parental cells (Figure 4.17B, bottom panel and Table 4.3). However, the NIKS cells that co-expressed the E6E7 genes were not susceptible to eupatorin treatment with a IC_{50} value higher than parental cells (0.226 ± 0.016 µM vs. 0.199 ± 0.026 µM).

Taken together, the TC4 treatment did not display significant cytotoxicity effects on the HPV16 models in line with the previous study by Anasamy et al., 2017 in which TC4 was used to treat breast cancer cells.

CHAPTER 5

DISCUSSION

5.1 Characteristics of NIKS Modified to Harbour the HPV16 Genome in Episomal Form and the HPV16 E6 and/or E7 Oncogenes

The life cycle of human papillomavirus (HPV) is closely integrated with the differentiation of the host epithelial cells and is initiated following infection of the proliferative basal keratinocytes by the virus (Kajitani et al., 2012; Pinidis et al., 2016). Monolayer culture of human keratinocytes, NIKS cells, was selected to generate the models in the present study. The main reason for this choice is that NIKS cells resemble normal keratinocytes in many aspects. Like normal keratinocytes, NIKS cells exhibit cell-to-cell contact inhibition and anchorage-dependence. They require growth-arrested 3T3 feeder cells to support its growth *in vitro*, a requirement that is similar to that of primary human keratinocytes (Allen-hoffmann et al., 2000). NIKS cells possess the wild-type p53 tumour suppressor gene, a feature that which is important for the study of the relationship between E6 and p53 (Allen-hoffmann et al., 2000; D. A. Galloway, 2009; Wang et al., 2009; Zhang et al., 2015). Additionally, the wild type p53 is believed to play a role in the increased susceptibility of HPV-associated cancers to radiation and chemotherapy compared to non-HPV associated cancers.

In this study, NIKS cells were genetically modified to represent two key steps/stages of HPV16-associated carcinogenesis. Persistent infection by HR-HPV such as HPV types 16 and 18 is a prerequisite for the process of cellular transformation. In this stage, the virus genome is present in the host cell largely as episomes. Hence the precancerous model, NIKS-HPV_{EPI} in which the HPV 16 genome is maintained in episomal form in the cells. On the other hand, the HPV genome is integrated into the host cell genome in the majority of HPV-associated cancers. Therefore, we modified the NIKS cells to harbour the E6 and/or E7 oncogenes to simulate the cancerous stage of the disease process (viz NIKS-HPV_{INT}).

These HPV16 models were established with the aim of using them as cell-based drug screening platforms. It is proposed that such a drug screening platform can act as a reproducible model system since NIKS cells are able to grow abundantly *in vitro* unlike primary cells which are quite limited in supply. All the HPV16 models were examined with respect to their morphology, oncogene transcription and protein expression (Figures 4.5 & 4.9). In addition, for the precancerous model, the episomal and integration status of the HPV were also studied (Figure 4.5).

The HPV16 precancerous model generated by using the full HPV16 genome in NIKS cells, demonstrated the ability to maintain the HPV16 episomes up to 21 cell passages. In a study by Laurson *et al*., 2010, it was shown that HPV16 episomes were maintained up to passage 12 in NIKS cells without any reduction of episomal copy number. In another study which involved the

use of human cervical keratinocytes derived from an early stage of cervical cancer, the W12 cell line, it was shown that the cells were able to maintain the HPV16 episomes up to passages 34 and 83, in different cell replicates (Gray *et al*., 2010). In this study, NIKS cells retained HPV16 episomes at early passages in the culture but HPV16 genome integration occurred in prolonged culture, suggesting that different culture conditions or distinct cell types may have different frequencies of HPV16 integration. However, the HPV16 integration did not result in increased mRNA levels of the E6 and E7 oncogenes, findings similar to that reported for HPV16-immortalised human foreskin keratinocytes and oropharyngeal squamous carcinoma cells, OPSCC (Olthof et al., 2014; Scarpini et al., 2014; Lace et al., 2011). However, the protein expression for E6 in NIKS cells carrying HPV16 episomes (precancerous model) and E7 in NIKS cells harbouring the E6E7 gene (cancerous model) were found to be upregulated with extended passaging in culture. The upregulated expression of the E6 or E7 genes in both the models could indicate that the introduction of HPV16 episomes or E6E7 oncogenes may lead to epigenetic alteration of the host cells and contribute to differential gene expression in different model system as suggested by Alvarez-Rios, 2016.

5.2 Increased Sensitivity of HPV16 Models to Cisplatin Treatment Compared to the Parental NIKS Cells

Cisplatin-based regimens are the standard treatment for HPV16-associated cancers especially for advanced and recurrent cervical cancers (Kamura and Ushijima, 2013). Previous studies have shown that HPV16-

positive cells are more sensitive to chemotherapeutic drug treatment compared to HPV16-negative cells *in vivo* and *in vitro* (Ziemann et al., 2015; Ang et al., 2010) . Thus, to determine whether this observation can be reproduced in our established models, cytotoxicity profile of the HPV16 models was tested using cisplatin. The relative drug sensitivities between the parental NIKS cells and the HPV16 models were evaluated. As demonstrated in Figure 4.12A and 4.12B (top panels), cisplatin inhibited cell proliferation of the HPV16 precancerous and cancerous models to a much greater degree compared to cells harbouring the empty vector and the NIKS controls. This observation is consistent with previous studies which reported increased sensitivity to cisplatin treatment of HPV16-positive head-and-neck cancer cell lines compared to the HPV16-negative cell lines (Thomas et al., 2016; Ziemann et al., 2015). Furthermore, it was also shown that the presence of HPV16 E6 and HPV16 E6E7 oncogenes in primary human foreskin keratinocytes improved cisplatin sensitivity and induced cell apoptosis (Liu et al., 2000).

Cisplatin treatment of HPV16-positive cells has been shown to deregulate E6 and E7 expression (Ziemann et al., 2015; Zhen et al., 2016; Butz et al., 1996). Therefore, it is proposed here that the chemosensitivity demonstrated by the HPV16 models upon cisplatin treatment is likely to be associated at least in part with the repression of E6 and E7 oncogene expression thereby allowing the escape of p53 and pRb proteins from the E6- or E7-mediated degradation activity. This in turn promotes the accumulation of the p53 protein to trigger apoptosis (Zhen et al., 2016). A proposed scheme of interactions between the HPV16 E6 or E7 oncogenes and cisplatin at the cellular

level is shown in Figure 5.1. This scheme, suggests that cisplatin treatment, restores the apoptotic function of p53 and pRb (retinoblastoma) by supressing the expression of E6 (1a) and E7 (1b), respectively. In addition, a previous study have indicated that the formation of DNA adducts (1c) by cisplatin induces the activation of the ataxia telangiectasia mutated (ATM) (1d) pathway which leads to inhibition of DNA damage repair mechanisms, results in activation of p53-dependent apoptosis (1e) (Basu and Krishnamurthy, 2010). Restoration of the activity of the tumour suppressor gene, p53, induces the upregulation of cyclin-dependent kinase inhibitor, p21 (2a), to inhibit the cyclin-dependent kinase 2-cyclin E (CDK2-cyclin E) (2b) at the G1 phase, hence, inducing the G1/S phase cell cycle arrest (2c). Furthermore, cisplatin treatment was reported to upregulate GADD45 expression in HPV-positive cancer cell lines, CaSki and SiHa cells as well as in head-and-neck cancer cell lines, CCL23, CCL23AS, and CAL27 (Butz et al., 1999; HT et al., 2006). It is possible therefore that upregulation of the GADD45 protein (3a), which is the downstream target protein of p53 may partially explain the finding in this study. Activation of GADD45 plays an essential role in the suppression of tumour growth through inhibition of cyclin-dependent kinase 1-cyclin B (CDK1-cyclin B), thereby inducing G2/M phase cell-cycle arrest (3c) in response to DNA damage (Tamura et al., 2012; Jin et al., 2002; Butz et al., 1999). In addition, GADD45 also interacts with MEKK (3d) and results in the induction of apoptosis (3f) via the JNK/p38 (3e) pathways (Tamura et al., 2012). Another pro-apoptotic protein, BAX, is upregulated by p53 protein (4a) to induce apoptosis through permeabilising the outer membrane of the mitochondria to release cytochrome C (4c), which, in turns, leads to the activation of the caspase

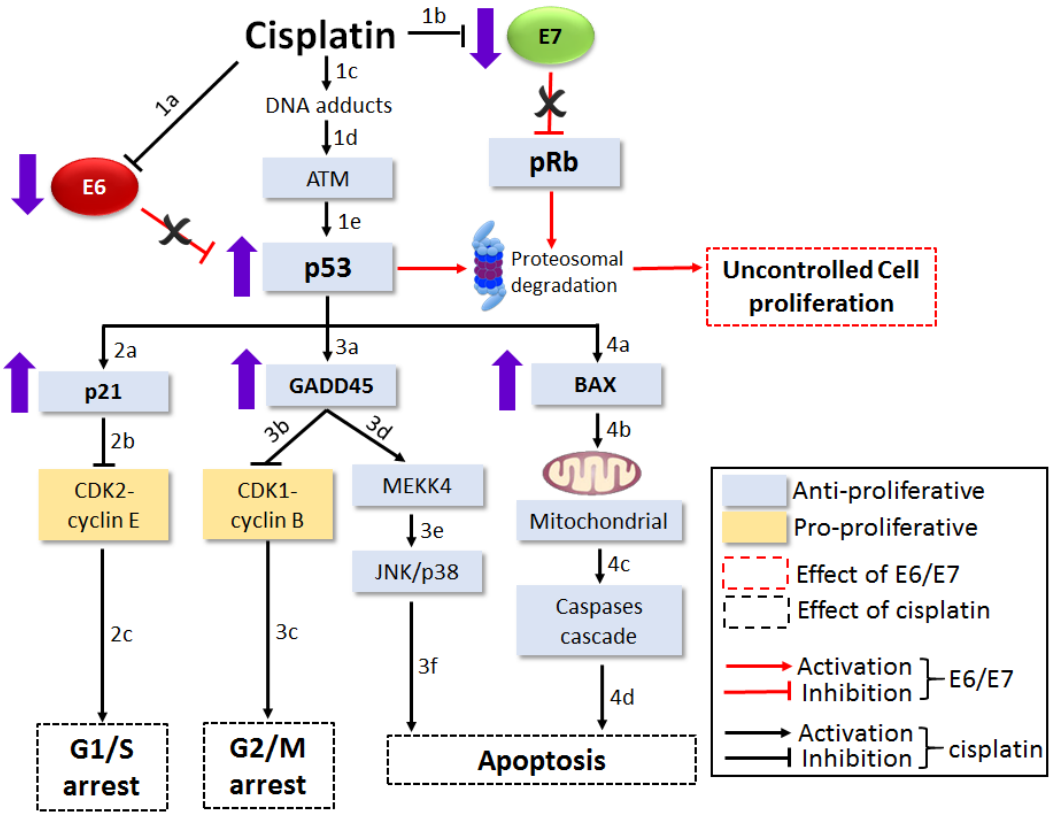

Figure 5.1 Proposed pathways of the interactions between the HPV16 E6 or E7 oncogenes and cisplatin. The anti- or pro-proliferative genes are indicated in blue and yellow boxes, respectively; effects of E6/E7 or cisplatin are boxed in red and black dashes. Blunt-ended arrows or lines in red or black indicate the predicted gene activation or inhibition, respectively, by E6/E7 oncogenes or cisplatin. The thick purple arrows indicate the up- or down-regulation of gene or protein expression. Refer to Discussion section 5.2 for further details. All of the information was extracted and modified from Ziemann et al., 2015; Zhen et al., 2016; Meng et al., 1999; Butz et al., 1996.

cascade (4c) and subsequently cell death (4d) (Westphal et al., 2011; Tait and Green, 2010).

In summary, the proposed scheme illustrates the possible mechanisms of cisplatin-induced chemosensitivity in the HPV-associated neoplasms which could, at least in part, explain the results of our study using the models harbouring the E6 or E7 gene alone. The exact underlying mechanisms, however, need to be further investigated.

5.3 Topotecan Induces the Highest Growth Inhibition in NIKS Cells Expressing the E7 Gene Alone

Topotecan hydrochloride is a topoisomerase I enzyme inhibitor that prevents the topoisomerase I from repairing the cleaved DNA during DNA replication and, thus promotes the accumulation of DNA breaks and eventually triggering the DNA damaging response system or apoptosis pathway (Coleman, 2002). Topotecan is often used in combination with cisplatin or other chemotherapeutic agents to reduce its hematologic toxicity (Lee et al., 2010; Robati et al., 2008). Topotecan treatment has been shown to reduce E6 mRNA level and upregulate p53 expression in the HPV16-positive cervical cancer cell line, SiHa; however the topotecan-induced apoptosis was shown to be p53-independent (Koivusalo and Hietanen, 2004).

In this study, topotecan was shown to be highly effective on NIKS cells expressing the E7 gene alone compared the other HPV16 models. A proposed

model illustrating the interaction between HPV16 E7 gene and topotecan action is provided in Figure 5.2. The cdc25a promoter was previously reported to be transactivated in HPV16 E7-expressing cells which promotes G1/S phase progression (Katich et al., 2001). It is suggested that NIKS cells expressing the E7 gene promotes G1/S phase transition by targeting CDC25a protein. In the presence of topotecan, DNA double-stranded breaks induced by the topotecan action leads to phosphorylation of the checkpoint kinase 1 (CHK1) (1b) (Kim et al., 2015; Cliby et al., 2002). In turn, CHK1 negatively regulates the cdc25a promoter (1c) and prevents the activation of downstream kinases including CDK2-cyclin E and CDK2-cyclin A (1d), thereby mediating the G1/S phase cell cycle arrest (1e) (Xiao et al., 2003). In addition, CHK1 has also been shown to degrade CDC25a (2a) triggered by topotecan treatment, in a p53-dependent manner (Tomicic et al., 2005). The proposed mechanisms could account for the NIKS cell containing E7 gene to be highly sensitive to topotecan treatment. However, further investigations are required to confirm this.

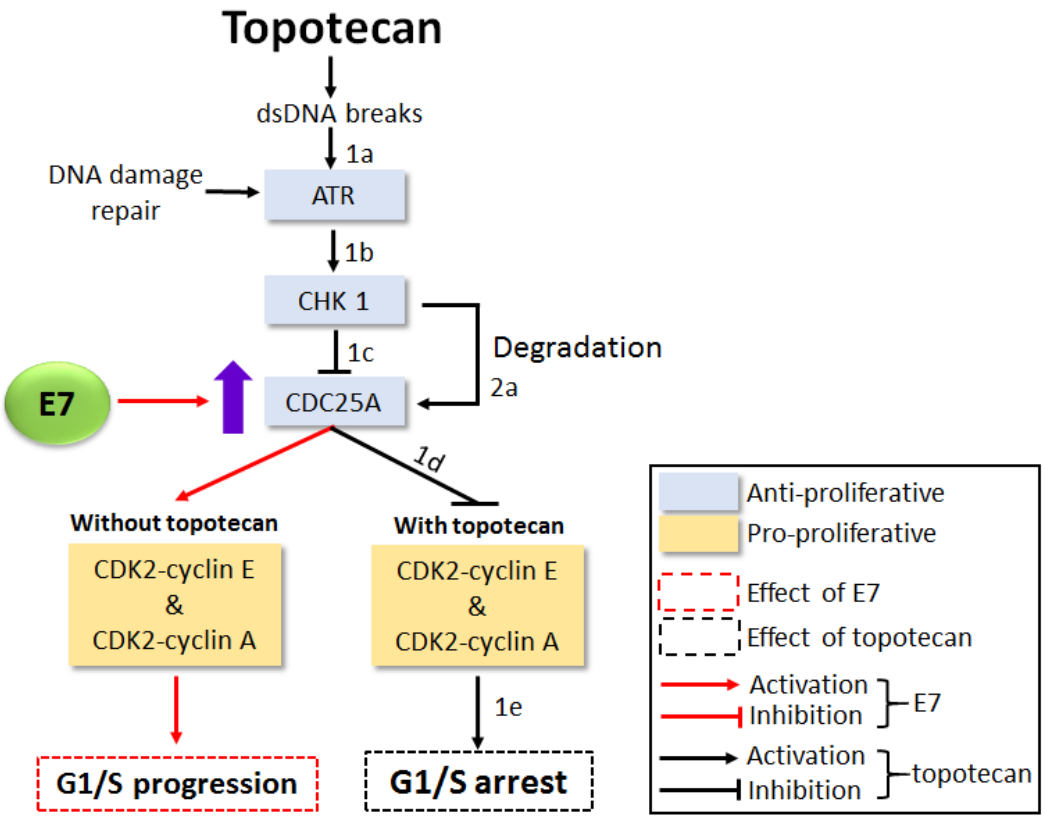

Figure 5.2 Proposed pathways of the interactions between the HPV16 E7 oncogenes and topotecan. The anti- or pro-proliferative genes are shown in blue and yellow boxes, respectively; effects of E7 or topotecan are boxed in red and black dashes. The blunt-ended arrows or lines in red or black indicate the predicted gene activation or inhibition by E7 oncogenes or topotecan. See also Figure 5.1 and refer to Discussion section 5.3 for further details. All of the information was extracted and modified from Koivusalo and Hietanen, 2004; Coleman, 2002; Katich et al., 2001

5.4 Eupatorin and Sinensetin Exert Higher Growth Inhibition when E6 or E7 was Acting Alone than when E6 and E7 are Co-expressed

In this study, both the natural compounds, eupatorin and sinensetin were shown to exert a similar growth inhibition pattern on the HPV16 models. NIKS cells that express E6 or E7 alone were more sensitive to the treatment by natural compounds compared to the NIKS cells that co-expressed the E6E7 genes (Table 4.2). A previous study has demonstrated that exposure of the HPV18-positive cervical adenocarcinoma cell line, HeLa, to eupatorin significantly reduced cell viability and induced cell-cycle arrest at the G2/M phase. Eupatorin has been shown to trigger apoptosis via both the p53-dependent and p53-independent pathways (Lee et al., 2016). Eupatorin treatment was also reported to not only exert cell growth inhibition and apoptosis on cancer cell lines, such as MCF7 (breast cancer cell line), HL-60 (human promyelocytic leukemia cells) and HUVEC (endothelial cells), but also interfere with angiogenesis via inhibition of vascular endothelial growth factor receptor (VEGFR) (Dolečková et al., 2012)

A proposed mechanism of eupatorin-induced anti-proliferative effects on the HPV16 models based on data from the literature is illustrated in Figure 5.3. It has been suggested that the anti-proliferative effects observed in the NIKS cells harbouring the E6 or E7 gene alone are associated with the (1) p53-dependent and (2) p53-independent pathways. Another possible pathway that may be applicable *in vivo* is the angiogenic pathway whereby suppression of

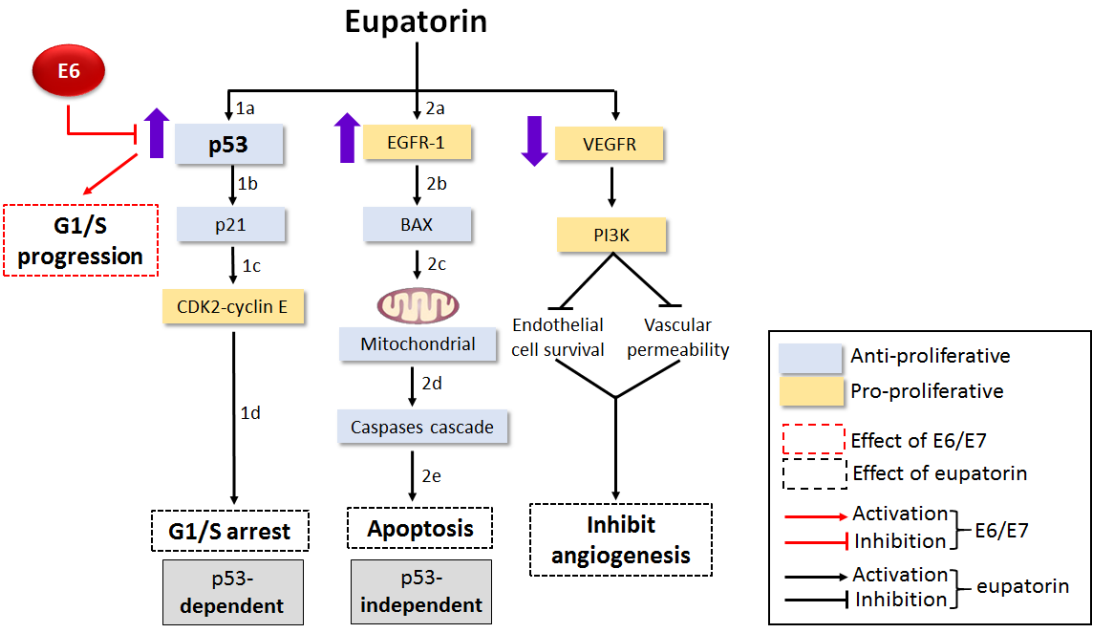

Figure 5.3 Proposed mechanism of action of eupatorin. See also Figure 5.1 and refer to Discussion section 5.4 for further details. All of the information was extracted and modified from Dolečková et al., 2012; Lee et al., 2016.

VEGFRs by eupatorin reduces angiogenesis, resulting in cell death (Lee et al., 2016; Ahamed et al., 2012; Dolečková et al., 2012).

In the p53-dependent pathway, eupatorin treatment may, upregulate the basal p53 acitivity (1a) despite the presence of E6 gene. This will enhance the inhibition action of the p21 protein (1b) on CDK2-cyclin E (1c). CDK2-cyclin E inhibition subsequently leads to cell-cycle arrest at G1 (1d), preventing the cells from entering the S phase and, thus, growth of the cancer cells is suppressed. In the p53-independent pathway, eupatorin treatment upregulates the expression of epidermal growth factor 1 (EGFR-1) gene (2a) and subsequently expression of the pro-apoptotic protein, BAX (2b). Activation of the BAX gene permeabilises the mitochondrial membrane and the release of cytosolic cytochrome C (2c) (Westphal et al., 2011), resulting in activation of the downstream caspase (2d) cascade and leading to cell death (2e). Taken together, the proposed predictive pathways may provide a working hypothesis for further investigation of mechanism that induced chemosensitivity by eupatorin in the cells expressing either the E6 or E7 gene alone.

Sinensetin is a methylated flavone that is isolated from the leaves of *Orthosiphon stamineus* and from orange peel. Sinensetin from these two sources share the same structure and methoxy groups (Amzad Hossain and Ismail, 2016; Hossain and Mizanur Rahman, 2015). Sinensetin has been reported to exhibit anti-angiogenesis effects on human umbilical vein endothelial cells (HUVECs) down regulating expression of the angiogenesis genes, *FLT1*, *KDR1* and *HRAS* in zebrafish and trigger cell cycle arrest at G0/G1

(Lam et al., 2012). Furthermore, Dong et al., (2011) showed that sinensetin treatment induced growth inhibition on human AGS gastric cancer cells and displayed apoptotic effects by causing cell-cycle arrest in the G2/M phase. In the same study, expression of p53 and its downstream effector gene, p21, was found to be elevated (Dong et al., 2000) and it was suggested that the increased expression of these proteins may play a role in the anti-proliferative and apoptosis pathways.

Results of this study demonstrated that only NIKS cells carrying the E6 gene alone was significantly sensitive to sinensetin treatment; none of the other HPV16 models were. The mechanism of action of sinensetin is illustrated in Figure 5.4 (right panel). Briefly, it has been proposed that sinensetin causes G1 arrest in a p53-dependent pathway. In contrast, HPV16 E6 blocks p53 function resulting in cellular proliferation. It is unclear how sinensetin affects E6 expressing cells to abrogate its effect on the host cell, thereby leading in the observed sensitivity of the cells to this compound.

5.5 TC1 but not TC4 Induces Growth Inhibition in the HPV16 Precancerous Models

The tribenzyltin carboxylates compounds 1 and 4 (TC1 & 4) are derived from organotin and are categorised as halogenated tribenzyltin complexes. The two compounds possess different functional groups and demonstrate different degree of growth inhibition effects. To date, there is only one published study

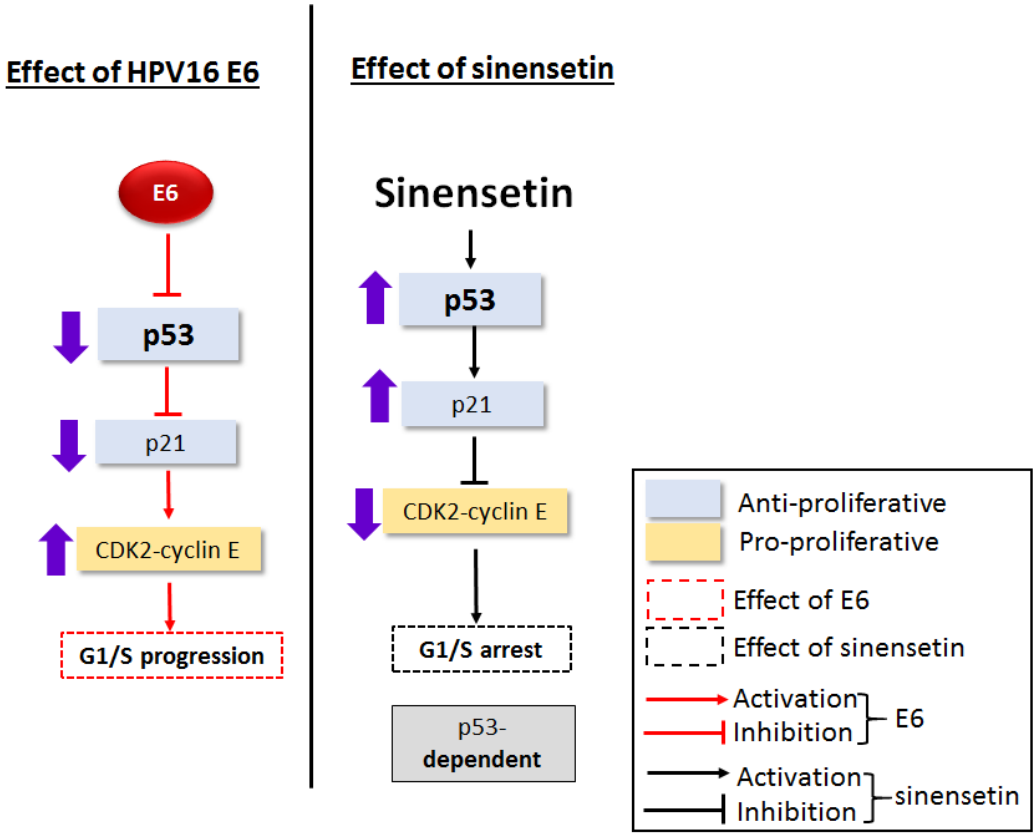

Figure 5.4 Proposed mechanism of action of sinensetin. The anti- or pro-proliferative proteins are shown in blue and yellow boxes, respectively; effects of E6 or sinensetin on cellular proliferation are boxed in red and black dashes. The arrows in red or black indicate the mechanism of action of E6 & sinensetin respectively; blunt-ended line in red indicate p53 and p21 inhibition by E6. For further details, refer to Figure 5.1. and section 5.4 (Discussion). All of the information was extracted from Dong et al., 2000; Lace et al., 2011; Lam et al., 2012.

on the use of these synthetic compounds on breast cancer cell lines (Anasamy et al., 2017). The TC1 was reported to inhibit proliferation of breast cancer cells, MCF-7, MDA-MB231 and 4T1, and triggered apoptosis via the caspase cascade-dependent pathway, but not the TC4 (Anasamy et al., 2017). This observation is consistent with the data obtained in this study as none of the HPV16 models was significantly inhibited by TC4 treatment, in contrast to TC1 treatment which rendered the NIKS cells harbouring the HPV16 episomes or the E6 gene alone to be more drug sensitive and with significant growth inhibition compared to the parental cells.

The pathway of TC1-induced cellular effects, summarised in Figure 5.5 is based on the results of a previous study (Anasamy et al., 2017). The higher growth inhibition induced by TC1 may be associated with the activation of caspase-9 and caspase-8 in the intrinsic and/or extrinsic apoptosis pathways as suggested by the study.

It has been suggested that truncated or mutants form of p53 that are lacking in transcriptional activity may be capable of triggering the apoptotic function via the intrinsic apoptosis pathway (Caelles et al., 1994). It has further been suggested that the basal level of p53, regardless of the presence of HPV16 E6, is activated to directly trigger the pemeabilisation of mitrochondrial outer membrane by interacting with the proapoptotic Bcl-2 family members, either BAX or BAK (Fulda and Debatin, 2006). Subsequently, release of cytochrome C from the mitochondria to the cytosol will then trigger the apoptotic protease activating factor (APAF1) to form an apoptosome to activate caspase-9

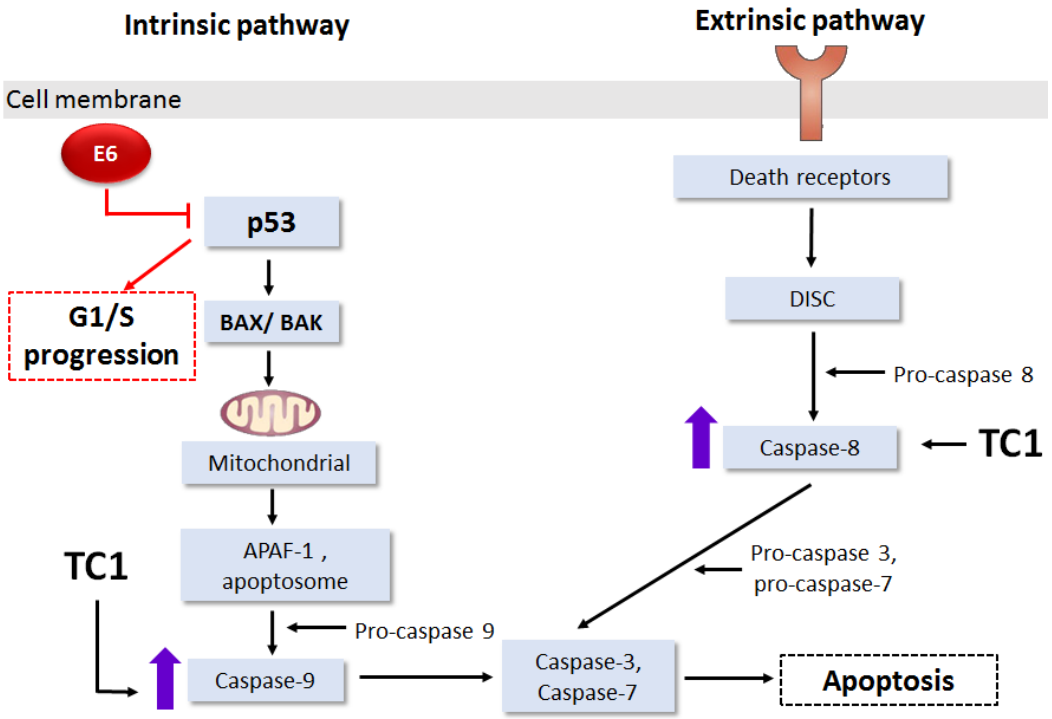

Figure 5.5 Proposed mechanism of action of tribenzyltin carboxylates 1 (TC1). See also Figure 5.1. Refer to Discussion section 5.5 for further details. All of the information was extracted and modified from Anasamy et al., 2017.

(Ichim and Tait, 2016; Vaseva and Moll, 2009). The activation of caspase-9 results in activation of caspase-3 and caspase-7, which leads to apoptosis.

In contrast, in the extrinsic apoptosis pathway, death receptors (DR) such as, CD95, tumour necrosis factor (TNF)-related apoptosis-inducing ligand (TRAIL) receptor 1 or 2 (TRAIL-R1 or TRAIL-R2) and FAS that reside in the cell membrane undergo translational modifications upon ligand binding to their cognate ligand (Ichim and Tait, 2016; Dickens et al., 2012). The recruitment of apoptotic proteins at the death receptor leads to the formation of death domain, known as the death inducing signalling complex (DISC) (Ichim and Tait, 2016). The formation of DISC stimulates the activation of caspase cascade including caspase-8, caspase-3 and caspase-7, eventually leading to apoptosis. It is possible that TC1 may upregulate caspase-9 in the intrinsic and caspase-8 in the extrinsic pathway to further enhance the apoptosis process, which subsequently contributes to increase cell death in NIKS cells harbouring the E6 gene.

CHAPTER 6

CONCLUSION

6.1 Major Findings of the Present Study

A normal immortalised keratinocytes cell line (NIKS) was used to express the HPV16 episomes or oncogenes in this study as an *in vitro* cell-based model for drug screening purpose. This model could serve as a platform for the search for potential therapeutic agents for treatment of HPV-associated neoplasms. Although immortalised keratinocytes cell line (NIKS) is widely used to study the HPV16 infection in vitro, however, majority of the researches were conducted to study the life cycle of high-risk HPV (Holmgren et al., 2005; Griffin et al., 2014; Lambert et al., 2006) and functional roles of viral gene expression in cancer progression (Isaacson Wechsler et al., 2012; Jackson et al., 2016).

The originality of the present study is that cells of the established *in vitro* HPV16 models were morphologically similar to that of the parental NIKS cells while exhibiting continued expression of HPV16 E6 and/or E7. A functional and episomal full-length HPV16 genome was successfully delivered into NIKS cells to represent the precancerous stage of the oncogenic process in HPV16-associated neoplasms. Cells harbouring and constitutively expressing the E6 and/or E7 oncogenes in prolonged culture were developed to represent the

cancerous stage of the process. The rationale of these approaches are based on the observation that episomal forms of the virus is maintained in chronic HPV infection, and integration of the viral gene is strongly associated with the large majority of HPV-associated cancers. It is believed that chronic infection is a prerequisite to the event of integration of the virus genome into the host.

Proof of concept studies verified that the HPV16 models were more sensitive to cisplatin and topotecan relative to the control cells. Of particular note is the significant increased sensitivity of cells expressing E7 to topotecan (15.2-fold change in IC_{50}). In addition, the HPV16 models expressing either E6 or E7 alone but not in E6E7 together were sensitive to the natural flavones, eupatorin and sinensetin. Furthermore, we have demonstrated that treatment with TC1 but not TC4 effectively inhibited proliferation of cells harbouring the HPV16 episomes. In which these findings have never been reported in the literature on the HPV models.

6.2 Limitations of the Study

Although NIKS cells resemble primary keratinocytes cells with respect to its characteristics, they may suffer from genetic drift as they divide in prolonged culture and lose some characteristic of the primary cells (Carter and Shieh, 2015; Irfan Maqsood et al., 2013). Hence, it is important to periodically validate the characteristic of the cultured cells to ensure experimental reproducibility and reliability. We acknowledge that the HPV16 modified NIKS models were not functionally validated - the effects of E6E7 on the downstream

key cellular target genes, particularly p53 and pRb tumour suppressor genes were not evaluated. Secondly, apoptosis assays following treatment of the cells with the chemotherapeutic agents or natural/ synthetic compounds which would have indicated whether the observed cell death was by apoptosis or necrosis were not performed. It is finally noted that the models used are not truly oncogenic despite cellular mortality. They merely represent a change for the parental NIKS cells with respect to the presence of HPV, in episomal and integrated forms, both features of which are present in HPV-associated neoplasms, both *in vitro* and *in vivo*.

The HPV16 cell-based *in vitro* models established in this study could be useful as drug screening platforms. In this study, the cell lines were subjected to cytotoxic assay using only a limited number of compounds. More work need to be carried out to determine the nature of cell death and its underlying mechanisms. Elucidation of the possible molecular mechanism in drug sensitivity induced for example by tribenzyltin carboxylates 1 (TC1) in suppressing the HPV16-harbouring cells should be carried out as this compound may be a new therapeutic option for use in the early stage of HPV16-positive cancers.

Further investigations are also needed to elucidate the molecular pathway of cellular transformation and carcinogenesis of HPV16 E6 and E7 *in vitro* and *in vivo*. Furthermore, the precise role of cell cycle regulators such as p53 and pRb in (i) HPV-associated carcinogenesis and (ii) response of HPV-associated cancers to chemotherapy will need more intensive studies.

REFERENCES

Agorastos, T. et al., 2015. Primary screening for cervical cancer based on high-risk human papillomavirus (HPV) detection and HPV 16 and HPV 18 genotyping, in comparison to cytology. *PLOS ONE*, 10(3), pp.1–23.

Akowuah, G.A. et al., 2004. Sinensetin, eupatorin, 3'-hydroxy-5, 6, 7, 4'-tetramethoxyflavone and rosmarinic acid contents and antioxidative effect of Orthosiphon stamineus from Malaysia. *Food Chemistry*, 87(4), pp.559–566.

Alama, A., Tasso, B., Novelli, F. and Sparatore, F., 2009. Novel Organotins as Antitumour Agents. *Discovery Antitumour Agents*, pp.50–53.

Alfaro, A. et al., 2016. Different Association of Human Papillomavirus 16 Variants with Early and Late Presentation of Cervical Cancer. *PLOS ONE*, 11(12), pp.1–13.

Alkatout, I. et al., 2015. Vulvar cancer: epidemiology, clinical presentation, and management options. *International Journal of Women's Health*, 7, pp.305–313.

Allen-hoffmann, B.L. et al., 2000. Normal growth and differentiation in a spontaneously immortalized near-diploid human keratinocyte cell line, NIKS. *Journal of Investigative Dermatology*, 114(3), pp.444–455.

Alvarez-Rios, J.O.-N. and E., 2016. Role of HR-HPVs E6 and E7 Oncoproteins in Cervical Carcinogenesis. *Journal of Molecular and Genetic Medicine*, 10(2), pp.1–11.

Ameer, O.Z. et al., 2012. Orthosiphon stamineus : Traditional Uses, Phytochemistry, Pharmacology, and Toxicology. *Journal of Medicinal Food*, 15(8), pp.678–690.

Amzad Hossain, M. and Ismail, Z., 2016. Quantification and enrichment of sinensetin in the leaves of Orthosiphon stamineus. *Arabian Journal of Chemistry*, 9, pp.S1338–S1341.

Anacker, D. and Moody, C., 2012. Generation of Organotypic Raft Cultures from Primary Human Keratinocytes. *Journal of Visualized Experiments : JoVE*, (60), p.3668.

Anasamy, T. et al., 2017. Tribenzyltin carboxylates as anticancer drug candidates: Effect on the cytotoxicity, motility and invasiveness of breast cancer

cell lines. *European Journal of Medicinal Chemistry*, 125, pp.770–783.

Ang, K.K. et al., 2010. Human Papillomavirus and Survival of Patients with Oropharyngeal Cancer. *The New England Journal of Medicine*, 363(1), pp.24–35.

Archambault, J. and Melendy, T., 2013. Targeting human papillomavirus genome replication for antiviral drug discovery. *Antiviral Therapy*, 18(3), pp.271–283.

Arjmand, F., Parveen, S., Tabassum, S. and Pettinari, C., 2014. Organo-tin antitumor compounds: Their present status in drug development and future perspectives. *Inorganica Chimica Acta*, 423(PB), pp.26–37.

Ault, K.A., 2006. Epidemiology and natural history of human papillomavirus infections in the female genital tract. *Infectious Diseases in Obstetrics and Gynecology*, 2006, p.40470.

Autier, P., Coibion, M., Huet, F. and Grivegnee, A.R., 1996. Transformation zone location and intraepithelial neoplasia of the cervix uteri. *British Journal of Cancer*, 74(3), pp.488–490.

Awale, S., Tezuka, Y., Banskota, A.H. and Kadota, S., 2003. Siphonols A–E: Novel nitric oxide inhibitors from Orthosiphon stamineus of Indonesia. *Bioorganic & Medicinal Chemistry Letters*, 13(1), pp.31–35.

Bansal, A., Singh, M.P. and Rai, B., 2016. Human papillomavirus-associated cancers: A growing global problem. *International Journal of Applied and Basic Medical Research*, 6(2), pp.84–89.

Baseman, J.G. and Koutsky, L. a, 2005. The epidemiology of human papillomavirus infections. *Journal of clinical virology : the official publication of the Pan American Society for Clinical Virology*, 32 Suppl 1, pp.S16-24.

Basu, A. and Krishnamurthy, S., 2010. Cellular Responses to Cisplatin-Induced DNA Damage. *Journal of Nucleic Acids*, 2010, pp.1–16.

Basu, P. et al., 2013. Efficacy and safety of human papillomavirus vaccine for primary prevention of cervical cancer: A review of evidence from phase III trials and national programs. *South Asian Journal of Cancer*, 2(4), pp.187–192.

Bechtold, V., Beard, P. and Raj, K., 2003. Human papillomavirus type 16 E2 protein has no effect on transcription from episomal viral DNA. *Journal of Virology*, 77(3), pp.2021–2028.

Bergvall, M., Melendy, T. and Archambault, J., 2013. The E1 proteins. *Virology*, 445(0), pp.1–47.

Bodily, J. and Laimins, L. a, 2011. Persistence of human papillomavirus infection: keys to malignant progression. *Trends in Microbiology*, 19(1), pp.33–39.

Boscolo-Rizzo, P. et al., 2013. New insights into human papillomavirus-associated head and neck squamous cell carcinoma. *Acta Otorhinolaryngologica Italica*, 33(2), pp.77–87.

Braaten, K.P. and Laufer, M.R., 2008. Human Papillomavirus (HPV), HPV-Related Disease, and the HPV Vaccine. *Reviews in Obstetrics and Gynecology*, 1(1), pp.2–10.

Bravo, I.G. and Félez-Sánchez, M., 2015. Papillomaviruses: viral evolution, cancer and evolutionary medicine. *Evolution, Medicine, and Public Health*, 2015(1), pp.32–51.

Brimer, N. and Vande Pol, S.B., 2014. Papillomavirus E6 PDZ interactions can be replaced by repression of p53 to promote episomal human papillomavirus genome maintenance. *Journal of Virology*, 88(5), pp.3027–3030.

Burd, E.M., 2003. Human papillomavirus and cervical cancer. *Clinical Microbiology Reviews*, 16(1), pp.1–17.

Burk, R.D., Harari, A. and Chen, Z., 2013. Human papillomavirus genome variants. *Virology*, 445(1–2), pp.232–243.

Butz, K. et al., 1996. Cellular responses of HPV-positive cancer cells to genotoxic anti-cancer agents: Repression of E6/E7-oncogene expression and induction of apoptosis. *International Journal of Cancer*, 68(4), pp.506–513.

Bzhalava, D. et al., 2013. A systematic review of the prevalence of mucosal and cutaneous human papillomavirus types. *Virology*, 445(1–2), pp.224–231.

Bzhalava, D., Eklund, C. and Dillner, J., 2015. International standardization and classification of human papillomavirus types. *Virology*, 476, pp.341–344.

Campo, M.S. et al., 2010. HPV-16 E5 down-regulates expression of surface HLA class I and reduces recognition by CD8 T cells. *Virology*, 407(1), pp.137–142.

Carter, M. and Shieh, J., 2015. Cell Culture Techniques BT - Guide to Research

Techniques in Neuroscience (Second Edition). In: *Guide to Research Techniques in Neuroscience (Second Edition)*. Academic Press, San Diego, pp. 295–310.

Cerqueira, C. et al., 2013. Heparin increases the infectivity of human papillomavirus type 16 independent of cell surface proteoglycans and induces L1 epitope exposure. *Cellular Microbiology*, 15(11), pp.1818–1836.

Chang, M.H. and Jeang, K.T., 2013. The role of human papillomavirus in oncogenesis. In: Chang, M.H. and Jeang, K.-T., (eds.) *Viruses and Human Cancer: From Basic Science to Clinical Prevention*. Springer Science & Business Media, pp. 135–148.

Chen, W. et al., 2007. Human papillomavirus causes an angiogenic switch in keratinocytes which is sufficient to alter endothelial cell behavior. *Virology*, 367(1), pp.168–174.

Choi, M. and Lee, C., 2015. Immortalization of Primary Keratinocytes and Its Application to Skin Research. *Biomolecules & Therapeutics*, 23(5), pp.391–399.

Choo, C.K., Rorke, E. a and Eckert, R.L., 1994. Differentiation-independent constitutive expression of the human papillomavirus type 16 E6 and E7 oncogenes in the CaSki cervical tumour cell line. *The Journal of general virology*, 75 (Pt 5)(1994), pp.1139–1147.

Choo, K., Pan, C., Liu, M. and Ng, H., 1987. Presence of Episomal and Integrated Human Papillomavirus DNA Sequences in Cervical Carcinoma. *Journal of Medical Virology*, 21, pp.101–107.

Cliby, W.A., Lewis, K.A., Lilly, K.K. and Kaufmann, S.H., 2002. S Phase and G2 Arrests Induced by Topoisomerase I Poisons Are Dependent on ATR Kinase Function. *Journal of Biological Chemistry*, 277(2), pp.1599–1606.

Clower, R. V, Fisk, J.C. and Melendy, T., 2006. Papillomavirus E1 protein binds to and stimulates human topoisomerase I. *Journal of Virology*, 80(3), pp.1584–1587.

Coleman, R.L., 2002. Emerging role of topotecan in front-line treatment of carcinoma of the ovary. *The oncologist*, 7(5), pp.46–55.

Conway, M.J. and Meyers, C., 2009. Replication and Assembly of Human Papillomaviruses. *Journal of Dental Research*, 88(4), pp.307–317.

Coutlée, F., Rouleau, D., Ferenczy, A. and Franco, E., 2005. The laboratory

diagnosis of genital human papillomavirus infections. *The Canadian Journal of Infectious Diseases & Medical Microbiology*, 16(2), pp.83–91.

Cubie, H.A., 2013. Diseases associated with human papillomavirus infection. *Virology*, 445(1), pp.21–34.

Culp, T.D., Budgeon, L.R. and Christensen, N.D., 2006. Human papillomaviruses bind a basal extracellular matrix component secreted by keratinocytes which is distinct from a membrane-associated receptor. *Virology*, 347(1), pp.147–159.

D'Souza, G. et al., 2007. Case–Control Study of Human Papillomavirus and Oropharyngeal Cancer. *New England Journal of Medicine*, 356(19), pp.1944–1956.

D'Souza, G. and Dempsey, A., 2011. The role of HPV in head and neck cancer and review of the HPV vaccine. *Preventive Medicine*, 53(Suppl 1), pp.S5–S11.

Das, R. et al., 2014. Improved chemosensitivity in cervical cancer to cisplatin: Synergistic activity of mahanine through STAT3 inhibition. *Cancer Letters*, 351(1), pp.81–90.

Dasari, S. and Bernard Tchounwou, P., 2014. Cisplatin in cancer therapy: molecular mechanisms of action. *European Journal of Pharmacology*, 740(0), pp.364–378.

Deligeoroglou, E. et al., 2013. HPV Infection: Immunological Aspects and Their Utility in Future Therapy. *Infectious Diseases in Obstetrics and Gynecology*, 2013, pp.1–9.

Diao, M.-K. et al., 2015. Integrated HPV genomes tend to integrate in gene desert areas in the CaSki, HeLa, and SiHa cervical cancer cell lines. *Life Sciences*, 127, pp.46–52.

Dickens, L.S., Powley, I.R., Hughes, M.A. and MacFarlane, M., 2012. The 'complexities' of life and death: Death receptor signalling platforms. *Experimental Cell Research*, 318(11), pp.1269–1277.

Digiuseppe, S. et al., 2015. Topography of the human papillomavirus minor capsid protein L2 during vesicular trafficking of infectious entry. *Journal of Virology*, 89(20), pp.10442–10452.

DiMaio, D. and Mattoon, D., 2001. Mechanisms of cell transformation by papillomavirus E5 proteins. *Oncogene*, 20(54), pp.7866–7873.

Dimaio, D. and Petti, L.M., 2013. The E5 proteins. *Virology*, 445, pp.99–114.

Dolečková, I. et al., 2012. Antiproliferative and antiangiogenic effects of flavone eupatorin, an active constituent of chloroform extract of Orthosiphon stamineus leaves. *Fitoterapia*, 83(6), pp.1000–1007.

Dong, Y. et al., 2000. Effects of sinensetin on proliferation and apoptosis of human gastric cancer AGS cells. *China journal of Chinese materia medica*, 36(6), pp.790–794.

Doorbar, J. et al., 2015. Human papillomavirus molecular biology and disease association. *Reviews in Medical Virology*, 25(1), pp.2–23.

Doorbar, J. et al., 2012. The biology and life-cycle of human papillomaviruses. *Vaccine*, 30, pp.F55–F70.

Doorbar, J., 2013. The E4 protein ; structure , function and patterns of expression. *Virology*, 445(1–2), pp.80–98.

Doorbar, J., 2005. The papillomavirus life cycle. *Journal of Clinical Virology*, 32, pp.7–15.

Dufour, X., Beby-Defaux, A., Agius, G. and Lacau St Guily, J., 2012. HPV and head and neck cancer. *European Annals of Otorhinolaryngology, Head and Neck Diseases*, 129(1), pp.26–31.

Durzynska, J., Lesniewicz, K. and Poreba, E., 2017. Human papillomaviruses in epigenetic regulations. *Mutation Research/Reviews in Mutation Research*, 772, pp.36–50.

Egawa, N. et al., 2017. HPV16 and 18 genome amplification show different E4-dependence, with 16E4 enhancing E1 nuclear accumulation and replicative efficiency via its cell cycle arrest and kinase activation functions. *PLOS Pathogens*, 13(3), pp.1–38.

Egawa, N., Egawa, K., Griffin, H. and Doorbar, J., 2015. Human papillomaviruses; epithelial tropisms, and the development of neoplasia. *Viruses*, 7(7), pp.3863–3890.

Fakhry, C. et al., 2008. Improved survival of patients with human papillomavirus-positive head and neck squamous cell carcinoma in a prospective clinical trial. *J Natl Cancer Inst.*, 100(4), pp.261–269.

Fani, S. et al., 2015. Synthesis, structural characterization, and anticancer

activity of a monobenzyltin compound against MCF-7 breast cancer cells. *Drug Design, Development and Therapy*, 9, pp.6191–6201.

Feller, L., Khammissa, R.A., Wood, N.H. and Lemmer, J., 2009. Epithelial maturation and molecular biology of oral HPV. *Infect Agent Cancer.*, 4, p.16.

Florea, A.-M. and Büsselberg, D., 2011. Cisplatin as an Anti-Tumor Drug: Cellular Mechanisms of Activity, Drug Resistance and Induced Side Effects. *Cancers*, 3(1), pp.1351–1371.

Francis, D.A., Schmid, S.I. and Howley, P.M., 2000. Repression of the Integrated Papillomavirus E6/E7 Promoter Is Required for Growth Suppression of Cervical Cancer Cells. *Journal of Virology*, 74(6), pp.2679–2686.

Frattini, M.G., Lim, H.B., Doorbar, J. and Laimins, L.A., 1997. Induction of human papillomavirus type 18 late gene expression and genomic amplification in organotypic cultures from transfected DNA templates. *Journal of Virology*, 71(9), pp.7068–7072.

Frazer, I.H., 2004. Prevention of cervical cancer through papillomavirus vaccination. *Nature Reviews Immunology*, 4(1), pp.46–55.

de Freitas, A.C., de Oliveira, T.H.A., Barros, M.R. and Venuti, A., 2017. hrHPV E5 oncoprotein: immune evasion and related immunotherapies. *Journal of Experimental & Clinical Cancer Research*, 36(1), p.71.

Fulda, S. and Debatin, K.-M., 2006. Extrinsic versus intrinsic apoptosis pathways in anticancer chemotherapy. *Oncogene*, 25(34), pp.4798–4811.

Funk, J.O. et al., 1997. Inhibition of CDK activity and PCNA-dependent DNA replication by p21 is blocked by interaction with the HPV-16 E7 oncoprotein. *Genes & Development*, 11(16), pp.2090–2100.

Galloway, D.A., 2009. Human papillomaviruses: a growing field. *Genes & Development*, 23(2), pp.138–142.

Galloway, D.A., 2009. NIH Public Access. *Genes & Development*, 23(2), pp.138–142.

Ganti, K. et al., 2015. The human papillomavirus E6 PDZ binding motif: from life cycle to malignancy. *Viruses*, 7(7), pp.3530–3551.

Garbuglia, A.R., 2014. Human papillomavirus in head and neck cancer. *Cancers*, 6(3), pp.1705–1726.

Garner-Hamrick, P.A. and Fisher, C., 2002. HPV Episomal Copy Number Closely Correlates with Cell Size in Keratinocyte Monolayer Cultures. *Virology*, 301(2), pp.334–341.

Garnett, T.O. and Duerksen-Hughes, P.J., 2006. Modulation of Apoptosis by Human Papillomavirus (HPV) Oncoproteins. *Archives of Virology*, 151(12), pp.2321–2335.

Garst, J., 2007. Topotecan: An evolving option in the treatment of relapsed small cell lung cancer. *Therapeutics and Clinical Risk Management*, 3(6), pp.1087–1095.

Gillison, M.L. et al., 2000. Evidence for a Causal Association Between Human Papillomavirus and a Subset of Head and Neck Cancers. *JNCI: Journal of the National Cancer Institute*, 92(9), pp.709–720.

Gillison, M.L., 2008. Human papillomavirus-related Diseases: Oropharynx Cancers and Potential Implications for Adolescent HPV Vaccination. *The Journal of adolescent health : official publication of the Society for Adolescent Medicine*, 43(4 Suppl), pp.S52–S60.

Gillison, M.L., Chaturvedi, A.K., Anderson, W.F. and Fakhry, C., 2015. Epidemiology of Human Papillomavirus–Positive Head and Neck Squamous Cell Carcinoma. *Journal of Clinical Oncology*, 33(29), pp.3235–3242.

Graham, S. V, 2010. Human papillomavirus: gene expression, regulation and prospects for novel diagnostic methods and antiviral therapies. *Future Microbiology*, 5(10), pp.1493–1506.

Graham, S. V and Faizo, A.A.A., 2017. Control of human papillomavirus gene expression by alternative splicing. *Virus Research*, 231, pp.83–95.

Gray, E. et al., 2010. In Vitro Progression of HPV16 Episome-Associated Cervical Neoplasia Displays Fundamental Similarities to Integrant-Associated Carcinogenesis. *Cancer research*, 70(10), pp.4081–4091.

Griffin, L.M., Cicchini, L., Xu, T. and Pyeon, D., 2014. Human Keratinocyte Cultures in the Investigation of Early Steps of Human Papillomavirus Infection. *Methods in molecular biology (Clifton, N.J.)*, 1195, pp.219–238.

Grisar, K. et al., 2018. Differences in human papillomavirus-positive and negative head and neck cancers in Belgium: an 8-year retrospective, comparative study. *Oral Surgery, Oral Medicine, Oral Pathology and Oral Radiology*, 121(5), pp.456–460.

Günes, Ç., Lichtsteiner, S., Vasserot, A.P. and Englert, C., 2000. Expression of the hTERT gene is regulated at the level of transcriptional initiation and repressed by Mad1. *Cancer Research*, 60(8), pp.2116–2121.

Hacker, N.F., Eifel, P.J. and van der Velden, J., 2015. Cancer of the vagina. *International Journal of Gynecology & Obstetrics*, 131, pp.S84–S87.

Hadjikakou, S.K. and Hadjiliadis, N., 2009. Antiproliferative and anti-tumor activity of organotin compounds. *Coordination Chemistry Reviews*, 253(1), pp.235–249.

Halim, T.A., Farooqi, A.A. and Zaman, F., 2013. Nip the HPV encoded evil in the cancer bud: HPV reshapes TRAILs and signaling landscapes. *Cancer Cell International*, 13, p.61.

zur Hausen, H., 2012. Papillomaviruses and cancer of the upper digestive. In: zur Hausen, H., (ed.) *Human Pathogenic Papillomaviruses*. Current Topics in Microbiology and Immunology. Springer Berlin Heidelberg, pp. 1–274.

zur Hausen, H., 2009. Papillomaviruses in the causation of human cancers - a brief historical account. *Virology*, 384(2), pp.260–265.

Hawley-Nelson, P. et al., 1989. HPV16 E6 and E7 proteins cooperate to immortalize human foreskin keratinocytes. *The EMBO Journal*, 8(12), pp.3905–3910.

Herfs, M. et al., 2012. A discrete population of squamocolumnar junction cells implicated in the pathogenesis of cervical cancer. *Proceedings of the National Academy of Sciences of the United States of America*, 109(26), pp.10516–10521.

Herfs, M., Soong, T.R., Delvenne, P. and Crum, C.P., 2017. Deciphering the multifactorial susceptibility of mucosal junction cells to HPV infection and related carcinogenesis. *Viruses*, 9(4), pp.85–98.

Hoe, K.K., Verma, C.S. and Lane, D.P., 2014. Drugging the p53 pathway: understanding the route to clinical efficacy. *Nature Reviews Drug Discovery*, 13(3), pp.217–236.

Hoffmann, R. et al., 2006. Different Modes of Human Papillomavirus DNA Replication during Maintenance. *Journal of Virology*, 80(9), pp.4431–4439.

Holmgren, S.C., Patterson, N. a, Ozbun, M. a and Lambert, P.F., 2005. The Minor Capsid Protein L2 Contributes to Two Steps in the Human Papillomavirus Type 31 Life Cycle The Minor Capsid Protein L2 Contributes

to Two Steps in the Human Papillomavirus Type 31 Life Cycle. *Journal of virology*, 79(7), pp.3938–3948.

Hong, S. and Laimins, L.A., 2013. Regulation of the life cycle of HPVs by differentiation and the DNA damage response. *Future microbiology*, 8, pp.1547–1557.

Horikawa, I. et al., 2002. Downstream E-Box–mediated Regulation of the Human Telomerase Reverse Transcriptase (hTERT) Gene Transcription: Evidence for an Endogenous Mechanism of Transcriptional Repression. *Molecular Biology of the Cell*, 13(8), pp.2585–2597.

Horvath, C. a J. et al., 2010. Mechanisms of cell entry by human papillomaviruses: an overview. *Virology journal*, 7(11), pp.1–7.

Hossain, M.A. and Mizanur Rahman, S.M., 2015. Isolation and characterisation of flavonoids from the leaves of medicinal plant Orthosiphon stamineus. *Arabian Journal of Chemistry*, 8(2), pp.218–221.

Hoste, G., Vossaert, K. and Poppe, W.A.J., 2013. The clinical role of HPV testing in primary and secondary cervical cancer screening. *Obstetrics and Gynecology International*, 2013, pp.1–7.

Howie, H.L., Katzenellenbogen, R.A. and Galloway, D.A., 2009. Papillomavirus E6 proteins. *Virology*, 384(2), pp.324–334.

Hutchinson, L., 2016. Drug therapy: Cetuximab or cisplatin in HNSCC? *Nature Reviews Clinical Oncology*, 13(2), p.66.

Hwang, L.Y. et al., 2009. Factors that influence the rate of epithelial maturation in the cervix of healthy young women. *The Journal of adolescent health : official publication of the Society for Adolescent Medicine*, 44(2), pp.103–110.

Hwang, S.G. et al., 2002. Human papillomavirus type 16 E7 binds to E2F1 and activates E2F1-driven transcription in a retinoblastoma protein-independent manner. *Journal of Biological Chemistry*, 277(4), pp.2923–2930.

Ichim, G. and Tait, S.W.G., 2016. A fate worse than death: apoptosis as an oncogenic process. *Nature reviews. Cancer*, 16(8), pp.539–548.

Irfan Maqsood, M., Matin, M.M., Bahrami, A.R. and Ghasroldasht, M.M., 2013. Immortality of cell lines: challenges and advantages of establishment. *Cell Biology International*, 37(10), pp.1038–1045.

Isaacson Wechsler, E. et al., 2012. Reconstruction of Human Papillomavirus Type 16-Mediated Early-Stage Neoplasia Implicates E6/E7 Deregulation and the Loss of Contact Inhibition in Neoplastic Progression. *Journal of Virology*, 86(11), pp.6358–6364.

Jackson, R. et al., 2016. Functional variants of human papillomavirus type 16 demonstrate host genome integration and transcriptional alterations corresponding to their unique cancer epidemiology. *BMC Genomics*, 17(1), p.851.

Jackson, R., Togtema, M., Lambert, P.F. and Zehbe, I., 2014. Tumourigenesis Driven by the Human Papillomavirus Type 16 Asian-American E6 Variant in a Three-Dimensional Keratinocyte Model. *PLOS ONE*, 9(7), p.e101540.

James, C.D. and Roberts, S., 2016. Viral interactions with PDZ domain-containing proteins—an oncogenic trait? *Pathogens*, 5(1), pp.8–30.

Jeon, S., Allen-Hoffmann, B.L. and Lambert, P.F., 1995. Integration of human papillomavirus type 16 into the human genome correlates with a selective growth advantage of cells. *Journal of Virology*, 69(5), pp.2989–2997.

Jiang, P. and Yue, Y., 2014. Human papillomavirus oncoproteins and apoptosis (Review). *Experimental and Therapeutic Medicine*, 7(1), pp.3–7.

Jing, M. et al., 2007. Degradation of tyrosine phosphatase PTPN3 (PTPH1) by association with oncogenic human papillomavirus E6 proteins. *Journal of Virology*, 81(5), pp.2231–2239.

Johansson, C. and Schwartz, S., 2013. Regulation of human papillomavirus gene expression by splicing and polyadenylation. *Nature Publishing Group*, 11(4), pp.239–251.

Jones, D.L., Alani, R.M. and Münger, K., 1997. The human papillomavirus E7 oncoprotein can uncouple cellular differentiation and proliferation in human keratinocytes by abrogating p21(Cip1)-mediated inhibition of cdk2. *Genes & Development*, 11(16), pp.2101–2111.

Juckett, G., Hartman-adams, H. and Virginia, W., 2010. Human Papillomavirus: Clinical Manifestations and Prevention. *American Family Psysician*, 82(10), pp.1209–1214.

Jung, H.S. et al., 2012. The synergistic therapeutic effect of cisplatin with Human papillomavirus E6/E7 short interfering RNA on cervical cancer cell lines in vitro and in vivo. *International Journal of Cancer*, 130(8), pp.1925–

1936.

Kadaja, M. et al., 2007. Genomic instability of the host cell induced by the human papillomavirus replication machinery. *The European Molecular Biology Organization Journal*, 26(8), pp.2180–2191.

Kadaja, M., Silla, T., Ustav, E. and Ustav, M., 2009. Papillomavirus DNA replication - from initiation to genomic instability. *Virology*, 384(2), pp.360–8.

Kajitani, N., Satsuka, A., Kawate, A., & Sakai, H., 2012. Productive lifecycle of human papillomaviruses that depends upon squamous epithelial differentiation. *Frontiers in Microbiology*, 3(April), p.152.

Kajitani, N., Satsuka, A., Kawate, A. and Sakai, H., 2012. Productive lifecycle of human papillomaviruses that depends upon squamous epithelial differentiation. *Frontiers in Microbiology*, 3(152), pp.1–12.

Kamura, T. and Ushijima, K., 2013. Chemotherapy for advanced or recurrent cervical cancer. *Taiwanese Journal of Obstetrics and Gynecology*, 52(2), pp.161–164.

Katich, S.C., Zerfass-thome, K. and Ho, I., 2001. Regulation of the Cdc25A gene by the human papillomavirus Type 16 E7 oncogene. *Oncogene*, 20(5), pp.543–550.

Katzenellenbogen, R. and Rachel, 2017. Telomerase Induction in HPV Infection and Oncogenesis. *Viruses*, 9(7), pp.180–192.

Khan, J. et al., 2011. Role of calpain in the formation of human papillomavirus type 16 E1^E4 amyloid fibers and reorganization of the keratin network. *Journal of Virology*, 85(19), pp.9984–9997.

Kim, S.H. et al., 2006. Human papillomavirus 16 E5 up-regulates the expression of vascular endothelial growth factor through the activation of epidermal growth factor receptor, MEK/ERK1,2 and PI3K/Akt. *Cellular and Molecular Life Sciences*, 63(7–8), pp.930–938.

Kim, S.M., 2016. Human papilloma virus in oral cancer. *Journal of the Korean Association of Oral and Maxillofacial Surgeons*, 42(6), pp.327–336.

Klingelhutz, A.J., Foster, S.A. and McDougall, J.K., 1996. Telomerase activation by the E6 gene product of human papillomavirus type 16. *Nature*, 380(6569), pp.79–82.

Klingelhutz, A.J. and Roman, A., 2012. Cellular transformation by human papillomaviruses: Lessons learned by comparing high- and low-risk viruses. *Virology*, 424(2), pp.77–98.

Koivusalo, R. and Hietanen, S., 2004. The cytotoxicity of chemotherapy drugs varies in cervical cancer cells depending on the p53 status. *Cancer Biology and Therapy*, 3(11), pp.1177–1183.

Kranjec, C. and Banks, L., 2011. A systematic analysis of human Papillomavirus (HPV) E6 PDZ substrates identifies MAGI-1 as a major target of HPV type 16 (HPV-16) and HPV-18 whose loss accompanies disruption of tight junctions. *Journal of Virology*, 85(4), pp.1757–1764.

Lace, M.J. et al., 2011. Human Papillomavirus Type 16 (HPV-16) Genomes Integrated in Head and Neck Cancers and in HPV-16-Immortalized Human Keratinocyte Clones Express Chimeric Virus-Cell mRNAs Similar to Those Found in Cervical Cancers. *Journal of Virology*, 85(4), pp.1645–1654.

Lam, I.K. et al., 2012. In vitro and in vivo structure and activity relationship analysis of polymethoxylated flavonoids: identifying sinensetin as a novel antiangiogenesis agent. *Molecular Nutrition & Food Research*, 56(6), pp.945–956.

Lambert, P.F. et al., 2006. Using an immortalized cell line to study the HPV life cycle in organotypic “raft” cultures BT - human papillomaviruses: methods and protocols. In: Davy, C. and Doorbar, J., (eds.) Humana Press, Totowa, NJ, pp. 141–155.

Laporta, R. and Taichman, L., 1982. Human papilloma viral DNA replicates as a stable episome in cultured epidermal keratinocytes. *Proc. Natl. Acad. Sci. USA*, 79, pp.3393–3397.

Laurson, J. et al., 2010. Epigenetic repression of E-cadherin by human papillomavirus 16 E7 protein. *Carcinogenesis*, 31(5), pp.918–926.

Lee, D. et al., 2016. Using Organotypic Epithelial Tissue Culture to Study the Human Papillomavirus Life Cycle. *Current Protocols in Microbiology*, 41, p.14B.8.1-14B.8.19.

Lee, J.M. et al., 2014. Phase I/Ib study of olaparib and carboplatin in BRCA1 or BRCA2 mutation-associated breast or ovarian cancer with biomarker analyses. *Journal of the National Cancer Institute*, 106(6), p.dju089.

Lee, K. et al., 2016. The natural flavone eupatorin induces cell cycle arrest at

the G2/M phase and apoptosis in HeLa cells. *Applied Biological Chemistry*, 59(2), pp.193–199.

Lee, Y.-Y. et al., 2010. Sequence-dependent hematologic side effects of topotecan and cisplatin in persistent or recurrent cervical cancer. *Gynecologic Oncology*, 119(1), pp.87–91.

Liu, X. et al., 2008. Cell-restricted immortalization by human papillomavirus correlates with telomerase activation and engagement of the hTERT promoter by Myc. *Journal of Virology*, 82(23), pp.11568–11576.

Liu, X. et al., 2009. HPV E6 protein interacts physically and functionally with the cellular telomerase complex. *Proceedings of the National Academy of Sciences*, 106(44), pp.18780–18785.

Liu, Y. et al., 2005. The mechanism of cisplatin-induced apoptosis in HeLa cells. *Chinese Journal of Clinical Oncology*, 2(6), pp.866–869.

Liu, Y., Lu, Z., Xu, R. and Ke, Y., 2016. Comprehensive mapping of the human papillomavirus (HPV) DNA integration sites in cervical carcinomas by HPV capture technology. *Oncotarget*, 7(5), pp.5852–5864.

Liu, Y., McKalip, A. and Herman, B., 2000. Human papillomavirus type 16 E6 and HPV-16 E6/E7 sensitize human keratinocytes to apoptosis induced by chemotherapeutic agents: roles of p53 and caspase activation. *Journal of Cellular Biochemistry*, 78(2), pp.334–349.

Llames, S. et al., 2015. Feeder Layer Cell Actions and Applications. *Tissue Engineering. Part B, Reviews*, 21(4), pp.345–353.

Long III, H.J., Laack, N.N.I. and Gostout, B.S., 2017. Prevention, Diagnosis, and Treatment of Cervical Cancer. *Mayo Clinic Proceedings*, 82(12), pp.1566–1574.

Longworth, M.S. and Laimins, L.A., 2004. Pathogenesis of Human Papillomaviruses in Differentiating Epithelia. *Microbiology and Molecular Biology Reviews*, 68(2), pp.362–372.

Loon, Y.H., Wong, J.W., Yap, S.P. and Yuen, K.H., 2005. Determination of flavonoids from Orthosiphon stamineus in plasma using a simple HPLC method with ultraviolet detection. *Journal of Chromatography B*, 816(1), pp.161–166.

López, J. et al., 2012. Human papillomavirus infections and cancer stem cells of tumors from the uterine cervix. *The Open Virology Journal*, 6, pp.232–240.

Lorincz, A., Castanon, A., Lim, A.W.W. and Sasieni, P., 2013. New Strategies for HPV-based Cervical Screening. *Women's health (London, England)*, 9(5), pp.1–16.

Lorusso, D. et al., 2010. Review role of topotecan in gynaecological cancers: Current indications and perspectives. *Critical Reviews in Oncology / Hematology*, 74(3), pp.163–174.

Lui, V.W.Y. and Grandis, J.R., 2012. Primary chemotherapy and radiation as a Treatment strategy for HPV-positive oropharyngeal cancer. *Head and Neck Pathology*, 6(Suppl 1), pp.91–97.

Magaldi, T.G. et al., 2012. Primary human cervical carcinoma cells require human papillomavirus E6 and E7 expression for ongoing proliferation. *Virology*, 422(1), pp.114–124.

Mantovani, F. and Banks, L., 2001. The human papillomavirus E6 protein and its contribution to malignant progression. *Oncogene*, pp.7874–7887.

Martinez-Zapien, D. et al., 2016. Structure of the E6/E6AP/p53 complex required for HPV-mediated degradation of p53. *Nature*, 529(7587), pp.541–545.
Maufort, J.P., Shai, A., Pitot, H.C. and Lambert, P.F., 2010. A role for HPV16 E5 in cervical carcinogenesis. *Cancer Res.*, 70(7), pp.2924–2931.

McBride, A. a, 2013. The papillomavirus E2 proteins. *Virology*, 445(1–2), pp.57–79.

McBride, A.A., 2008. Replication and partitioning of papillomavirus genomes. *Advances in Virus Research*, 72, pp.155–205.

McBride, A.A. and Warburton, A., 2017. The role of integration in oncogenic progression of HPV-associated cancers. *PLOS Pathogens*, 13(4), pp.1–7.

McIlwain, W.R., Sood, A.J., Nguyen, S.A. and Day, T.A., 2014. Initial symptoms in patients with HPV-positive and HPV-negative oropharyngeal cancer. *JAMA Otolaryngology - Head and Neck Surgery*, 140(5), pp.441–447.

Meng, X., Dong, Y. and Sun, Z., 1999. Mechanism of p53 downstream effectors p21 and Gadd45 in DNA damage surveillance. *Science in China Series C: Life Sciences*, 42(4), pp.427–434.

Miller, D.L. and Stack, M.S., 2015. Chapter 5 - Papillomavirus replication. *Human Papillomavirus (HPV)-Associated Oropharyngeal Cancer*. Springer International Publishing, Switzerland, pp. 103–132.

Miniggio, H.D., 2016. Biological significance of palatine tonsillar epithelium: microstructure and disease. *South African Dental Journal*, 71, pp.496–499.

Mischo, A. et al., 2013. Structural insights into a wildtype domain of the oncoprotein E6 and its interaction with a PDZ domain. *PLoS ONE*, 8(4), p.e62584.

Monie, A., Hung, C.-F., Roden, R. and Wu, T.-C., 2008. Cervarix(TM): a vaccine for the prevention of HPV 16, 18-associated cervical cancer. *Biologics : Targets & Therapy*, 2(1), pp.107–113.

Moody, C. a and Laimins, L. a, 2010. Human papillomavirus oncoproteins: pathways to transformation. *Nature Reviews. Cancer*, 10(8), pp.550–60.

Morandell, D. et al., 2012. The human papillomavirus type 16 E7 oncoprotein targets Myc-interacting zinc-finger protein-1. *Virology*, 422(2), pp.242–253.

Mori, S. et al., 2009. An Anchorage-Independent Cell Growth Signature Identifies Tumors with Metastatic Potential. *Oncogene*, 28(31), pp.2796–2805.

Morrison, B., 2014. Risk Factors and Prevalence of Penile Cancer. *The West Indian Medical Journal*, 63(6), pp.559–560.

Morshed, K., Polz-Gruszka, D., Szymanski, M. and Polz-Dacewicz, M., 2014. Human Papillomavirus (HPV) - Structure, epidemiology and pathogenesis. *Otolaryngologia Polska*, 68(5), pp.213–219.

Moscicki, A.-B. and Palefsky, J.M., 2011. HPV in men: an update. *Journal of Lower Genital Tract Disease*, 15(3), pp.231–234.

Müller, M., Prescott, E.L., Wasson, C.W. and Macdonald, A., 2015. Human papillomavirus E5 oncoprotein: function and potential target for antiviral therapeutics. *Future Virology*, 10(1), pp.27–39.

Münger, K. et al., 2004. Minireview: Mechanisms of human papillomavirus-induced oncogenesis. *Journal of Virology*, 78(21), pp.11451–11460.

Nguyen, M.L. et al., 2003. The PDZ Ligand Domain of the Human Papillomavirus Type 16 E6 Protein Is Required for E6's Induction of Epithelial Hyperplasia In Vivo. *Journal of Virology*, 77(12), pp.6957–6964.

Nicolaides, L. et al., 2011. Stabilization of HPV16 E6 protein by PDZ proteins, and potential implications for genome maintenance. *Virology*, 414(2), pp.137–145.

Nucci, M.R. and Oliva, E., 2009. Cervical neoplasia. In: Nucci, M.R. and Oliva, E., (eds.) *Gynecologic Pathology*. ClinicalKey 2012. Churchill Livingstone/Elservier, p. 710.

Olthof, N.C. et al., 2014. Comprehensive analysis of HPV16 integration in OSCC reveals no significant impact of physical status on viral oncogene and virally disrupted human gene expression. *PLOS ONE*, 9(2), p.e88718.

Ozbun, M.A. and Patterson, N.A., 2014. Using organotypic (raft) epithelial tissue cultures for the biosynthesis and isolation of infectious human papillomaviruses. *Current protocols in microbiology*, 34, p.14B.3.1-14B.3.18.

Pabla, N. and Dong, Z., 2008. Cisplatin nephrotoxicity: Mechanisms and renoprotective strategies. *Kidney International*, 73(9), pp.994–1007.

Pai, S.I. and Westra, W.H., 2009. Molecular pathology of head and neck cancer: implications for diagnosis, prognosis, and treatment. *Annual review of pathology*, 4, pp.49–70.

Palefsky, J.M., 2010. Human papillomavirus-related disease in men: not just a women's issue. *The Journal of adolescent health : official publication of the Society for Adolescent Medicine*, 46(4 Suppl), pp.S12–S19.

Paradise, W.A., Fischer, D.J., B, E.J. and Radosevich, J.A., 2013. Head & Neck Cancer: Current Perspectives, Advances, and Challenges. In: Radosevich, J.A., (ed.) *Head & Neck Cancer: Current Perspectives, Advances, and Challenges*. SpringerLink : B{ü}cher. Springer Netherlands, p. 1070.

Parish, J.L. et al., 2006. E2 Proteins from High- and Low-Risk Human Papillomavirus Types Differ in Their Ability To Bind p53 and Induce Apoptotic Cell Death E2 Proteins from High- and Low-Risk Human Papillomavirus Types Differ in Their Ability To Bind p53 and Induce Apoptotic Cell. *Journal of Virology*, 80(9), pp.4580–4590.

Pedroza-Saavedra, A., Lam, E.W.-F., Esquivel-Guadarrama, F. and Gutierrez-Xicotencatl, L., 2010. The human papillomavirus type 16 E5 oncoprotein synergizes with EGF-receptor signaling to enhance cell cycle progression and the down-regulation of p27Kip1. *Virology*, 400(1), pp.44–52.

Pendleton, K.P. and Grandis, J.R., 2013. Cisplatin-Based Chemotherapy Options for Recurrent and/or Metastatic Squamous Cell Cancer of the Head and Neck. *Clinical medicine insights. Therapeutics*, 740(0), pp.364-378

Petignat, P. and Roy, M., 2007. Diagnosis and management of cervical cancer. *BMJ : British Medical Journal*, 335(7623), pp.765–768.

Pim, D. et al., 2012. Human papillomaviruses and the specificity of PDZ domain targeting. *FEBS Journal*, 279(19), pp.3530–3537.

Pinidis, P., Tsikouras, P., Iatrakis, G., Zervoudis, S., Koukouli, Z., Bothou, A., … Vladareanu, S., 2016. Human Papilloma Virus' Life Cycle and Carcinogenesis. *Mædica*, 11(1), pp.48–54.

Psyrri, A. and DiMaio, D., 2008. Human papillomavirus in cervical and head-and-neck cancer. *Nature Reviews Clinical Oncology*, 5(1), pp.24–31.

Pyeon, D. et al., 2009. Establishment of human papillomavirus infection requires cell cycle progression. *PLOS Pathogens*, 5(2), pp.1–9.

Rasheed, Z.A. and Rubin, E.H., 2003. Mechanisms of resistance to topoisomerase I-targeting drugs. *Oncogene*, 22(47), pp.7296–7304.

Rashid, N.N., Rothan, H.A. and Yusoff, M.S.M., 2015. The association of mammalian DREAM complex and HPV16 E7 proteins. *American Journal of Cancer Research*, 5(12), pp.3525–3533.

Rautava, J. and Syrjänen, S., 2012. Biology of human papillomavirus infections in head and neck carcinogenesis. *Head and Neck Pathology*, 6(Suppl 1), pp.3–15.

Robati, M., Holtz, D. and Dunton, C.J., 2008. A review of topotecan in combination chemotherapy for advanced cervical cancer. *Therapeutics and Clinical Risk Management*, 4(1), pp.213–218.

Rodríguez-Carunchio, L. et al., 2015. HPV-negative carcinoma of the uterine cervix: A distinct type of cervical cancer with poor prognosis. *BJOG: An International Journal of Obstetrics and Gynaecology*, 122(1), pp.119–127.

Ryser, M.D., Myers, E.R. and Durrett, R., 2015. HPV Clearance and the neglected role of stochasticity. *PLOS Computational Biology*, 11(3), pp.1–16.

Sanders, C.M. and Stenlund, A., 1998. Recruitment and loading of the E1 initiator protein: an ATP-dependent process catalysed by a transcription factor. *The EMBO Journal*, 17(23), pp.7044–7055.

de Sanjose, S. et al., 2013. Age-specific occurrence of HPV16- and HPV18-related cervical Cancer. *Cancer Epidemiology, Biomarkers & Prevention*, 22(7),

pp.1313–1318.

Scarpini, C.G. et al., 2014. Virus transcript levels and cell growth rates after naturally occurring HPV16 integration events in basal cervical keratinocytes. *The Journal of Pathology*, 233(3), pp.281–293.

Schiffman, M. et al., 2016. Carcinogenic human papillomavirus infection. *Nature Reviews Disease Primers*, 2, p.16086.

Schiffman, M. et al., 2007. Human papillomavirus and cervical cancer. *The Lancet*, 370(9590), pp.890–907.

Schiffman, M. and Wentzensen, N., 2013. Human papillomavirus (HPV) infection and the multi-stage carcinogenesis of cervical cancer. *Cancer epidemiology, biomarkers & prevention : a publication of the American Association for Cancer Research, cosponsored by the American Society of Preventive Oncology*, 22(4), pp.553–560.

Schlichte, M.J. and Guidry, J., 2015. Current cervical carcinoma screening guidelines. *Journal of Clinical Medicine*, 4(5), pp.918–932.

Shabbir, M., Barod, R., Hegarty, P.K. and Minhas, S., 2013. Primary prevention and vaccination for penile cancer. *Therapeutic Advances in Urology*, 5(3), pp.161–169.

Shah, C.A. et al., 2009. Factors Affecting Risk of Mortality in Women With Vaginal Cancer. *Obstetrics and gynecology*, 113(5), pp.1038–1045.

Shin, S.I., Freedman, V.H., Risser, R. and Pollack, R., 1975. Tumorigenicity of virus-transformed cells in nude mice is correlated specifically with anchorage independent growth in vitro. *Proceedings of the National Academy of Sciences of the United States of America*, 72(11), pp.4435–4439.

Siddik, Z.H., 2003. Cisplatin: mode of cytotoxic action and molecular basis of resistance. *Oncogene*, 22(47), pp.7265–7279.

Silverberg, S.G. and Loffe, O.B., 2003. Pathology of cervical cancer. *The Cancer Journal*, 9(5), pp.335–347.

Soeda, E., Ferran, M.C., Baker, C.C. and McBride, A.A., 2006. Repression of HPV16 early region transcription by the E2 protein. *Virology*, 351(1), pp.29–41.

Song, D., Li, H., Li, H. and Dai, J., 2015. Effect of human papillomavirus infection on the immune system and its role in the course of cervical cancer.

Oncology Letters, 10(2), pp.600–606.

Soumya, D. and Arun, K.R., 2011. A Brief Assessment on Cervical Cancer. *Journal of Cancer Science & Therapy*, 3(17), pp.1–5.

Spanos, W. et al., 2009. Immune response during therapy with cisplatin or radiation for human papillomavirus–related head and neck cancer. *Archives of Otolaryngology–Head & Neck Surgery*, 135(11), pp.1137–1146.

Spanos, W.C. et al., 2008. The PDZ binding motif of human papillomavirus type 16 E6 induces PTPN13 loss, which allows anchorage-independent growth and synergizes with Ras for invasive growth. *Journal of Virology*, 82(5), pp.2493–2500.

Spence, T., Bruce, J., Yip, K.W. and Liu, F.-F., 2016. HPV associated head and neck cancer. *Cancers*, 8(8), p.75.

Stanley, M. a, 2012. Epithelial cell responses to infection with human papillomavirus. *Clinical microbiology reviews*, 25(2), pp.215–22.

Stanley, M.A., Masterson, P.J. and Nicholls, P.K., 1997. In vitro and animal models for antiviral therapy in papillomavirus infections. *Antiviral Chemistry & Chemotherapy*, 8(5), pp.381–400.

Stein, A.P. et al., 2014. Prevalence of Human Papillomavirus in Oropharyngeal Squamous Cell Carcinoma in the United States Across Time. *Chemical Research in Toxicology*, 27(4), pp.462–469.

Sudenga, S.L. and Shrestha, S., 2013. Key considerations and current perspectives of epidemiological studies on human papillomavirus persistence, the intermediate phenotype to cervical cancer. *International Journal of Infectious Diseases*, 17(4), pp.e216–e220.

Sultana, H. et al., 2003. Chemosensitivity and p53-Bax pathway-mediated apoptosis in patients with uterine cervical cancer. *Annals of Oncology*, 14(2), pp.214–219.

Suprynowicz, F.A. et al., 2010. The human papillomavirus type 16 E5 oncoprotein inhibits epidermal growth factor trafficking independently of endosome acidification. *Journal of virology*, 84(20), pp.10619–29.

Taichman, L.B., Breitburd, F., Croissant, O. and Orth, G., 1984. The search for a culture system for papillomavirus. *Journal of Investigative Dermatology*, 83(1), pp.S2–S6.

Tait, S.W.G. and Green, D.R., 2010. Mitochondria and cell death : outer membrane permeabilization and beyond. *Nature reviews. Molecular cell biology*, 11(9), pp.621–632.

Tamura, R.E. et al., 2012. GADD45 proteins: central players in tumorigenesis. *Current molecular medicine*, 12(5), pp.634–651.

Thomas, M., Pim, D. and Banks, L., 1999. The role of the E6-p53 interaction in the molecular pathogenesis of HPV. *Oncogene*, 18, pp.7690–7700.

Thomas, R., Oleinik, N. and Ogretmen, B., 2016. HPV16-E7 Oncoprotein Enhances Ceramide-Mediated Lethal Mitophagy by Regulating the Rb/E2F5/Drp1 Signaling Axis. *The FASEB Journal*, 30(1), p.1.

Tomaić, V., 2016. Functional roles of E6 and E7 oncoproteins in HPV-induced malignancies at diverse anatomical sites. *Cancers*, 8(10), p.95.

Tommasino, M., 2014. The human papillomavirus family and its role in carcinogenesis. *Seminars in Cancer Biology*, 26, pp.13–21.

Tsuda, N., Watari, H. and Ushijima, K., 2016. Chemotherapy and molecular targeting therapy for recurrent cervical cancer. *Chinese Journal of Cancer Research*, 28(2), pp.241–253.

Urban, D., Corry, J. and Rischin, D., 2014. What is the best treatment for patients with human papillomavirus–positive and –negative oropharyngeal cancer? *Cancer*, 120(10), pp.1462–1470.

Vaseva, A. V and Moll, U.M., 2009. The mitochondrial p53 pathway. *Biochimica et Biophysica Acta (BBA) - Bioenergetics*, 1787(5), pp.414–420.

Vermeer, P.D. et al., 2013. Targeting ERBB receptors shifts their partners and triggers persistent ERK signaling through a novel ERBB-EFNB1 complex. *Cancer research*, 73(18), pp.5787–5797.

de Villiers, E.-M. et al., 2004. Classification of papillomaviruses. *Virology*, 324(1), pp.17–27.

de Villiers, E.-M., 2013. Cross-roads in the classification of papillomaviruses. *Virology*, 445(1), pp.2–10.

Vokes, E.E., Agrawal, N. and Seiwert, T.Y., 2015. HPV-Associated Head and Neck Cancer. *Journal of the National Cancer Institute*, 107(12), pp.1–7.

Walker, J., Smiley, L.C., Ingram, D. and Roman, A., 2011. Expression of Human Papillomavirus Type 16 E7 Is Sufficient to Significantly Increase Expression of Angiogenic Factors But Is Not Sufficient to Induce Endothelial Cell Migration. *Virology*, 410(2), pp.283–290.

Wang, J.W. and Roden, R.B.S., 2013. Virus-like particles for the prevention of human papillomavirus-associated malignancies. *Expert Review of Vaccines*, 12(2), pp.1–22.

Wang, Q. et al., 2009. Phosphorylation of the human papillomavirus type 16 E1--E4 protein at T57 by ERK triggers a structural change that enhances keratin binding and protein stability. *Journal of Virology*, 83(8), pp.3668–3683.

Watt, F.M., 1998. Epidermal stem cells : markers , patterning and the control of stem cell fate. *Philosophical Transactions of the Royal Society B: Biological Sciences*, 353(1370), pp.831–837.

Węsierska-Gądek, J., Schloffer, D., Kotala, V. and Horky, M., 2002. Escape of p53 protein from E6-mediated degradation in HeLa cells after cisplatin therapy. *International Journal of Cancer*, 101(2), pp.128–136.

Westphal, D., Dewson, G., Czabotar, P.E. and Kluck, R.M., 2011. Molecular biology of Bax and Bak activation and action. *Biochimica et Biophysica Acta (BBA) - Molecular Cell Research*, 1813(4), pp.521–531.

White, M.D., 2014. Pros, cons, and ethics of HPV vaccine in teens—Why such controversy? *Translational Andrology and Urology*, 3(4), pp.429–434.

Williams, V.M., Filippova, M., Soto, U. and Duerksen-Hughes, P.J., 2011. HPV-DNA integration and carcinogenesis: putative roles for inflammation and oxidative stress. *Future Virology*, 6(1), pp.45–57.

Xiao, Z. et al., 2003. Chk1 mediates S and G2 arrests through Cdc25A degradation in response to DNA damaging agents. *The Journal of Biological Chemistry*, 278(13), pp.21767–21773.

Xu, F. et al., 2015. Integration of the full-length HPV16 genome in cervical cancer and Caski and Siha cell lines and the possible ways of HPV integration. *Virus Genes*, 50(2), pp.210–220.

Xu, M. et al., 2008. NFX1 interacts with mSin3A/histone deacetylase to repress hTERT transcription in keratinocytes. *Molecular and Cellular Biology*, 28(15), pp.4819–4828.

Xue, J., Vesper, B.J. and Radosevich, J.A., 2012. *HPV and Cancer* Radosevich, J.A., (ed.), Springer Netherlands, Netherlands.

Yang, A., Farmer, E., Wu, T.C. and Hung, C.-F., 2016. Perspectives for therapeutic HPV vaccine development. *Journal of Biomedical Science*, 23(1), p.75.

Yoshimatsu, Y. et al., 2017. Roles of the PDZ-binding motif of HPV 16 E6 protein in oncogenic transformation of human cervical keratinocytes. *Cancer Science*, 108(7), pp.1303–1309.

Zerfass-Thome, K. et al., 1997. Inactivation of the CDK inhibitor p27KIP1 by the human papillomavirus type 16 E7 oncoprotein. *Oncogene*, 13, pp.2323–2330.

Zhang, B., Srirangam, A., Potter, D.A. and Roman, A., 2005. HPV16 E5 protein disrupts the c-Cbl-EGFR interaction and EGFR ubiquitination in human foreskin keratinocytes. *Oncogene.*, 24(15), pp.2585–2588.

Zhang, C.X. and Lippard, S.J., 2003. New metal complexes as potential therapeutics. *Current Opinion in Chemical Biology*, 7(4), pp.481–489.

Zhang, W. et al., 2015. Role of cdk1 in the p53-independent abrogation of the postmitotic checkpoint by human papillomavirus E6. *Journal of Virology*, 89(5), pp.2553–2562.

Zhang, W., Kazakov, T., Popa, A. and DiMaio, D., 2014. Vesicular trafficking of incoming human papillomavirus 16 to the golgi apparatus and endoplasmic reticulum requires - secretase. *mBio*, 5(5), pp.1–11.

Zhen, S. et al., 2016. In Vitro and In Vivo Synergistic Therapeutic Effect of Cisplatin with Human Papillomavirus16 E6/E7 CRISPR/Cas9 on Cervical Cancer Cell Line. *Translational Oncology*, 9(6), pp.498–504.

Zheng, Z.-M., 2010. Viral Oncogenes, Noncoding RNAs, and RNA Splicing in Human Tumor Viruses. *International Journal of Biological Sciences*, 6(7), pp.730–755.

Zheng, Z.-M. and Baker, C.C., 2006. Papillomavirus genome structure, expression, and post-transcriptional regulation. *Frontiers in Bioscience : a Journal and Virtual Library*, 11, pp.2286–2302.

Ziemann, F. et al., 2015. Increased sensitivity of HPV-positive head and neck cancer cell lines to x-irradiation ± Cisplatin due to decreased expression of E6 and E7 oncoproteins and enhanced apoptosis. *American Journal of Cancer*

Research, 5(3), pp.1017–1031.

APPENDICES

APPENDIX A

Plasmid map of pBABE-neo

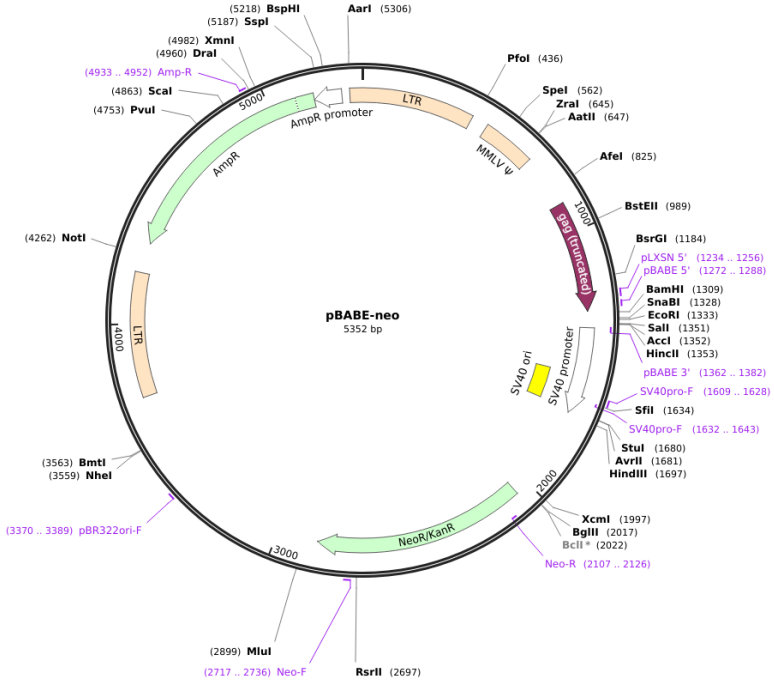

Plasmid map features

Colour	Features
Bar(s) / arrow(s)	
Yellow	Origin of replication (Ori)
White	Promoter region
Green	Antibiotic resistance selectable marker
Maroon	Truncated moloney murine leukemia virus, MMLV gag gene lacking the start codon
Peach	I. LTR – long terminal repeats II. MMLV ψ – packaging signal of MMLV
Grey	Basis of mobility region from pBR322
Fonts	
Purple	Location of 5' and 3' primers
Black	Restriction enzymes recognition sites.

The figure is adapted from Addgene. (Link: https://www.addgene.org/1767/).

APPENDIX B

Plasmid map of pLXSN-HPV16E6

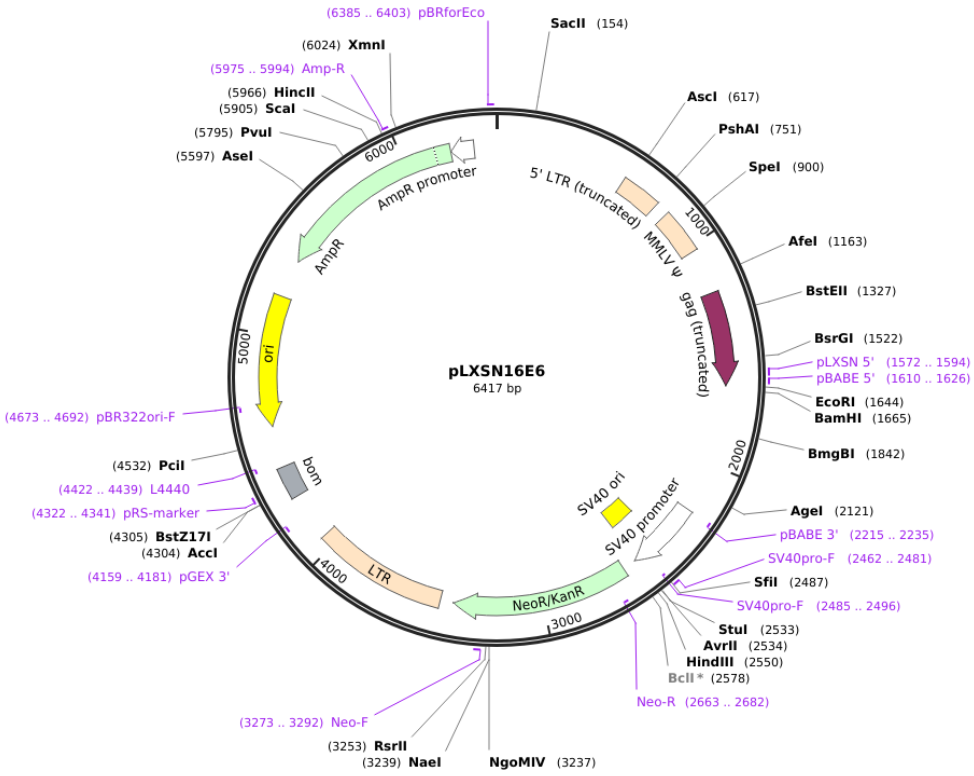

The figure is adapted from Addgene (Link: https://www.addgene.org/52395/).

See also table to Appendix A.

APPENDIX C

Plasmid map of pLXSN-HPV16E7

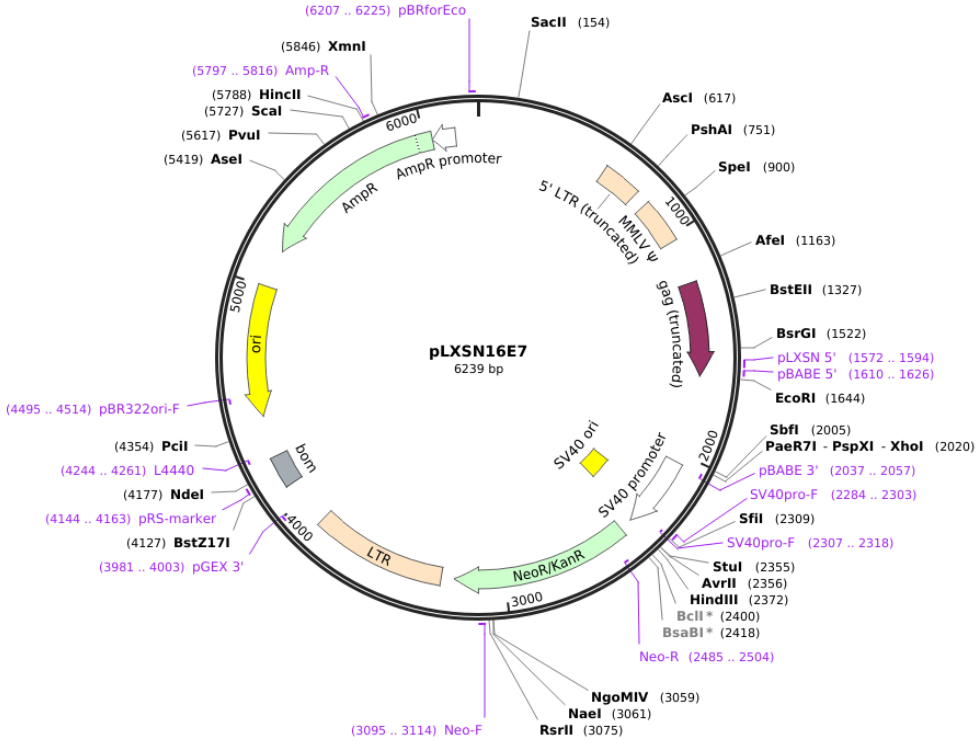

The figure is adapted from Addgene (Link: https://www.addgene.org/52396/). See also table to Appendix A.

APPENDIX D

Plasmid map of pLXSN _HPV16E6E7

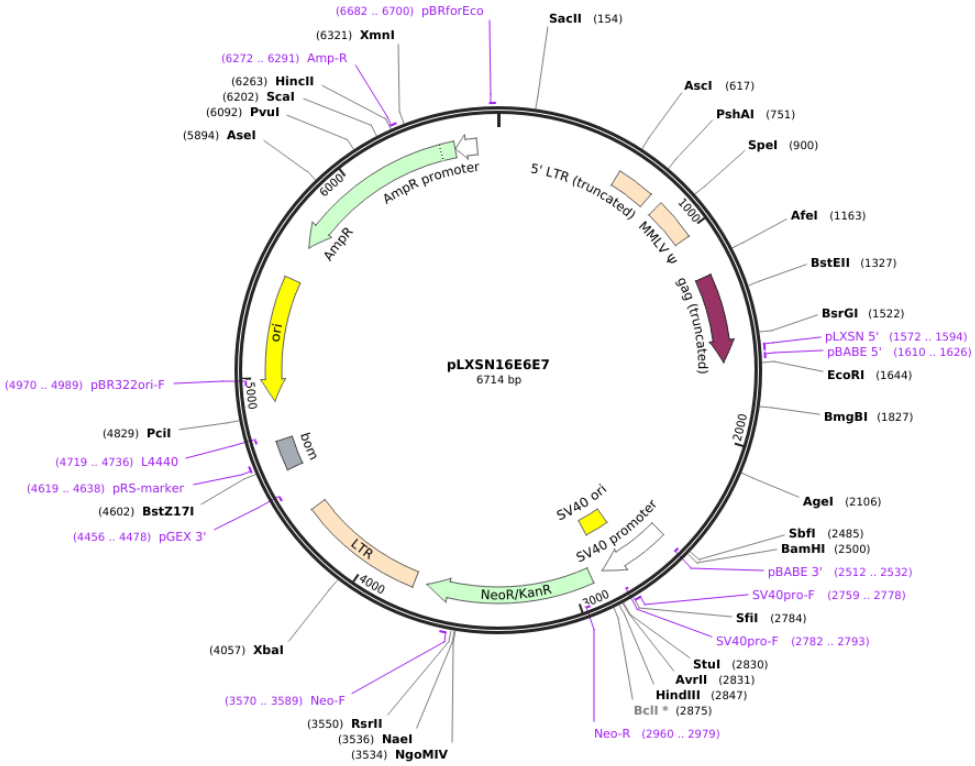

The figure is adapted from Addgene (Link: https://www.addgene.org/52394/).

See also table to Appendix A.

APPENDIX E

Plasmid map of pMX-GFP

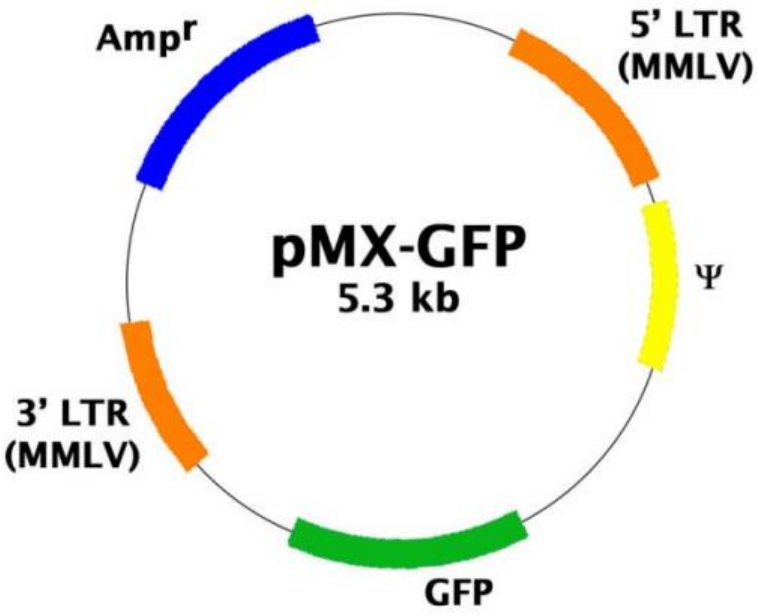

The figure is the plasmid map of pMX-GFP. Blue bar indicates the ampicillin-resistance gene; orange bars as the long terminator region (LTR) of moloney murine leukemia virus, MMLV; green bar as the reporter gene (green fluorescence protein, GFP), yellow bar as the packaging signal of MMLV. This figure is adapted from Cell Biolabs, Inc (Link: http://www.cellbiolabs.com/pmx-gfp-retroviral-control-vector)

APPENDIX F

Plasmid map of pcDNA6/ myc-His A

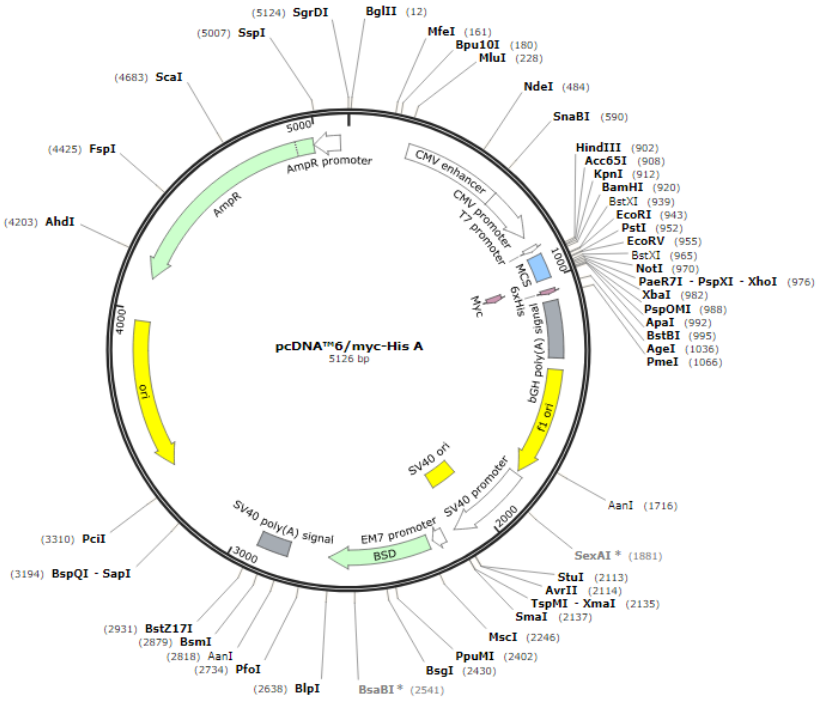

Plasmid map features

Bar(s) / arrow(s)	
Yellow	Origin of replication (Ori)
White	Promoter region
Green	Antibiotic resistance selectable marker
Maroon	Truncated moloney murine leukemia virus, MMLV gag gene lacking the start codon
Grey	Polyadenylation signal
Purple	Epitope / affinity tag
Blue	Multiple cloning site (MCS)
Fonts	
Black	Restriction enzymes recognition sites.

Figure adapted from SnapGene (Link: http://www.snapgene.com/resources/plasmid_files/mammalian_expression_vectors/pcDNA6_myc-His_A/).

APPENDIX G

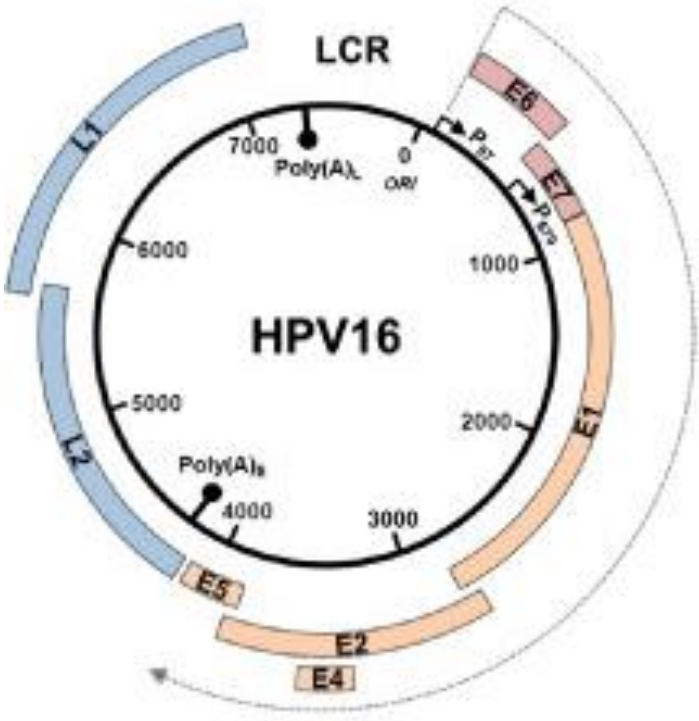

The figure is the genomic map of 7.9-kb HPV16 genome. Blue bars indicate the late (L) genes region; orange and pink bars as the early (E) genes region. HPV16-E6 and E7 genes are the major transforming protein that drive the infected cells to malignancy. LCR refers to long control region. This figure is adapted from Groves and Coleman, 2014.

(Link: https://www.researchgate.net/publication/269286889_Pathogenesis_of_human_papillomavirus-associated_mucosal_disease).

APPENDIX H

A

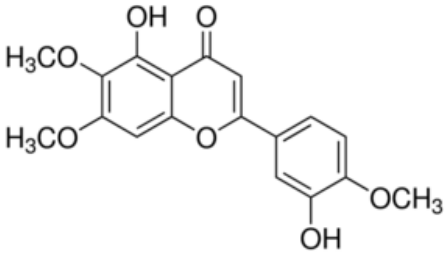

B

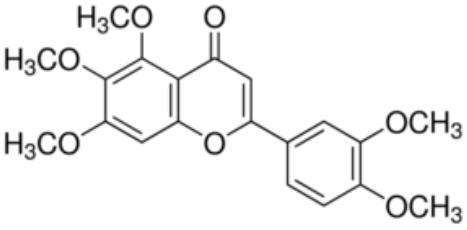

C

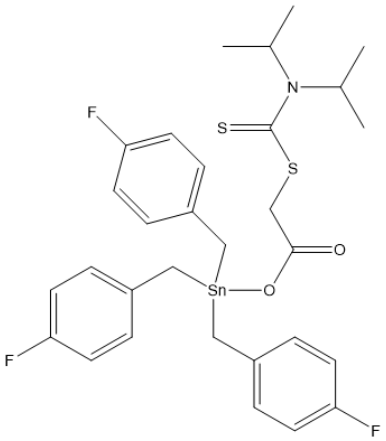

D

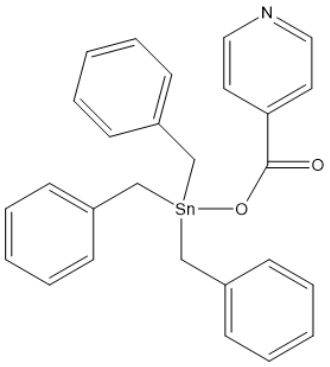

Chemical structure of natural flavone and novel synthetic compounds. (A) Eupatorin; (B) sinensetin; (C) tribenzyltin carboxylates 1 (TC1) and (D) tribenzyltin carboxylated 4 (TC4).

APPENDIX I

E6 mRNA expression in NIKS transduced with HPV16 (precancerous model)

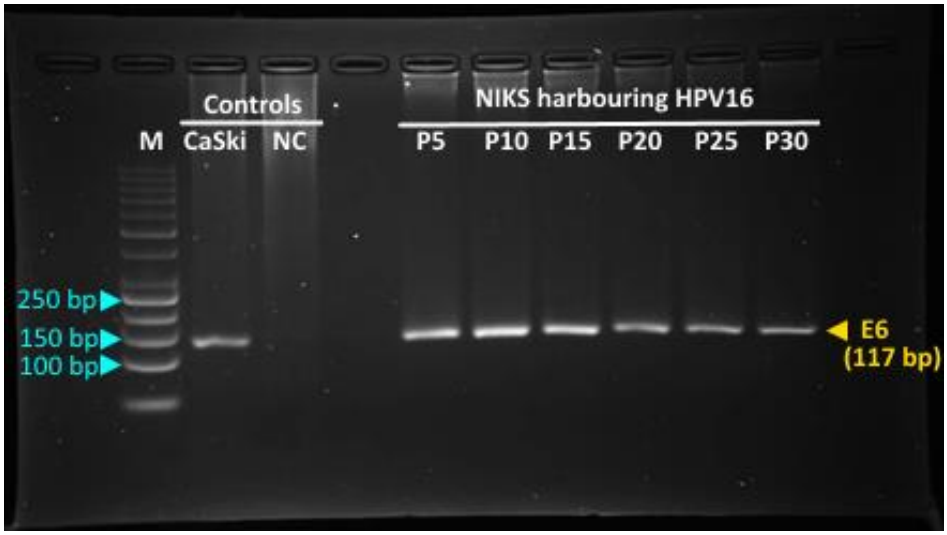

NIKS cells expressing the HPV16 were harvested from passage (P) 5 to 30 post-transfection. The E6 mRNA transcription detected by RT-PCR using the E6 primers. Expected bands at 117 bp were observed. CaSki was used as the HPV16-positive control; M, 50-bp DNA marker and NC, negative control without template.

APPENDIX J

E7 mRNA expression in NIKS transduced with HPV16 (precancerous model)

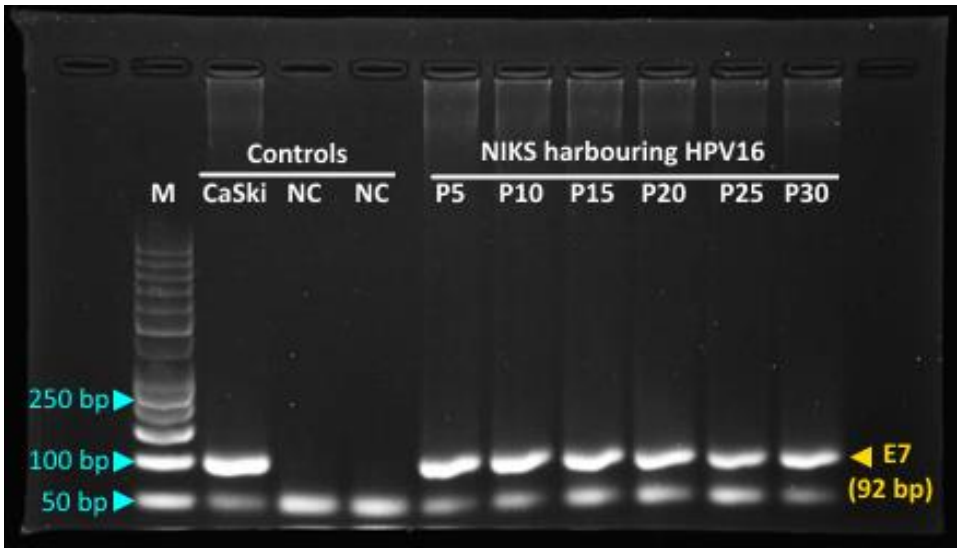

NIKS cells expressing the HPV16 were harvested from passage (P) 5 to 30 post-transfection. The E7 mRNA transcription detected by RT-PCR using the E7 primers. Expected bands at 92 bp were observed and bands below 50 bp were primer dimers. CaSki was used as the HPV16-positive control; M, 50-bp DNA marker and NC, negative control without template.

APPENDIX K

GAPDH mRNA expression in NIKS transduced with HPV16 (precancerous model)

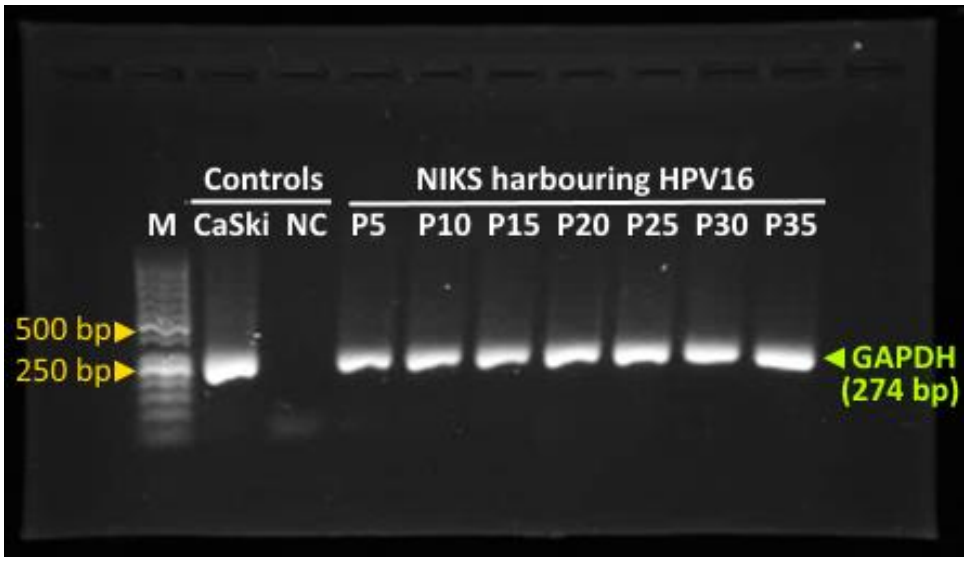

NIKS cells expressing the HPV16 were harvested from passage (P) 5 to 30 post-transfection. The GAPDH mRNA transcription detected by RT-PCR using the GAPDH primers. Expected bands at 274 bp were observed. CaSki was used as the HPV16-positive control; M, 50-bp DNA marker and NC, negative control without template.

APPENDIX L

E6 mRNA expression in NIKS transduced with HPV16 E6 gene (cancerous model)

NIKS cells expressing the HPV16 E6 gene were harvested from passage (P) 5 to 30 post-transduction. The E6 mRNA transcription detected by RT-PCR using the E6 primers. Expected bands at 117 bp were observed. CaSki was used as the HPV16-positive control; M, 50-bp DNA marker and NC, negative control without template.

APPENDIX M

E7 mRNA expression in NIKS transduced with HPV16 E7 gene (cancerous model)

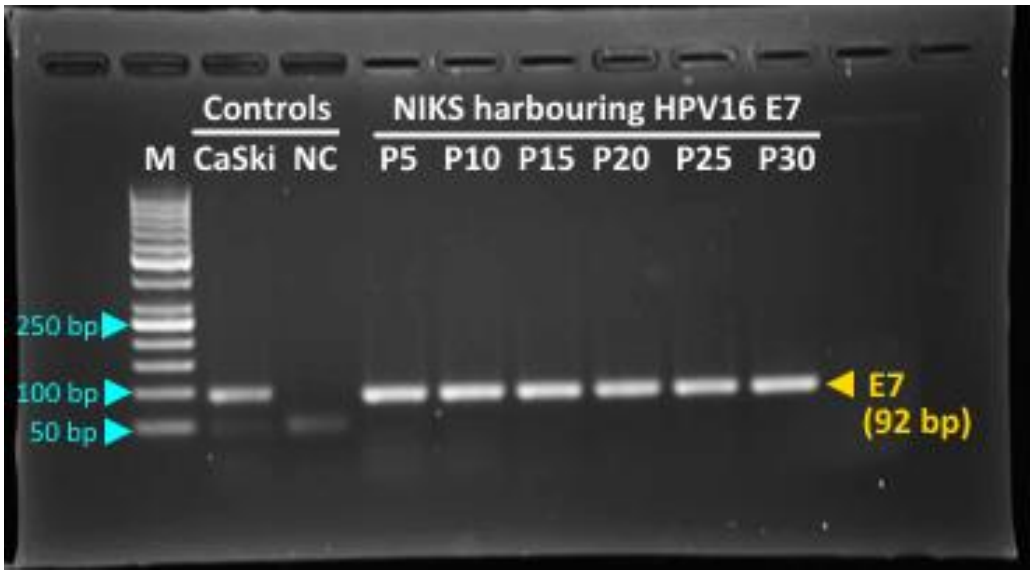

NIKS cells expressing the HPV16 E7 gene were harvested from passage (P) 5 to 30 post-transduction. The E7 mRNA transcription detected by RT-PCR using the E7 primers. Expected bands at 92 bp were observed and bands below 50 bp were primer dimers. CaSki was used as the HPV16-positive control; M, 50-bp DNA marker and NC, negative control without template.

APPENDIX N

E6 mRNA expression in NIKS transduced with HPV16 E6E7 gene (cancerous model)

NIKS cells expressing the HPV16 E6E7 gene were harvested from passage (P) 5 to 30 post-transduction. The E6 mRNA transcription detected by RT-PCR using the E6 primers. Expected bands at 117 bp were observed. CaSki was used as the HPV16-positive control; M, 50-bp DNA marker and NC, negative control without template.

APPENDIX O

E7 mRNA expression in NIKS transduced with HPV16 E6E7 gene (cancerous model)

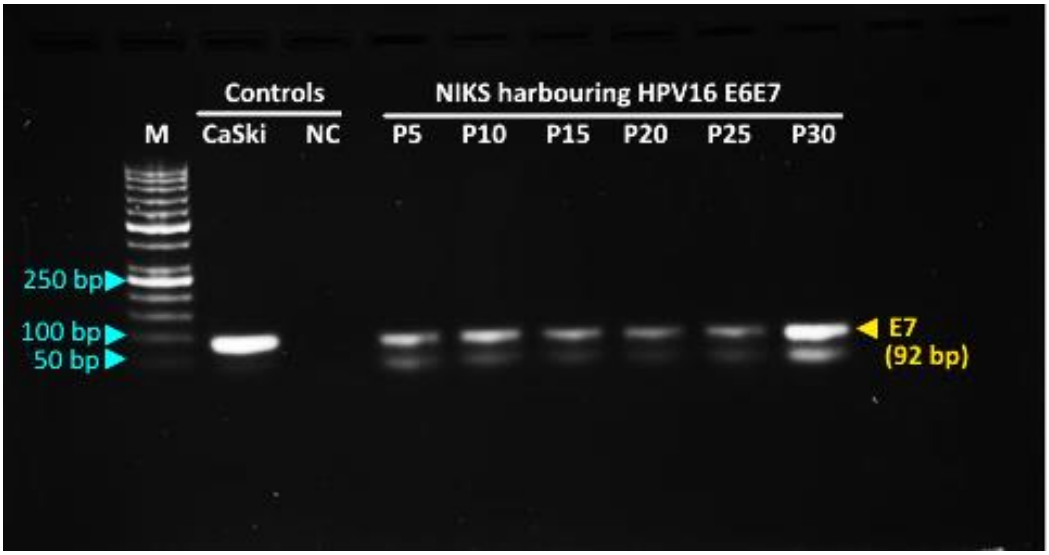

NIKS cells expressing the HPV16 E6E7 gene were harvested from passage (P) 5 to 30 post-transduction. The E7 mRNA transcription detected by RT-PCR using the E7 primers. Expected bands at 92 bp were observed and bands below 50 bp were primer dimers. CaSki was used as the HPV16-positive control; M, 50-bp DNA marker and NC, negative control without template.

APPENDIX P

GAPDH mRNA expression in NIKS transduced with HPV16 E6 gene (cancerous model)

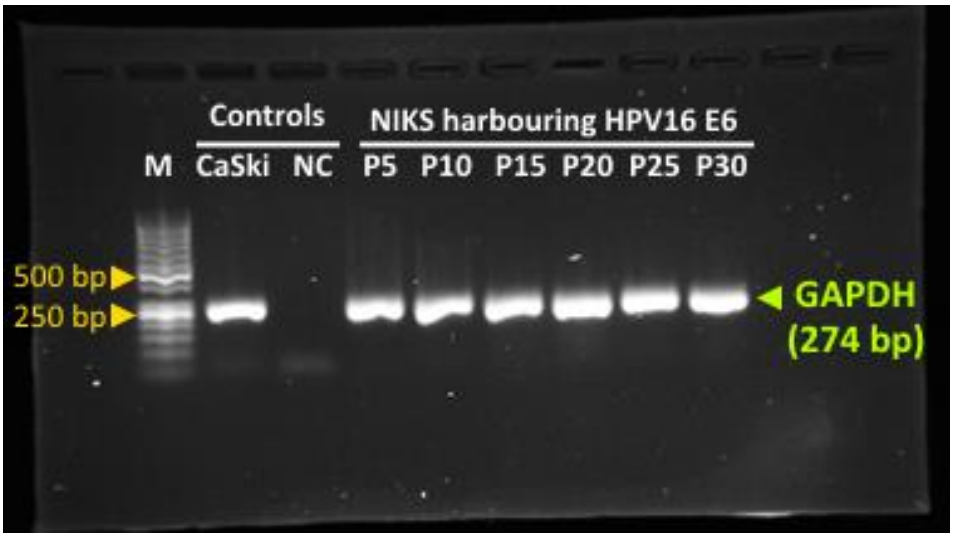

NIKS cells expressing the HPV16 E6 gene were harvested from passage (P) 5 to 30 post-transduction. The GAPDH mRNA transcription detected by RT-PCR using the GAPDH primers. Expected bands at 274 bp were observed. CaSki was used as the HPV16-positive control; M, 50-bp DNA marker and NC, negative control without template.

APPENDIX Q

GAPDH mRNA expression in NIKS transduced with HPV16 E7 gene (cancerous model)

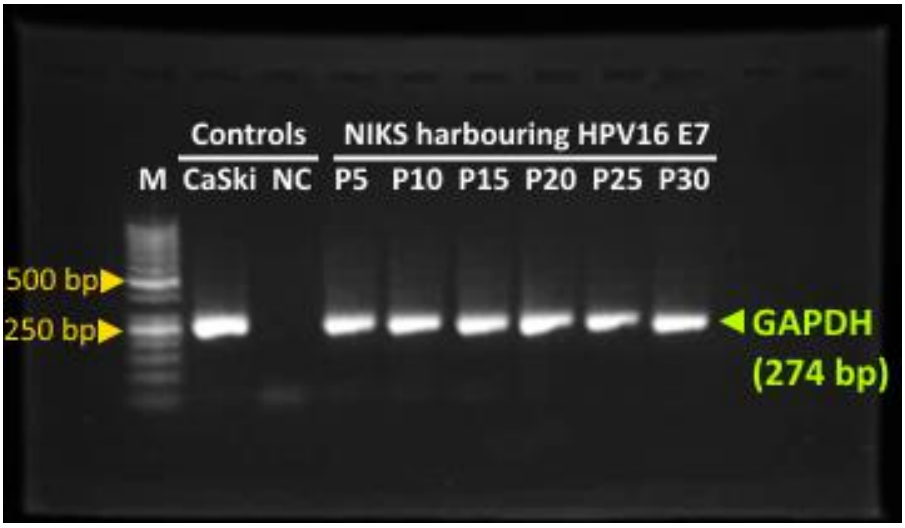

NIKS cells expressing the HPV16 E7 gene were harvested from passage (P) 5 to 30 post-transduction. The GAPDH mRNA transcription detected by RT-PCR using the GAPDH primers. Expected bands at 274 bp were observed. CaSki was used as the HPV16-positive control; M, 50-bp DNA marker and NC, negative control without template.

APPENDIX R

GAPDH mRNA expression in NIKS transduced with HPV16 E6E7 gene (cancerous model)

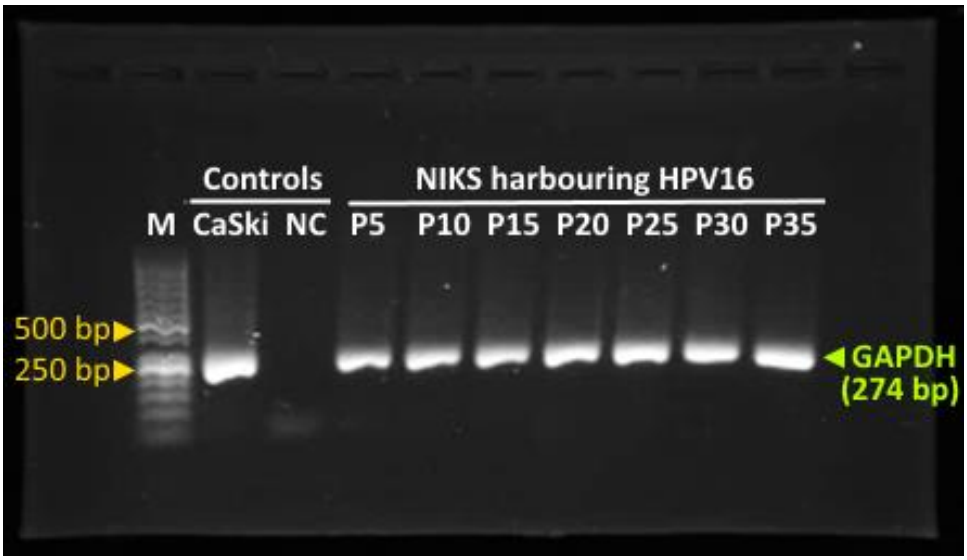

NIKS cells expressing the HPV16 E6E7 gene were harvested from passage (P) 5 to 30 post-transduction. The GAPDH mRNA transcription detected by RT-PCR using the GAPDH primers. Expected bands at 274 bp were observed. CaSki was used as the HPV16-positive control; M, 50-bp DNA marker and NC, negative control without template.